



**The Joint Meeting of the
Polish Synchrotron Radiation Society
and SOLARIS Users**

meeting summary

programme

presentations abstracts

Selected topics of the Synchrotron X-ray Absorption Spectroscopy (SXAS)

Andrzej Kisiel

Bulletin of the Polish Synchrotron Radiation Society

Vol.20, November 2020

SYNCHROTRON RADIATION IN NATURAL SCIENCE



Dear Readers,

On behalf of the Editorial Team, it is my pleasure to deliver the second issue of "Synchrotron Radiation in Natural Science" this year. The current release follows the Joint Meeting of Polish Synchrotron Radiation Society and SOLARIS Users. Due to the COVID-19 pandemic, the conference was prepared and executed online on 9-11 September. The conference was a great success, with over 200 participants from 66 Institutes and Universities all over the world. Within the present issue of "Synchrotron Radiation in Natural Science", we publish abstracts of the Joint Meeting of the Polish Synchrotron Radiation Society and SOLARIS Users conference. It is

important to note that abstracts cover very broad aspects of synchrotron radiation and X-ray Free Electron Lasers, including recent achievements in fundamental and applied research and novel applications in various research fields. The present Bulletin issue is further supplemented with a broad, and very didactic review on synchrotron-based X-ray absorption spectroscopy prepared by professor Andrzej Kisiel from the Jagiellonian University. We hope that each reader will find interesting and inspiring materials and research results with the present issue.

On behalf of Editorial Team,

Editor-In-Chief

Jakub Szlachetko

jakub.szlachetko@ifj.edu.pl
Institute of Nuclear Physics
Polish Academy of Sciences
Radzikowskiego 152
31-342 Kraków, Poland

Editorial board

Co-Editor, Graphics & Style

Zuzanna Pietralik-Molińska

Faculty of Physics
Adam Mickiewicz University
Uniwersytetu Poznańskiego 2
61-614 Poznań, Poland



Co-Editor, Auxiliary Editing

Joanna Czapla-Masztafiak

Institute of Nuclear Physics
Polish Academy of Sciences
Radzikowskiego 152
31-342 Kraków, Poland



Co-Editor, Graphics & Style

Augustyn Moliński

Faculty of Physics
Adam Mickiewicz University
Uniwersytetu Poznańskiego 2
61-614 Poznań, Poland



Co-Editor, Research Section

Wojciech Błachucki

Institute of Nuclear Physics
Polish Academy of Sciences
Radzikowskiego 152
31-342 Kraków, Poland



Co-Editor, Scientific News

Edyta Piskorska-Hommel

Institute of Low Temperature
and Structure Research
Polish Academy of Sciences
Okólna 2, 50-422 Wrocław, Poland



*Co-Editor, Scientific News
& Administrative management*

Anna Wach

Institute of Nuclear Physics
Polish Academy of Sciences
Radzikowskiego 152
31-342 Kraków, Poland



Co-Editor, SOLARIS news

Emilia Król

National Synchrotron Radiation
Centre SOLARIS
Jagiellonian University,
Czerwone Maki 98
30-392 Kraków, Poland



Layout and cover design by Z. Pietralik-Molińska and A. Moliński

Cover photo SOLARIS FACILITY by E. Król

ISSN 1644-7190

**JOINT MEETING OF POLISH SYNCHROTRON RADIATION SOCIETY
AND SOLARIS USERS**

KRAKÓW, POLAND, SEPTEMBER 9 - 11, 2020

**Ladies and Gentlemen,**

We would like to thank all the people and institutions who contributed to the success of the first Joint Meeting of the Polish Synchrotron Radiation Society (PTPS) and Users of The National SOLARIS Synchrotron Radiation Center (NCPS). The conference was held on September 9-11, 2020. Due to the situation related to the COVID-19 pandemic, we decided to organize the "Joint Meeting of the Polish Synchrotron Radiation Society and SOLARIS Users" as an online conference.

The Polish Synchrotron Radiation Society has been organizing the National Symposium of Synchrotron Radiation Users (KSUPS) every two years since 1991. Thanks to the fine efforts of the scientific community associated with the Polish Synchrotron Consortium and members of the Polish Synchrotron Radiation Society the construction of the National Synchrotron Radiation Center - the SOLARIS synchrotron in Krakow began in 2010. Since 2018, research groups from various centers, not only from Poland, have been conducting experiments on beamlines at the SOLARIS synchrotron, which has become a unique research center in Poland. SOLARIS is continuously expanding its research offer, and recently, apart from the synchrotron, the most advanced cryo-electron microscope in Poland is available to scientists.

The program of this year's 1st edition of the joint conference included an overview of research performed at synchrotron and alternative radiation sources as well as at X-ray free electron lasers. The scientific presentations were focused on current scientific and technological achievements and development trends in the field of research using synchrotron radiation. We hope that the 1st edition of the Joint Meeting of the Polish Synchrotron Radiation Society (PTPS) and SOLARIS Users contributed significantly to the integration of the community of synchrotron radiation users in Poland. We would like to mention that a relatively large number of 240 participants from 66 universities/institutes took part in the virtual meeting, while over 100 listeners attended each oral presentation. The online poll completed during the conference registration showed that the general scientific interest of participants was focused mostly on synchrotron and X-ray free electron laser research, as well as on Cryo-EM technique (distribution is presented in Figure 1). We would also like to note the relatively large contribution of participants affiliated with foreign Institute/University (Figure 2). Among Polish Institutes/Universities, the most participants were from SOLARIS National Synchrotron Radiation Centre (36), AGH University of Science and Technology (28), Institute of Physics Polish Academy of Sciences (20), Institute of Nuclear Physics Polish Academy of Science (16), Jagiellonian University (15) and Gdańsk University of Technology (14).

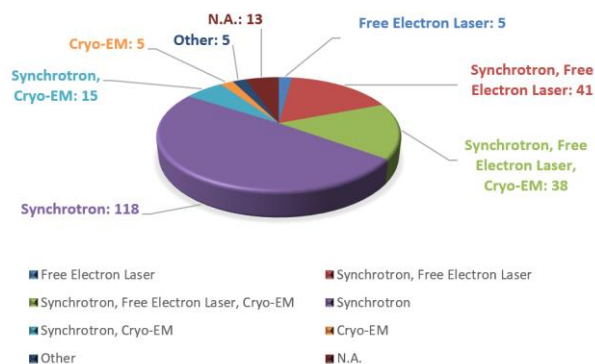


Figure 1: Poll results of the scientific interest among the conference participants.

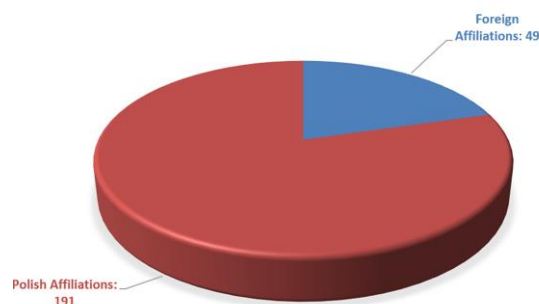


Figure 2: Distribution of affiliations for conference participants.

We would like to thank all the speakers, invited guests, and participants for active participation in the first Joint Meeting of the Polish Synchrotron Radiation Society (PTPS) and SOLARIS Users. We would like to thank the Polish Synchrotron Radiation Society, the National Radiation Synchrotron Centre SOLARIS, the Jagiellonian University, the Institute of Nuclear Physics Polish Academy of Science, and the National Centre For Nuclear Research for active support, participation, and help in organizing this event. Our warm thanks also go to the Scientific Committee for active participation in preparing the conference's scientific program.

We are hoping that the second Joint Meeting of the Polish Synchrotron Radiation Society (PTPS) and Users of The National SOLARIS Synchrotron Radiation Center (NCPS) can be conducted in a classical, face-to-face form.

With kind regards,

Chairs of the organizing committee:

dr hab. Jakub Szlachetko and prof. Marek Stankiewicz

On behalf of the Organizing Committee:

dr Katarzyna Bester-Ostrowska, the SOLARIS National Synchrotron Radiation Centre
 dr Wojciech Błachucki, the Institute of Physical Chemistry of the Polish Academy of Sciences
 dr Agata Chrzęścijanek, the SOLARIS National Synchrotron Radiation Centre
 dr Joanna Czapla-Masztafiak, the Institute of Nuclear Physics of the Polish Academy of Sciences
 dr Sebastian Glatt, the Malopolska Centre of Biotechnology
 mgr Alicja Górkiewicz, the SOLARIS National Synchrotron Radiation Centre
 dr Marcin Klepka, the Institute of Physics of the Polish Academy of Sciences
 mgr Emilia Król, the SOLARIS National Synchrotron Radiation Centre
 dr Anna Wach, the Institute of Nuclear Physics of the Polish Academy of Sciences.

CONFERENCE PROGRAMME

Wednesday, 9th September			
Time	Title	Speaker	Page
9:15 – 9:30	Conference Opening	Wojciech M. Kwiatek	
Session: Research with synchrotrons and free electron lasers			
9:30 – 10:00	SOLARIS - Present Status and Development Plans	Marek Stankiewicz	
10:00 – 10:30	The European XFEL – A new x-ray source offering new research opportunities	Thomas Tschentscher	
10:30 – 10:50	Band structure of Pb/NbP interface – an ARPES study	Bogdan Kowalski	
10:50 – 11:10	Coffee break		
11:10 – 11:40	The Evolution of Electronic Complexity in Biology: 2p3d and 1s3p RIXS of Iron Sulfur Clusters	Serena DeBeer	
11:40 – 12:00	Serial Crystallography Reveals Cap Methylation in SARS-CoV-2	Mateusz Wilamowski	
12:00 – 12:20	Scattering rates and superconductivity in ferropnictides	Rafał Kurlito	
12:20 – 12:40	Remote access to Research Infrastructure and Data	Roberto Pugliese	
12:40 – 13:40	Lunch break		
Session: Research with synchrotrons and free electron lasers			
13:40 – 14:10	Spin cross-over dynamics and charge transfer in biology	Majed Chergui	
14:10 – 14:30	Development of Fast HPC Detectors for Synchrotron Applications	Pawel Grybos	
14:30 – 14:50	X-ray spectroscopy with polychromatic sources for laboratory and synchrotron research	Wojciech Błachucki	
14:50 – 15:10	RIXS-MCD as selective probe to characterize structure and magnetization of nanoparticles in solution	Juliusz Kuciakowski	
15:10 – 15:30	Electronic structure of LaAgSb ₂	Marcin Rosmus	
15:30 – 15:40	Coffee Break		
15:40 – 16:10	Virtual Tour SOLARIS		
16:10 – 18:10	PTPS: General Assembly		

Thursday, 10th September			
Time	Title	Speaker	Page
Session: SOLARIS - current status and new opportunities			
9:00 – 9:30	New beamlines at SOLARIS	Jacek Szade	
9:30 – 10:00	Recent progress in the construction of SOLCRYS beamline at SOLARIS National Synchrotron Radiation Centre	Maciej Kozak	
10:00 – 10:30	Seeing is Believing - How single particle Cryo-EM is changing structural biology	Sebastian Glatt	
10:30 – 10:50	Coffee Break		
Session: SOLARIS beamlines			
10:50 – 11:10	Performance of SOLARIS synchrotron	Adriana Wawrzyniak	
11:10 – 11:40	Research potential of PEEM/XAS beamline	Marcin Zając & Tomasz Giela	
11:40 – 12:00	Research potential of UARPES beamline	Natalia Olszowska	
12:00 – 12:20	First scientific highlight from SOLARIS	Michał Ślęzak	
12:20 – 12:30	News from User Office	Alicja Górkiewicz	
12:30 – 13:15	Lunch Break		
Session: SOLARIS beamlines under development			
13:15 – 13:45	Synchrotron infrared spectroscopy and imaging: Opportunities, and new challenges	Paul Dumas	
13:45 – 14:00	SOLAIR beamline	Tomasz Wrobel	
14:00 – 14:15	PHLIX beamline	Magdalena Szczepanik-Ciba	
14:15 – 14:30	POLYX beamline	Pawel Korecki	
14:30 – 14:45	SOLABS beamline	Henning Lichtenberg	
14:45 – 15:00	XMCD beamline	Tolek Tyliczszak & Krzysztof Matlak	
15:00 – 15:20	Coffee Break		
15:20 – 16:30	Poster Session		

Friday, 11th September			
Time	Title	Speaker	Page
Session: Research with synchrotrons and free electron lasers			
9:00 – 9:30	SOLARIS and MAX IV: A unique example of international collaboration	Nils Mårtensson	
9:30 – 10:00	X-ray photoelectron study of polymers surface after modification by extreme ultraviolet radiation	Krystyna Jablonska	
10:00 – 10:20	The status and scope of SOLARIS within the European landscape of CERIC-ERIC	Carlo Rizzuto	
10:20 – 10:40	Coffee break		
Session: Research with synchrotrons and free electron lasers			
10:40 – 11:00	Polish Free Electron Laser- User Facility	Krzysztof Kurek	
11:00 – 11:30	Observation of the reduction of Ce ⁴⁺ to Ce ³⁺ in Ce _{0.7} Yb _{0.2} Pd _{0.1} O _{2-δ} catalyst	Edyta Piskorska-Hommel	
11:30 – 11:50	Scanning photoelectron microscopy study of local electronic structure of p-type ZnO films doped with nitrogen	Elżbieta Guzewicz	
11:50 – 12:10	Spectroscopic insight into properties of nanostructured magnetic oxides	Krzysztof Pitala	
12:10 – 12:20	Closing Remarks		

SOLARIS - present status and development plans

Keynote Lecture
Wednesday 09.09.2020
09:30-10:00

M. Stankiewicz*

SOLARIS National Synchrotron Radiation Centre, Jagiellonian University
ul. Czerwone Maki 98, 30-392 Kraków

*e-mail: m.j.stankiewicz@uj.edu.pl

National Synchrotron Radiation Centre SOLARIS in Kraków is the most modern and largest multidisciplinary research facility in Poland. The Centre was built between 2010 and 2015. The investment was co-financed by the European Union with funds from the European Regional Development Fund, as part of the Innovative Economy Operational Program for 2007-2013. As a strategic investment for the development of science, SOLARIS has been included on the Polish Roadmap for Research Infrastructures. Since 2016 SOLARIS joined Central European Research Infrastructure Consortium - CERIC-ERIC where it has become one of the key research facilities.

SOLARIS has been built using the groundbreaking design of magnetic double bend achromats developed at MAX-lab facility in Lund, Sweden, resulting in outstanding properties of generated synchrotron light which places SOLARIS firmly at the cutting edge of devices of this type. SOLARIS synchrotron operates at 1.5GeV energy with up to 500mA stored electron beam. It is powered by 600MeV S-band linac.

SOLARIS can provide synchrotron radiation for up to 18 beamlines from bending magnets and insertion devices. Within the scope of the project budget two state of the art beamlines (PEEM/XAS and UARPES) have been constructed.

In April 2018 SOLARIS opened the first call for measurements at these beamlines. Since then the number of applications from all over the world exceeds the available time and International Evaluation Committee is providing advice and ranking of the applications on the scientific merit basis. Today SOLARIS is undergoing very intense development constructing 6 new beamlines which will significantly broaden available research options.

The presentation will focus on the current status of the Center, its National and International position as well as on the plans for the future development.

Acknowledgements: Author would like to acknowledge the privilege of working with all members of SOLARIS Team whose deep and persisting involvement during construction and development of the center have put SOLARIS on the world map of research facilities. Support of numerous Polish and International researchers and experts has to be acknowledged. The project would not be possible without their involvement.

References

1. Reich, E. S. Ultimate upgrade for US synchrotron. *Nature* 501, 148–149 (2013).
2. All countries, great and small, *Nature* 535, S56–S61 (2016).

The European XFEL – A new x-ray source offering new research opportunities

Keynote Lecture
Wednesday 09.09.2020
10:00-10:30

T. Tschentscher*

European XFEL, Holzkoppel 4, 22869 Schenefeld, Germany

*e-mail: thomas.tschentscher@xfel.eu

European XFEL is an international large-scale user facility for research using x-ray FEL radiation. It offers opportunities for x-ray FEL research in the range from 0.25 to 25 keV at initially six science instruments, each dedicated to a specific area of application. European XFEL offers the unique possibility to deliver up to 27.000 x-ray pulses per second and User operation started in 2017 after about 8 yrs of construction.

In the focus of scientific applications of the European XFEL are those of the ultrafast time and high-field domain. Applications target many different types of samples – from highly excited ions via complex solids to huge bio-machines – in a huge variety of environments – from vacuum via natural solvents to extreme pressures and field strength – by also applying ultrashort lasers of variable wavelength to study non-equilibrium dynamics. Experiments support fundamental research applications to e.g. solve the structure of complex bio-matter, study ultrafast chemical processes, disentangle electronic state dynamics of complex materials, or reveal the properties of matter under extreme conditions.

In the presentation a brief overview of the facility and available instrumentation, exemplary results from first experiments, and some general findings are shown.

Band structure of Pb/NbP interface – an ARPES study

B. J. Kowalski^{1*}, P. Iwanowski^{1,2}, A. Wadge², A. Wiśniewski^{1,2}, N. Olszowska,³
J. Kołodziej³

Oral Presentation
Wednesday 09.09.2020
10:30-10:50

¹Institute of Physics, Polish Academy of Sciences, Aleja Lotników 32/46, PL-02668 Warsaw, Poland

²International Research Centre MagTop, Institute of Physics, Polish Academy of Sciences, Aleja Lotników 32/46, PL-02668 Warsaw, Poland

³National Synchrotron Radiation Centre SOLARIS, Jagiellonian University, Czerwone Maki 98, PL-30392 Kraków, Poland

*e-mail: kowab@ifpan.edu.pl

In Weyl semimetals (WSMs), the bulk quasiparticle excitations manifest themselves as Weyl fermions, massless particles theoretically predicted and never before observed experimentally. So, these materials, e. g. NbP, appear to be a playground for testing some concepts of quantum field theory but also may find applications in very fast electronics and quantum computing. Their crucial feature is existence (or not) time-reversal and inversion symmetries. Breaking one of them leads to a Weyl semimetal. If both symmetries are broken, the system may convert into a Weyl superconductor. Recently, an idea of introducing superconductivity in WSMs by the proximity effect at the superconductor/WSM interface has been developed¹. It was predicted that such system can support the zero-energy modes that are equivalent to Majorana fermions, which have potential for realization of fault-tolerant topological quantum computation².

We used the ARPES technique to study the early stage of Pb/NbP interface formation and to follow the surface states modifications due to appearance of Pb atoms on both P- and Nb-terminated NbP(001) faces. The data were collected for surfaces covered by approx. 0.5 ML of Pb and gave us an experimental evidence that Pb deposition quantitatively changed surface band structure on both faces. In particular the Fermi surface pockets marked out by Fermi arcs on P-terminated face, the fingerprints of Weyl semimetal character of the investigated system, were changed. Surprisingly, the contours appearing close to the X and Y points of the Brillouin zone for the Pb-covered P-terminated surface were similar to the Fermi arcs (between the Weyl points which still exist) obtained by calculations for the P-terminated TaP surface covered with 1 ML of potassium³. The conservation of the Weyl points during the Pb deposition supports the idea of inducing superconductivity in WSMs by the proximity effect at the Pb/NbP interface, as independently confirmed by our detailed magneto-transport studies of (Nb, Pb, In)/NbP systems⁴.

References

1. Bachmann, M. D., Nair, N., Flicker, F., Ilan, R., Meng, T., Ghimire, N. J., Bauer, E. D., Ronning, F., Analytis, J. G. & Moll P. J. W. Inducing superconductivity in Weyl semimetal microstructures by selective ion sputtering. *Sci. Adv.* 3, e1602983 (2017).
2. Lian, B., Sun, X.-Q., Vaezi, A., Qi, X.-L. & Zhang, S.-C. Topological quantum computation based on chiral Majorana fermions. *Proc. Natl Acad. Sci. USA* 115, 10938–10942 (2018).
3. Sun, Y., Wu, S.-C. & Yan, B. Topological surface states and Fermi arcs of the noncentrosymmetric Weyl semimetals TaAs, TaP, NbAs, and NbP. *Phys. Rev. B* 92, 115428 (2015).
4. Grabecki, G., Dąbrowski, A., Iwanowski, P., Hruban, A., Kowalski, B. J., Olszowska, N., Kołodziej, J., Chojnacki, M., Dybko, K., Łusakowski, A., Wojtowicz, T., Wojciechowski, T., Jakiela, R. & Wiśniewski A. Conductance spectra of (Nb, Pb, In)/NbP superconductor/Weyl semimetal junctions. *Phys. Rev. B* 101, 085113 (2020).

The Evolution of Electronic Complexity in Biology: 2p3d and 1s3p RIXS of Iron Sulfur Clusters

Keynote Lecture
Wednesday 09.09.2020
11:10-11:40

S. DeBeer*

Max Planck Institute for Chemical Energy Conversion, Stiftstr. 34-36, Mülheim an der Ruhr, D-45470, Germany

*e-mail: serena.debeer@cec.mpg.de

Iron sulfur proteins are ubiquitous in nature, performing essential roles in electron transfer processes, redox chemistry, regulatory sensing and catalysis. The metal active sites of these proteins range from simple single iron sites to complex eight iron clusters. Perhaps the most complex iron sulfur cluster that has been identified to date is the iron molybdenum cofactor (or FeMoco) of nitrogenase, which is capable of cleaving the strong triple bond of dinitrogen. The fundamental question that arises is how does nature evolve complexity in order to enable challenging transformations? In our view, a deeper understanding of the complex geometric and electronic structure of iron sulfur clusters requires the pursuit of novel experimental approaches for integrating their electronic structure in a detailed and quantitative fashion. To this end, we are applying both 2p3d and 1s3p resonant inelastic X-ray scattering (2p3d RIXS), in order to obtain deeper insights into the electronic structure of these important clusters. These data provide an experimental measure of the d-d transitions and allow for more detailed insights into the nature of the multiplet structure. The utility of these methods for understanding the electronic structure of nitrogenase will be highlighted. The challenges that RIXS spectroscopy presents for theoretical modeling will also be discussed.

Serial Crystallography Reveals Cap Methylation in SARS-CoV-2

Oral Presentation
Wednesday 09.09.2020
11:40-12:00

M. Wilamowski^{1,2*}, D. A. Sherrell³, G. Minasov⁴, Y. Kim^{1,3}, L. Shuvalova⁴,
A. Lavens³, R. Chard⁵, K. Michalska^{1,3}, K.J.F. Satchell⁴, A. Joachimiak^{1,2,3}

¹Center for Structural Genomics of Infectious Diseases, University of Chicago, USA

²Department of Biochemistry and Molecular Biology, University of Chicago, USA

³Structural Biology Center, X-ray Science Division, Argonne National Laboratory, USA

⁴Center for Structural Genomics of Infectious Diseases, Northwestern University, USA

⁵Mathematics and Computer Science Division, Argonne National Laboratory, USA

*e-mail: mwilamowski@anl.gov

The genome of the SARS-CoV-2 coronavirus contains 29 proteins, including 15 nonstructural proteins (Nsp). The complex of Nsp10 and Nsp16 is a 2'-O methyltransferase required for the capping of viral RNA at the 5' end¹. The methylation reaction is dependent on the S-adenosyl-L-methionine which is the donor of the methyl group that is moved to Cap-0 to produce Cap-1. The occurrence of the Cap-1 allows viral RNAs mimic eukaryotic transcripts and avoids initiation of innate immune response. Therefore, molecules that affect activity of Nsp10/Nsp16 and inhibits viral RNA maturation are potential drug targets for COVID-19. To investigate 2'-O methyltransferase mechanism of SARS-CoV-2 Nsp10/Nsp16, we used fixed-target serial synchrotron crystallography (SSX). SSX allows to collect data from thousands of crystals at room-temperature and reduce the dose of X-ray required to solve a crystal structure². Therefore, SSX decreases impact of radiation damage on crystal structure. Using SSX system developed at Structural Biology Center 19-ID beamline at APS we determined 295K temperature structures of Nsp10/Nsp16 (Fig. A). Our data shows the structure before and after the methylation of RNA Cap (Fig. B). We solved the first structure of Nsp10/Nsp16 in a complex with Cap-1. These structures can help with rational drug designs that inhibit viral RNA maturation, making SARS-CoV-2 sensitive to human innate response.

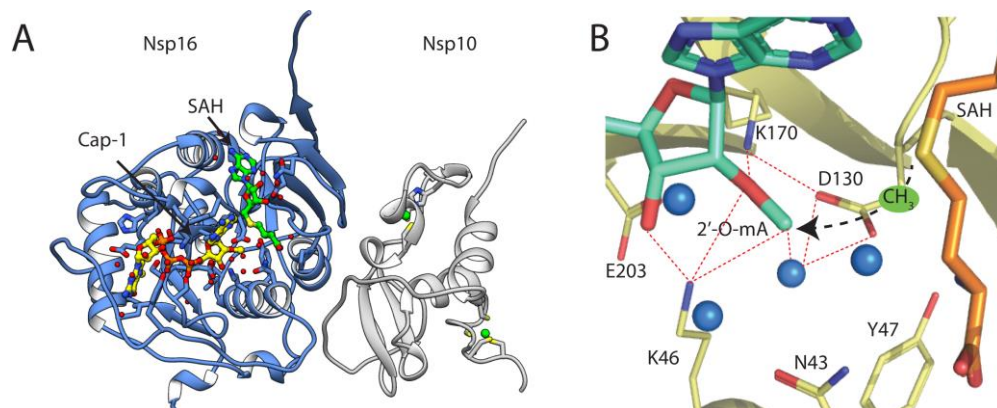


Fig. 1 A) Crystal structure of the SARS-CoV-2 Nsp10/Nsp16 heterodimer B) Active site of the Nsp10/Nsp16 2'-O MTase in a complex with Cap-1 and S-adenosyl-L-homocysteine (SAH)

References

1. Bouvet, M. et al. In Vitro Reconstitution of SARS-Coronavirus mRNA Cap Methylation. PLoS Pathog. 6, e1000863 (2010).
2. Sherrell, D. A. et al. A modular and compact portable mini-endstation for high-precision, high-speed fixed target serial crystallography at FEL and synchrotron sources. J. Synchrotron Radiat. 22, 1372–1378 (2015).

Scattering rates and superconductivity in ferropnictides

R. Kurlito^{1,2*}, E. D. L. Rienks³, M. Yao⁴, J. Bannies⁴, J. Fink^{1,4,5}

Oral Presentation
Wednesday 09.09.2020
12:00-12:20

¹Leibniz Institute for Solid State and Materials Research Dresden, Helmholtzstr. 20, D-01069 Dresden, Germany

²M. Smoluchowski Institute of Physics, Jagiellonian University, Łojasiewicza 11, 30-348, Kraków, Poland

³Helmholtz-Zentrum Berlin, Albert-Einstein-Strasse 15, 12489 Berlin, Germany

⁴Max Planck Institute for Chemical Physics of Solids, D-01187 Dresden, Germany

⁵Institut für Festkörperphysik, Technische Universität Dresden, D-01062 Dresden, Germany

*e-mail: rkurlito@gmail.com

In this contribution I describe our recent results on iron-based superconductors obtained by means of angle-resolved photoelectron spectroscopy (ARPES). Electronic structure of hole doped ferropnictides ($\text{Ba}_{1-x}\text{K}_x\text{Fe}_2\text{As}_2$, $\text{Eu}_{1-x}\text{K}_x\text{Fe}_2\text{As}_2$, $\text{Ba}_{1-x}\text{Na}_x\text{Fe}_2\text{As}_2$, $\text{Ba}(\text{Fe}_{1-x}\text{Co}_x)_2\text{As}_2$, $\text{NaFe}_{1-x}\text{Co}_x\text{As}$, BaCr_2As_2 , BaFe_2As_2) has been measured at the 12 and 13-ARPES end stations at BESSY synchrotron. All data have been collected in the normal state (5-50 K). The scattering rates of the inner hole pocket have been analyzed using novel, recently developed all-at-once (aao) method. They exhibit marginal Fermi liquid behavior. We have observed that the slope of scattering rate Γ/E scales with the critical temperature, what is in line with spin fluctuation model of superconductivity. Large value of Γ/E (c.a. 3), which is well above Planckian limit (i.e., $\Gamma/E=1$), was observed in case of optimally doped compound. This points to highly incoherent charge carriers in the normal state.

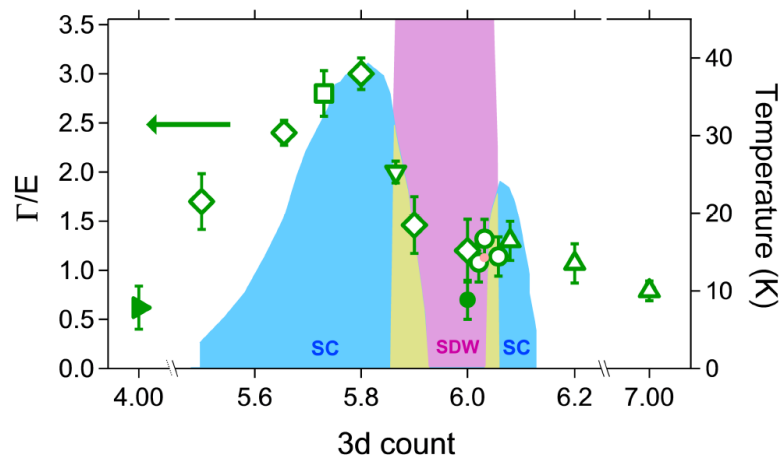


Fig. 1 Γ/E derived from ARPES as a function of 3d count. The ARPES data are compared with the range of the superconducting phase (blue), the spin density wave phase (magenta), and the range where both phases overlap (yellow)¹.

Acknowledgements: This work has been supported by the Deutsche Forschungsgemeinschaft (DFG) through the Priority Programme SPP1458.

References

1. Hardy, F. et al. Strong correlations, strong coupling, and s-wave superconductivity in hole-doped BaFe_2As_2 single crystals. Phys. Rev. B 94, 205113 (2016).

Remote access to Research Infrastructure and Data

Oral Presentation
Wednesday 09.09.2020
12:20-12:40

R. Pugliese^{1,2*}

¹Elettra Sincrotrone Trieste

²CERIC-ERIC

*e-mail: roberto.pugliese@elettra.eu

Covid-19 represents a challenge for research infrastructure. We will present a set of IT solutions that help to address the operational challenges during Covid-19. We will see how these technologies developed with the help of European Commission funded projects like PaNOSC¹, ExPaNDs² and CalipsoPlus³ can permit our users to remotely access data, acquisition computers, computing resources. We will also have a look to new technologies like distributed logbooks, wearable cameras, telepresence robots, voice user interfaces that even not essential can help giving the user a better experience. We will also cover the important advantages offered by a better quality of data management following the FAIR data principles.

All this will allow us to do science during lockdowns but also to improve the scientific workflow after lockdown providing us the freedom to choose if carrying on the experiment in presence or remotely via sample mailing.



Fig. 1 A Telepresence Robot operating at TwinMic beamline.

Acknowledgements: Authors would like to thank G. Kourousias, R.Borghes, F.Billè, R.Passuello, I.Gregori, M.Del Bianco, I.Andrian, M.Lonza from Synchrotron Elettra⁴, Trieste and M. De Simone, A.Olivo, E.Coghetto, A.Hafner, A. Lorenzon, from CERIC-ERIC⁵ for their huge effort in developing all the infrastructure.

References

1. PaNOSC (Photon and Neutron Open Science Cloud) project: <https://www.panosc.eu>.
2. ExPaNDs (European open science cloud Photon and Neutron Data service) project: <https://www.expands.eu>.
3. CalipsoPlus (Convenient Access to Light Sources Open to Innovation, Science and to the World.) project: <https://www.calipsoplus.eu>.
4. Elettra Sincrotrone Trieste, <http://www.elettra.eu>.
5. CERIC-ERIC, <https://www.ceric-eric.eu>.

Spin cross-over dynamics and charge transfer in biology

M. Chergui*

Keynote Lecture
Wednesday 09.09.2020
13:40-14:10

Ecole Polytechnique Fédérale de Lausanne, Lausanne centre for Ultrafast Science, 1015 Lausanne, Switzerland

*e-mail: majed.chergui@epfl.ch

The past decades have witnessed a revolution in sources of ultrashort pulses, from the optical to the X-ray spectral domain. This has given rise to novel approaches to track the evolution of chemical systems, with element-, spin- and structural sensitivity. In this talk, I will show the capabilities and the new insights that can be obtained from such approaches in the study of biological and molecular systems, and of materials.

We have recently investigated the initial events of the respiratory function in heme proteins. The change of the low-spin (LS) hexacoordinated heme to the high spin (HS) pentacoordinated domed form upon ligand detachment and the reverse upon ligand binding, represents the “transition state” that ultimately drives the respiratory function. The mechanism of the ligand dissociation-recombination process has been hotly debated in the past 30 years, without reaching a unified picture. We have monitored the evolution of Myoglobin-NO (MbNO) from LS to the HS state and the reverse process upon ligand rebinding to the heme, after impulsive photodissociation of the NO ligand. We monitored the evolution of the system using femtosecond (fs) Fe K α and K β non-resonant X-ray emission spectroscopy (XES), which is a powerful marker of the spin state. We show that the entire ligand dissociation-recombination cycle in MbNO is a spin cross-over followed by a reverse spin cross-over process.¹ The transition from planar LS to domed HS is not limited to ferrous ones, as thought till now, but a general behavior of all hemes as our fs X-ray absorption and fs-XES studies of Ferric Cytochrome c show.² The latter is the most important electron transfer (ET) protein in humans, and the biological significance of doming is still to be established in the case of ferric hemes.

References

1. Kinschel, D. et al. Femtosecond X-ray emission study of the spin cross-over dynamics in haem proteins. *Nat Commun* 11, 4145 (2020).
2. Bacellar, C. et al. *Proceedings of the National Academy of Science* (in press).

Development of Fast HPC Detectors for Synchrotron Applications

Oral Presentation
 Wednesday 09.09.2020
 14:10-14:30

P. Grybos* on behalf of ASIC Design Group

AGH University of Science and Technology, Kraków, Poland

*e-mail: [presenting author e-mail address](#)

There is a growing interest in pixel Hybrid Photon Counting (HPC) X-ray detectors for biology, medicine, chemistry, and solid-state physics applications. Hybrid pixel detectors usually consist of a pixelated sensor and readout front-end electronics of pixel architecture connected by the bump-bonding technique (Fig. 1). Hybrid detectors allow the use of different sensor materials, depending on the X-ray energy needed for the application, while Readout Integrated Circuit (ROIC) can be designed in one of the very advanced technologies offered by the microelectronics industry¹.

Readout integrated circuits (ROIC) for hybrid pixel detectors working in single photon counting mode are going in the direction of using deep submicron technologies or 3D technologies, to place more complex functionality in a single pixel cell to improve detector parameters like speed, energy, and spatial resolution. Some such examples of fast HPC detectors developed recently by AGH-UST, Kraków (Poland) in collaboration with Rigaku Corporation (Japan) are presented together with their synchrotron applications at Argonne National Laboratory (ANL)² and Synchrotron SOLEIL³.

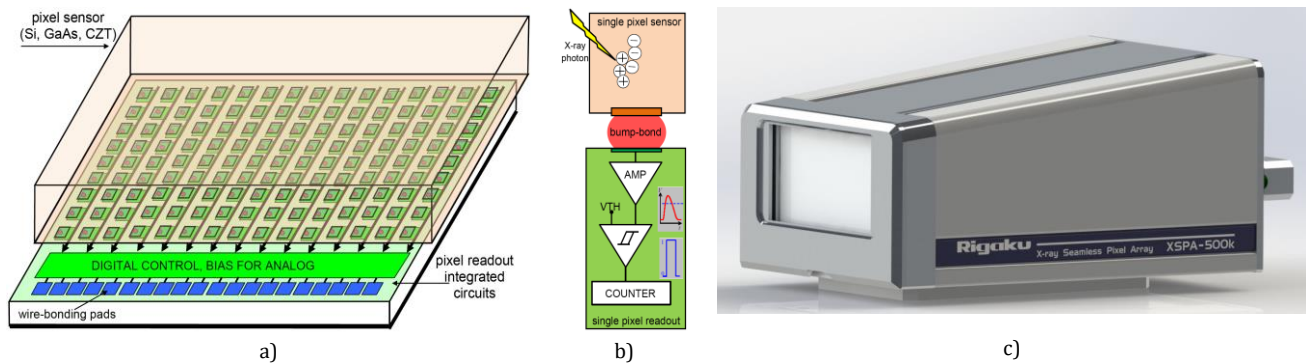


Fig. 1 a) SPC hybrid pixel detector – each detector’s pixel is connected to an independent readout channel on the IC, b) pulse processing in an SPC pixel, c) XSPA-500k HPC detector developed by Rigaku and AGH-UST with 500k, $76 \mu\text{m} \times 76 \mu\text{m}$ pixels over a $77.8 \times 38.9 \text{ mm}^2$ detection area³.

Acknowledgments: Authors would like to thank our collaborators from Rigaku Corporation Japan for common detector design, and Argonne National Laboratory and Synchrotron SOLEIL for beamline tests.

References

- Grybos, P. et al. 32k Channel Readout IC for Single Photon Counting Pixel Detectors with $75 \mu\text{m}$ Pitch, Dead Time of 85 ns, 9 e⁻ rms Offset Spread and 2% rms Gain Spread. IEEE TNS 63, 1155–1161 (2016).
- Zhang, Q. et al. Dynamic Scaling of Colloidal Gel Formation at Intermediate Concentrations. PRL 119, 178006 (2017).
- Nakaye, Y. et al. Characterization and performance evaluation of the XSPA-500k detector with synchrotron radiation (submitted to JSR 2020).

X-ray spectroscopy with polychromatic sources for laboratory and synchrotron research

Oral Presentation
Wednesday 09.09.2020
14:30-14:50

W. Błachucki^{1,*}, J. Czapla-Masztafiak¹, R. Fanselow², A. Wach¹, W. M. Kwiatek¹,
J. Szlachetko¹

¹Institute of Nuclear Physics, Polish Academy of Sciences, 31-342 Kraków, Poland

²Faculty of Chemistry, Jagiellonian University, Gronostajowa 2, 30-387 Kraków, Poland

*e-mail: wojciech.blachucki@ifj.edu.pl, jakub.szlachetko@ifj.edu.pl

With the advent of new technological solutions in the field of X-ray sources, optics and detectors, the development of efficient and compact X-ray spectroscopy systems is possible. We report an X-ray setup allowing X-ray emission and X-ray absorption spectroscopy (XES, XAS) measurements using polychromatic X-ray source equipped with focusing optics. Setup was developed at the Department of Applied Spectroscopy (NZ53) of the Institute of Nuclear Physics of the Polish Academy of Sciences¹. The available X-ray instrumentation and the supporting well-equipped chemistry and biology laboratories are routinely employed in fundamental research as well as in *in situ* time-resolved studies on electron dynamics and in particular in investigation of the role of metals in biological complexes, photo-chemical systems and materials important for renewable energy.

The X-ray equipment allows setting up two in-air crystal X-ray spectrometers in the von Hámos geometry² and gives large flexibility in the preparation of experiments. The spectrometers can be arranged not only independently, as two separate setups, but for instance they can share the X-ray source, enabling simultaneous measurement of XAS and XES spectra³ or two XES spectra in different energy regions (the so called *two-color mode*). The different experimental arrangements possible allow application of complex sample handling methods, such as, e. g., the liquid jet sample delivery. Our X-ray setups' capabilities will be further explored during user operation at the POLYX beamline of the SOLARIS synchrotron using the polychromatic beam from a bending magnet in combination with a focusing polycapillary X-ray optics. With the great X-ray flux available at the 3rd and 4th generation X-ray sources, the setups may be employed for time-resolved chemistry and biology research.

Acknowledgements: This work was supported by the National Science Centre (Poland) under the grants of numbers 2017/27/B/ST2/01890, 2016/21/D/ST4/00378, 2019/03/X/ST3/00035 and 2019/03/X/ST2/00949.

References

1. Błachucki, W., Wach, A., Czapla-Masztafiak, J., Kwiatek, W. & Szlachetko, J. Laboratory for high energy resolution X-ray spectroscopy at the Institute of Nuclear Physics of the Polish Academy of Sciences. *Synchrotron Radiation in Natural Science* 19, 5-7 (2020).
2. von Hámos, L. Röntgenspektroskopie und Abbildung mittels gekrümmter Kristallreflektoren. *Naturwissenschaften* 20, 705 (1932).
3. Błachucki, W., Czapla-Masztafiak, J., Sá, J. & Szlachetko, J. A laboratory-based double X-ray spectrometer for simultaneous X-ray emission and X-ray absorption studies. *Journal of Analytical Atomic Spectrometry* 34, 1409 (2019).

RIXS-MCD as selective probe to characterize structure and magnetization of nanoparticles in solution

Oral Presentation
Wednesday 09.09.2020
14:50-15:10

J. Kuciakowski^{1,2*}, M. Sikora², K. Pitala^{1,2}, S. L. Bielsa³, A. Kmita², D. Koziej⁴

¹ Faculty of Physics and Applied Computer Science, AGH University of Science and Technology, Cracow, Poland.

² Academic Centre for Materials and Nanotechnology, AGH University of Science and Technology, Cracow, Poland.

³ European Synchrotron Radiation Facility, Grenoble, France.

⁴ Institute for Nanostructures and Solid States Physics, Center for Hybrid Nanostructures, University of Hamburg, Hamburg, German

*e-mail: jkuciako@agh.edu.pl

Characterization of magnetic nanoparticles (MNP) in a solution is crucial in terms of the technologies development, since it is a natural state after synthesis and typical condition of use. Extraction of MNPs from solutions leads to changes in chemical state and structure, aggregation and strong dipole-dipole interactions and disregards the liquid-solid interaction. Capabilities of experimental techniques successfully applied to probe magnetic properties of nanoparticle films and nanopowders are strongly limited in case of liquid environment, e.g. due to lack of penetration or selectivity between solvent and nanoparticles. Recently, it was shown that X-ray Magnetic Circular Dichroism in Resonant Inelastic X-ray Scattering (RIXS-MCD) can be applied as sensitive, element selective probe of transition metal magnetic moment in bulk systems, nanopowders and frozen solutions of MNP^{1,2}. In 1s_{2p} RIXS-MCD sample is probed element-selectively at K edge of transition metal, upon collection of K α relaxation using high energy resolving spectrometer. It results in well-defined spectral features providing information about valence state and local environment of metal ions and strong MCD signal³. Weak self-absorption and significant penetration depth of hard x-rays allow for volume study through hard x-ray transparent window, while non-resonant signal is filtered out.

Presented are the results of in-situ magnetic characterization of iron oxide nanoparticles synthesized in especially designed cell for in-situ synthesis experiment⁴. Magnetite and cobalt ferrites were synthesized and measured on-the-fly to determine structural development, both on iron and cobalt edges. Evolution of magnetization of iron/cobalt ions were examined site-selectively during the reaction time. RIXS-MCD proves to be a good candidate for in-situ determination of structure and magnetization of nanoparticles in solutions. Supported by ex-situ characterization (size, zeta potential, etc.) it provides a comprehensive platform of description of magnetic nanoparticles in solution.

References

1. Juhin A., Lopez-Ortega A., Sikora M., Carvallo C., Estrader M., Estradé S., Peiró F., Baró M. D., Sainctavit P., Glatzel P. & Nogués J., *Nanoscale*, 6, 11911 (2014).
2. Daffé N., Daffé, Sikora M., Rovezzi M., Bouldi N., Gavrilov V., Neveu S., Choueikani F., Ohresser P., Dupuis V., Taverna D., Gloter A., Arrio M. A., Sainctavit P. & Juhin A., *Advanced Materials Interfaces*, 4, 1700599 (2017).
3. Sikora M., Juhin A., Simon G., Zając M., Biernacka K., Kapusta Cz., Morellon L., Ibarra M. R. & Glatzel P., *Journal of Applied Physics*, 111, 07E301 (2012).
4. Staniuk M., Hirsch O., Kränzlin N., Böhlen R., Beek W., Abdala P. M. & Koziej D., *Chemistry of Materials*, 26, p. 2086-2094 (2014).

Electronic structure of LaAgSb₂

Oral Presentation
Wednesday 09.09.2020
15:10-15:30

M. Rosmus^{1,2*}, N. Olszowska¹, J. J. Kołodziej^{1,2}, A. Ptok³, P. Piekarczyk³, M. Babij⁴,
Z. Bukowski⁴, P. Starowicz²

¹SOLARIS National Synchrotron Radiation Centre, Czerwone Maki 98, 30-392 Kraków

²M. Smoluchowski Institute of Physics, Jagiellonian University, Łojasiewicza 11, 30-348, Kraków, Poland

³Institute of Nuclear Physics, Polish Academy of Sciences. E. Radzikowskiego 152, PL-31342 Kraków, Poland

⁴Institute of Low Temperature and Structure Research, Polish Academy of Sciences, P.O. Box 1410, 50-950 Wrocław, Poland

*e-mail: marcin.rosmus@uj.edu.pl

LaAgSb₂ is an intermetallic compound that crystallizes in a tetragonal structure with characteristic atomic layers that indicate quasi-two-dimensional character of the electronic structure. It shows anisotropic transport properties.¹ It has been reported that LaAgSb₂ is a charge density wave (CDW) system with two transition temperature of $T_{1,CDW} = 207$ K and $T_{2,CDW} = 186$ K and their corresponding lattice modulation vectors equal $\tau_1 \sim 0.026(2\pi/a)$ and $\tau_2 \sim 0.16(2\pi/c)$.² Moreover, when the theoretical reports suggested the occurrence of states with non-trivial topology, this compound became particularly interesting.³

We have performed systematic investigations of electronic structure of LaAgSb₂ by means of angle-resolved photoemission spectroscopy (ARPES) at UARPES beamline of the Solaris synchrotron and at in-house laboratory. Measurements carried out with the use of a beam with different photon energies allowed to map a three-dimensional electronic structure and to find directions of high symmetry. Comparison of the measurements made for the series of values k_z , vertical and horizontal polarization of the excitation light and in different measurement geometries allowed to identify surface states, which are absent in the calculations based on the tight-binding model. The high-resolution measurements performed at in-house laboratory with helium lamp (photon energy of 21.2 eV) did not provide the clear evidence of the occurrence of a CDW energy gap in the investigated compound, however parts of Fermi surface show the characteristic features of the nesting compatible with the lattice modulation vector τ_1 .

References

1. Kefeng Wang and C. Petrovic, Multiband effects and possible Dirac states in LaAgSb₂ PHY. REV. B **86**, 155213 (2012).
2. C. Song, Jaehyun Park, Japil Koo, K.-B. Lee, J. Y. Rhee, S. L. Bud'ko, P. C. Canfield, B. N. Harmon, and A. I. Goldman, Charge-density-wave orderings in LaAgSb₂: An x-ray scattering study, Phys. Rev. B **68**, 035113 (2003).
3. Ruzsala P, Winiarski J, Samsel-Czekala M., Dirac-like band structure of LaTESb₂ (TE = Ni, Cu, and Pd) superconductors by DFT calculations, Comput. Mater. Sci. 154, 106-110 (2018).

New beamlines at SOLARIS

Keynote Lecture
Thursday 10.09.2020
09:00-09:30

J. Szade^{1,2}

¹NCPS SOLARIS

²A. Chełkowski Institute of Physics, University of Silesia

*e-mail: jacek.szade@uj.edu.pl

Synchrotron SOLARIS entered the new phase of its development. This phase can be characterized by a simultaneous work on several new beamlines which are at various stage of their formation.

PHELIX entered the commissioning stage. The beamline with the working name XMCD has changed its original shape and structure and will be completed in 2021. In the present shape it will comprise two microscopes – STXM and PEEM. The SOLABS beamline is being constructed. POLYX and SOLAIR are in the final design stage and first procurements have started. The same situation is with the SOLCRYX beamline which be placed in the extended experimental hall of SOLARIS.

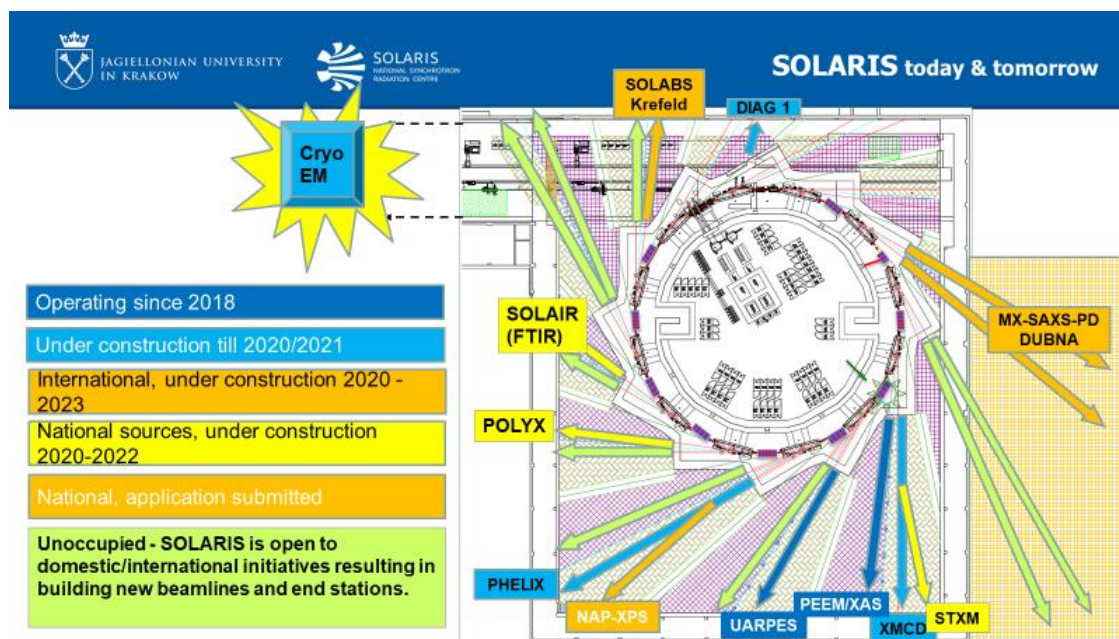


Fig. 1 Solaris today & tomorrow.

The planned timetable of the new beamlines realization and their basic parameters will be presented. The plan of the future development of our synchrotron will be given as well. SOLARIS is still open for new ideas and cooperation. There is still place for new beamlines. Good ideas are welcome!

Recent progress in the construction of SOLCRYM beamline at SOLARIS National Synchrotron Radiation Centre

Keynote Lecture
Thursday 10.09.2020
09:30-10:00

M. Kozak^{1,2*}, T. Kołodziej¹, A. Wawrzyniak¹, D. Paliwoda¹, G. Gazdowicz¹

¹SOLARIS National Synchrotron Radiation Centre, Jagiellonian University, Kraków, Poland

²Department of Macromolecular Physics, Adam Mickiewicz University, Poznań, Poland.

*e-mail: ma.kozak@uj.edu.pl

Macromolecular crystallography (MX) and bioSAXS beamlines are probably the most intensively utilised research systems in synchrotrons. Currently, there are over 100 such beamlines operating in synchrotrons worldwide¹.

The SOLCRYM beamline will be the first beamline, operating only in hard X-ray range from insertion device, installed at SOLARIS National Synchrotron Radiation Centre and will be dedicated to X-ray diffraction (especially macromolecular crystallography) and small angle X-ray scattering studies (SAXS). Its construction was planned already at the initial stages of NSRC construction. The X-ray source for SOLCRYM will be a superconducting wiggler ($B_0 = 4$ Tesla), which is currently being constructed by the Budker institute of Nuclear Physics RAS (Novosibirsk, Russia).

The synchrotron radiation beam, obtained from the wiggler, will be split by fixed mask into two independent beams for end stations (macromolecular crystallography, $E = 4-25$ keV and small angle X-ray scattering $E = 6-15$ keV). Both end stations will be fully equipped for experiments in ultra-low temperatures and for high pressure experiments. The diffraction experiments performed in helium atmosphere and at ultra-low temperature will reduce the radiation damages and improve the diffraction data quality^{3,4}. Therefore during the lecture the problem of radiation damages induced in macromolecular systems will be also discussed.

Recent situation caused by Covid-19 pandemic motivated us also to planning the remote access to SOLCRYM infrastructure. Therefore both end stations will be properly equipped for data collection via Internet on samples shipped by users directly to SOLARIS NSRC.

Acknowledgements: The SOLCRYM beamline is constructed in collaboration with Joint Institute for Nuclear Research (Dubna, Russia). The construction of extended experimental hall in NCPS SOLARIS is supported in part by Ministry of Science and Higher Education (Poland).

References

1. Owen, R.L., Juanhuix, J. & Fuchs, M. Current advances in synchrotron radiation instrumentation for MX experiments. Arch. Biochem. Biophys. 602, 21-31 (2016).
2. Kozak, M., Rypniewski, W. & Jaskólski, M. Koncepcja budowy linii pomiarowej MX/SAXS/XRD w NCPS SOLARIS. Synchr. Radiat. Nat. Sci. 11, 5-9 (2012).
3. Chinte, U., Shah, B., Chen, Y.-S., Pinkerton, A. A., Schall, C. A. & Hanson B. L. Cryogenic (<20 K) helium cooling mitigates radiation damage to protein crystals. Acta Cryst. D63, 486-492, (2007).
4. Panjikar, S., Thomsen, L., O'Donnell, K.M. & Riboldi-Tunnicliffe, A. A step towards long-wavelength protein crystallography: subjecting protein crystals to a vacuum. J Appl Crystallogr. 48, 913-916 (2015).

Performance of SOLARIS Synchrotron

Keynote Lecture
Thursday 10.09.2020
10:50-11:10

A. I. Wawrzyniak*, A. Curcio, R. Panaś, K. Guła, M. Jaglarz, M. Knafel, G. Kowalski,
A. Marendziak, M. Waniczek, M. Wiśniowski, G. Cioś, M. Madura,
M. Rozwadowski, T. Zbylut, M. Zając, M.J. Stankiewicz

*Solaris National Synchrotron Radiation Centre, Jagiellonian University, Czerwone Maki 98, 30-392
Krakow, Poland*

*e-mail: adriana.wawrzyniak@uj.edu.pl

SOLARIS synchrotron delivers the beam for users since October 2018. The storage ring is operating at an energy of 1.5 GeV in a decay mode with maximum current of 400 mA and total lifetime of 15 h¹. The injection to the storage ring is done twice per day and 22h/day of beam time is declared. Since 2018 high beam availability above 90 % was reached. Currently, 2912 h is dedicated to user operation and about 876 h is devoted to the accelerators' optimization as Solaris synchrotron is under permanent development. In the near future the new insertion device (superconducting wiggler) for hard X-ray beamline is planned to be installed and operational. Therefore the effort on linear and nonlinear optics optimisation with new devices is being done. The new diagnostic beamline (LUMOS) based on the visible light was installed in 2019 and is under commissioning now². It gives the possibility to measure the transversal as well as the longitudinal electron beam parameters. Recently, the longitudinal bunch profile was observed by using streak camera. There are also ongoing work on linear accelerator (linac) development and optimisation. Recently, the effort was put into bunch length measurements and linac optics optimisations, which results in better injection efficiency. During the presentation the current operational status and main parameters of Solaris synchrotron will be given.

References

1. Wawrzyniak, A. I. et al. Solaris a new class of low energy and high brightness light source. Nucl. Instrum. Methods Phys. Res B 411, 4-11 (2017).
2. Kisiel, A., Ptaszkiewicz, M., Cabala, S., Marendziak, A., Wawrzyniak, A. I., Zadworny I. & Zbylut, T. Diagnostic beamlines at the Solaris storage ring. IBIC'19, Malmö, Sweden, TUPP026, 366-368 (2019).

The PEEM/XAS beamline status presented on the magnetic material directed experiments

Oral presentation
Thursday 11.09.2020
11:10-11:40

M. Zając^{1*}, T. Giela¹, K. Freindl², J. Korecki^{2,3}, E. Madej², M. Sikora⁴, N. Spiridis², M. Stankiewicz¹, J. Stępień⁴, J. Szade¹, M. Ślęzak³, T. Ślęzak³, D. Wilgocka-Ślęzak²

¹National Synchrotron Radiation Centre SOLARIS at Jagiellonian University, ul. Czerwone Maki 98, 30-392 Kraków, Poland

²Jerzy Haber Institute of Catalysis and Surface Chemistry, Polish Academy of Sciences, ul. Niezapominajek 8, 30-239 Kraków, Poland

³Faculty of Physics and Applied Computer Science, AGH University of Science and Technology, Al. Mickiewicza 30, 30-059 Kraków, Poland

⁴Academic Centre of Materials and Nanotechnology, AGH University of Science and Technology, Al. Mickiewicza 30, 30-059 Kraków, Poland

*e-mail: mar.zajac@uj.edu.pl

The PEEM/XAS beamline has been optimized for the soft X-ray photon energy range (200-2000 eV) with the bending magnet as a synchrotron radiation source. It is equipped with two end stations: the Elmitec GmbH Photoemission Electron Microscope (SPE PEEM III) and exchangeable separate chamber for X-ray absorption spectroscopy measurements. Both end stations are composed of several vacuum chambers including dedicated chamber for sample preparation and characterization under UHV conditions. During our beamline presentation we will offer description of techniques available at each end stations. Among others the magnetic characterization may be used to study chemical and electronic, structural and magnetic properties by means of X-ray absorption spectroscopy (XAS), X-ray natural linear dichroism (XNLD), X-ray magnetic circular dichroism (XMCD), and X-ray magnetic linear dichroism (XMLD). These methods are suitable for probing element specific properties of surfaces, interfaces, thin films, nanomaterials and examining phenomena in catalysis and magnetism.

Synchrotron based PEEM microscope offers several advantages of contrast creation by utilizing XAS, X-ray Photoemission Spectroscopy (XPS) and XMCD. Both XAS and XPS modes of operation provide exquisite chemical contrast and XMCD is a direct and effective way for the characterization and measurement of magnetic materials.

The XAS end station was successfully used for XMCD and XMLD experiments on multilayers^{1,2} and superconductors.

The presentation will include description of experimental techniques available at both end stations, each illustrated with selected examples from recent measurements. The near future plans of the beamline development will be briefly discussed.

References

1. Ślęzak, M., Ślęzak, T., Drózdź, P., Matlak, B., Matlak, K., Kozioł-Rachwał, A., Zając, M. & Korecki, J. How a ferromagnet drives an antiferromagnet in exchange biased CoO/Fe(110) bilayers. *Sci. Rep* 9, 889 (2019).
2. Kozioł-Rachwał, A., Ślęzak, M., Zając, M., Drózdź, P., Janus, W., Szpytma, M., Nayyef, H., Ślęzak, T. Control of spin orientation in antiferromagnetic NiO by epitaxial strain and spin–flop coupling. *APL Materials* 8, 061107 (2020).

Research potential of UARPES beamline

N. Olszowska^{1*}, M. Rosmus^{1,2}, J.J. Kołodziej²

Oral presentation
Thursday 10.09.2020
11:40-12:00

¹NSRC Solaris, Czerwone Maki 98, 30-392 Kraków, Poland

²Institute of Physics, Jagiellonian University, Łojasiewicza 11, 30-348, Kraków, Poland

*e-mail: natalia.olszowska@uj.edu.pl

Understanding the collective behavior of electrons in solids (many-body interactions) is increasingly important as it give rise to many phenomena studied today in condensed matter physics.

Single electron in space is described by three quantum numbers: energy (E), momentum (k) and spin (S). With many-body interactions at play it is often still possible to retain this description within a so called quasiparticle theory.

Owing to its unique capability to probe the energy and momentum of electrons, angle-resolved photoemission spectroscopy (ARPES) has a leading role in achieving a comprehensive understanding of the electronic properties of solid state materials today. The knowledge about the band structures, i.e. $E(\mathbf{k})$ relations in solids, accessible with ARPES, is nowadays extensively employed for tailoring of functional materials and heterostructures for quantum-, opto-, spin- and magneto- electronic devices. UARPES beamline has been designed for studying fine effects in band structures of solids including topological insulators, superconductors and other strongly correlated systems, Dirac-type systems, Rashba-type systems, graphene and similar 2D materials, semiconductor and metal surfaces, Weyl metals, thin films and quantum well systems, solids containing charge and spin density waves and others. The beamline provides to users efficient ultra-high resolution angle-resolved photoelectron spectroscopy with the 8-150 eV photon energy and soft x-ray photoelectron spectroscopy with up to 600 eV photon energy. A source of photons for the beamline is quasiperiodic elliptically polarizing undulator (EPU) Apple II type, allowing for a full control over the photon beam polarization. The undulator radiation is monochromatized with Plane Grating Monochromator (PGM) or Normal Incidence Monochromator (NIM) which are available in range 12-600 eV and 8-20 eV, respectively. The heart of the end station is a hemispherical electron spectrometer VG SCIENTA DA-30L which can natively measure the 3D photocurrent map $I(\phi, \theta, E)$ which is then converted to $E(\mathbf{k})$ relation. Its angular resolution is 0.1° and the energy resolution is 1.8meV. Sample temperature can be stabilized in the range 7-500 K. Attached preparation chamber allows for samples preparation *in situ* and diagnostics of samples surface structure (available techniques: LEED, AES, RGA, QCM). The preparation chamber is also prepared for quick and easy installation of user devices such as effusion cells or vacuum suitcases.

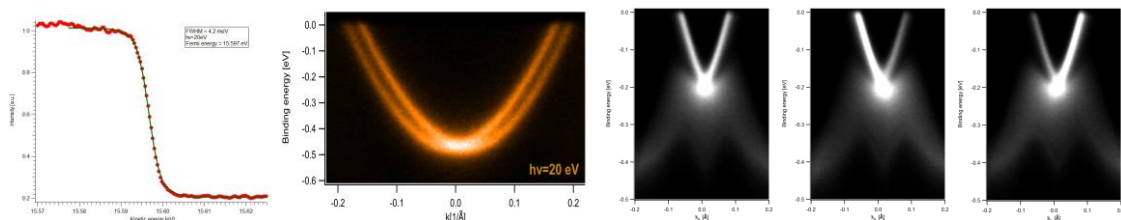


Fig. 1. The Fermi step at 8 K on polycrystalline gold and fitted a convolution of the Fermi distribution and the Gaussian (a); Rashba spin split Au(111) surface band (b); illustration of the photoemission circular dichroism effect on Be_2Te_3 - data for: horizontal (c), left (d) and right (e) circular polarization of the photon beam.

Some of the first experimental results from SOLARIS: resolving the spin structure of antiferromagnets at XAS/PEEM beamline

Oral presentation
Thursday 11.09.2020
12:10-12:20

M. Ślęzak^{1*}, M. Zając², P. Drózdź¹, K. Matlak^{1,2}, W. Janus¹, M. Szpytma¹,
A. Koziół-Rachwał¹, J. Korecki^{1,3}, T. O. Menteş⁴, F. Genuzio⁴, A. Locatelli⁴,
T. Ślęzak¹

¹AGH University of Science and Technology, Faculty of Physics and Applied Computer Science, Kraków, Poland

²National Synchrotron Radiation Centre SOLARIS, Jagiellonian University, Kraków, Poland

³Jerzy Haber Institute of Catalysis and Surface Chemistry PAS, Kraków, Poland

⁴Elettra - Sincrotrone Trieste, Basovizza, Trieste, Italy

*e-mail: mislezak@agh.edu.pl

While engineering of magnetic anisotropy (MA) in ferromagnets (FM) has been so far intensively studied, the control of antiferromagnets (AFM) is only nowadays in the focus of attention of the magnetism community. The aim of AFM spintronics is to complement or replace ferromagnets as the active components of spintronic devices. Magnetic control of AFM spins orientation includes either the application of a strong external magnetic field or, when AFM is exchange-coupled to a neighboring FM, its magnetic state can be controlled by relatively small external magnetic field.

Our X-ray magnetic linear and circular dichroism (XMLD and XMCD) measurements performed at the XAS end-station in Polish synchrotron SOLARIS enabled us to follow the magnetic properties of epitaxial CoO(111)/Fe(110)¹ and NiO(111)/Fe(110)² bilayers. In case of NiO/Fe bilayers our results were additionally complemented by micro-spectroscopic and spectro-microscopic studies performed in the spectroscopic photoemission and low energy electron microscope (SPELEEM) which is the end-station of the Nanospectroscopy beamline in Elettra synchrotron (Trieste, Italy).

We find that in both studied cases FM sublayer plays a dominant role and determines the magnetic state of the neighboring AFM, however completely different interaction mechanisms are involved. In CoO/Fe bilayers the AFM spins are totally frozen although their orientation is imprinted by magnetization of Fe layer when the system passes the Neel temperature of CoO. Once the Fe layer grafts the particular MA into the CoO overlayer, it later remains frozen and insensitive to external factors like external magnetic field or Fe magnetization direction¹. In contrast, for NiO/Fe bilayers we find that due to the weak intrinsic MA of NiO, the NiO spins are rotatable and always follow the reorientation of Fe magnetization that can be controlled by external magnetic field or via the temperature and thickness driven spin reorientation of Fe(110). In the case of the temperature induced spin reorientation transition in Fe(110), it allowed us to implement all-temperature, field-free switching of AFM moments in NiO/Fe bilayers².

References

1. Ślęzak, M., Ślęzak, T., Drózdź, P., Matlak, B., Matlak, K., Koziół-Rachwał, A., Zając, M. & Korecki, J. How a ferromagnet drives an antiferromagnet in exchange biased CoO/Fe(110) bilayers. *Scientific Reports* 9, 889 (2019).
2. Ślęzak, M., Drózdź, P., Janus, W., Nayyef, H., Koziół-Rachwał, A., Szpytma, M., Zając, M., Menteş, T. O., Genuzio, F., Locatelli, A. & Ślęzak, T. Fine tuning of ferromagnet/antiferromagnet interface magnetic anisotropy for field-free switching of antiferromagnetic spins. *Nanoscale* (accepted).

Synchrotron infrared spectroscopy and imaging: Opportunities, and new challenges

Keynote Lecture
Thursday 10.09.2020
13:15-13:45

P. Dumas^{1,2}

¹SOLEIL Synchrotron, L'Orme des Merisiers, 91191 Gif Sur Yvette- France

²CEA, DAM, DIF, Arpajon, France

*e-mail: paul.dumas@synchrotron-soleil.fr

The infrared emission from synchrotron radiation was long regarded with little interest until one realizes that the brightness of such source has enormous potential for application in spectroscopy and microscopy. Over the last twenty years, the exploitation of the emission of infrared photons has led to the implementation of dedicated beamlines in the majority of synchrotron facilities worldwide. The most recent example is SOLARIS and will be introduced during this meeting. The conditions for collecting the largest possible number of photons will be briefly introduced during my talk : sources of infrared emission in bending magnets, adapted optics for large source sizes..

The superior brightness of the synchrotron source has been exploited in the far- and mid- infrared region, more specifically in microscopy, with spatial resolution at the diffraction limit¹. Works in Biology, earth and space science, chemistry, archaeology/cultural heritage and solid state physics have provided a large number of publications , and few of them will be presented. Nevertheless, the demand for sub wavelength spatial resolution has markedly increased during the recent years. The first step forward was achieved using focal plane array detectors : the resolution could reach sub- micron range, using Point Spread Function deconvolution with a synchrotron infrared beam filling the area of the FPA detector. Infrared tomography is becoming an attractive add-on to beamline and this will be discussed within the context of the new infrared beamline at SOLARIS.

Nanometers resolution is, presently, the most exciting development of synchrotron IR. By combining the synchrotron beam with AFM detection, spectra and chemical images can be obtained with less than 20 to 40 nm of resolution.

The future of infrared synchrotron is bright with these recent developments , especially with the advent of complementary laser sources.

References

1. Dumas, P., Martin, M. C. & Carr G. L. IR spectroscopy and spectromicroscopy with synchrotron radiation in *Synchrotron Light Sources and Free-Electron Lasers* (eds. Jaeschke E., Khan S., Schneider J., Hastings J.) 2059-2113 (Springer, Cham, 2020).

Solaris Advanced InfraRed (SOLAIR) beamline capabilities

Keynote Lecture
Thursday 10.09.2020
13:45-14:00

T. P. Wróbel^{1*}, D. Liberda¹, A. I. Wawrzyniak¹, A. Marendziak¹, P. Nowak¹,
M. Zając¹, K. Małek², W. M. Kwiatek³, P. Dumas⁴, M. Stankiewicz¹

¹Solaris National Synchrotron Radiation Centre, Jagiellonian University, Czerwone Maki 98, 30-392 Krakow, Poland

²Faculty of Chemistry, Jagiellonian University in Krakow, Gronostajowa 2, 30-387 Krakow, Poland

³Institute of Nuclear Physics Polish Academy of Sciences, PL-31342, Krakow, Poland.

⁴SMIS beamline, SOLEIL synchrotron, L'orme des Merisiers, Gifsur Yvette, France

*e-mail: tomek.wrobel@uj.edu.pl

The Solaris Advanced InfraRed beamline (SOLAIR) is currently under construction. The large radiation extraction from a bending magnet will allow to collect a very wide wavelength range (0.4 - 500 μm), covering from the near (NIR) to the far (FIR) infrared spectral range. The extraction of infrared radiation from synchrotron radiation will be done using, first, a flat and slotted mirror (M1), which will be located inside the dipole chamber located at the bending magnet in storage ring. Figure 1 shows the distribution of infrared radiation intensity for two wavelengths: 10 μm (1000 cm^{-1}) and 200 μm (50 cm^{-1}) after M1.

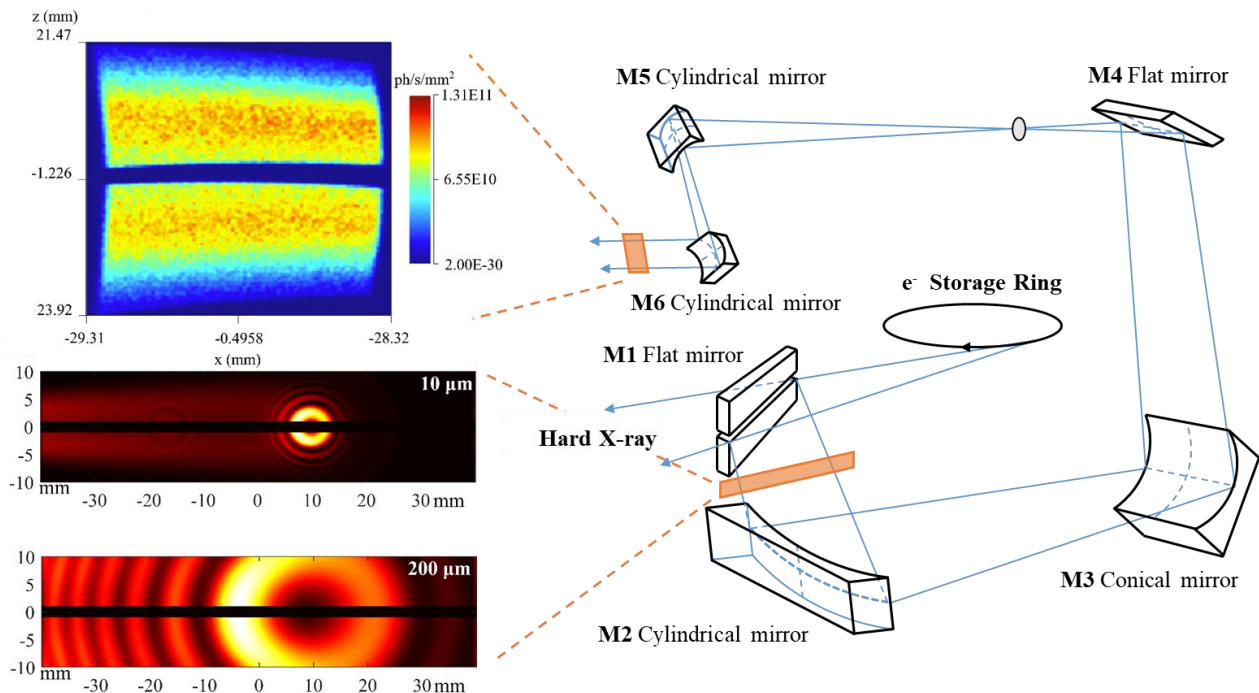


Fig. 1 Diagram of the optical system of M1 to M6 mirrors for the extraction of infrared radiation in the Solaris synchrotron with beam cross-sections behind the M1 mirror and after the M6 mirror.

The presentation will showcase the current status of the project along with the expected IR beam parameters. It will also highlight microscopic techniques planned to be used at the beamline with potential applications.

PHELIX beamline

Keynote Lecture
Thursday 10.09.2020
14:00-14:15

M. Szczepanik-Ciba^{1*}, T. Sobol^{1,2}, J. Szade^{1,2}

¹ National Synchrotron Radiation Centre SOLARIS in Kraków, Poland

² University of Silesia in Katowice, Poland

*e-mail: magdalena.szczepanik-ciba@uj.edu.pl

A recently constructed PHELIX beamline¹ at SOLARIS synchrotron² covers a soft X-ray energy range of radiation. It is designed to perform many kinds of complementary spectroscopic measurements under ultra-high vacuum conditions not only *ex situ* but also *in situ*, offering variety of preparation possibilities. All beamline and end-station components were customized and built from the ground up for those particular purposes. The source of the radiation is the elliptically polarizing undulator (EPU) giving variable polarization and exceptionally bright light in comparison to conventional X-ray sources. The available photon energy range is 50-1500 eV which is suitable for research on vast majority of materials used in state of the art electronic devices³, modern catalysts⁴ or fuel cells⁵. The design of the beamline and high quality optical elements ensure high radiation intensity transmission to the analysis chamber. The end-station provides not only the opportunity to measure resonant photoemission, circular-dichroic spectra or X-ray absorption spectra with total fluorescence and total electron yield modes but, most of all, to map band structures in three dimensional k-space with angle-resolved photoelectron spectra and to obtain direct 3D spin texture information. Performing measurements of this sort for one sample prepared in the same UHV system is very beneficial in terms of the high quality of the surface being a requirement for obtaining valuable results.

Acknowledgements: The PHELIX beamline was constructed grace to the funds of the Polish Ministry of Science and Higher Education under the decision no. 6582/IA/SP/2016. Authors are grateful the companies involved in the PHELIX beamline project (PREVAC, FMB, KYMA) for very good co-operation. The commitment of the SOLARIS staff in the construction of the beamline is highly appreciated.

References

1. Szczepanik-Ciba, M., Sobol, T. & Szade, J. PHELIX - a new soft X-ray spectroscopy beamline at SOLARIS synchrotron. Nucl. Instruments Methods Phys. Res. Sect. B Beam Interact. with Mater. Atoms (2020), submitted.
2. Wawrzyniak, A. I. et al. Performance of Solaris Storage Ring. IPAC 2017, Copenhagen 1–5 (2017).
3. Lv, B., Qian, T. & Ding, H. Angle-resolved photoemission spectroscopy and its application to topological materials. Nat. Rev. Phys. 1, 609–626 (2019).
4. Pereira-Hernández, X. I. et al. Tuning Pt-CeO₂ interactions by high-temperature vapor-phase synthesis for improved reducibility of lattice oxygen. Nat. Commun. 10 (2019).
5. Saveleva, V. A. et al. Operando Near Ambient Pressure XPS (NAP-XPS) Study of the Pt Electrochemical Oxidation in H₂O and H₂O/O₂ Ambients. J. Phys. Chem. C 120, 15930–15940 (2016).

PolyX beamline

Oral presentation
Thursday 10.09.2020
14:15-14:30

P. Korecki^{1,2*}, P. Wróbel³, T. Kołodziej², K.M. Sowa¹

¹*Institute of Physics, Jagiellonian University, Kraków, Poland*

²*National Synchrotron Radiation Centre SOLARIS, Jagiellonian University, Kraków, Poland*

³*Faculty of Physics and Applied Computer Science, AGH-University of Science and Technology, Kraków, Poland*

*e-mail: pawel.korecki@uj.edu.pl

PolyX will be a bending magnet beamline for multimodal X-ray microimaging, microspectroscopy and general/test purposes in the hard X-ray energy range of 4 keV – 16 keV. Commissioning of PolyX is planned in mid-2022. The name PolyX comes from structured polycapillary optics that will be used as focusing devices and from polychromatic X-rays that will be used to increase the X-ray flux.

PolyX is designed as a relatively short beamline with length <20 m and will be operated in three different modes: (i) white/pink beam, (ii) high flux mode using a double multilayer monochromator with bandwidth of 2–3 % and (iii) high energy mode with a Si(111) double crystal monochromator. Depending on the operation mode, PolyX, will deliver a collimated beam with a flux from 10⁹ to 10¹² photons/s/mm². Polycapillary optical elements with transmissions from 2-20% will enable to produce focused beams with sizes from 5 μm to 50 μm. In future, a compact KB mirror system is planned for generation of a sub-micron beam.

Main experimental techniques will be μXRF, μXAFS, μXRD and μCT. Setups for angle resolved spectroscopy with TXRF, TXRF-XANES, GI-XRF, GI-XANES are also planned. A special experimental area will be designed for non-standard user experiments. Experiments at PolyX will take benefit from recently developed X-ray imaging¹ and spectroscopic² setups. PolyX will be equipped with quad-SDD energy resolving detectors, hybrid-pixel detector(s), scintillator based X-ray camera, ionization chambers and photodiodes.

In this talk, we will describe the parameters, layout and present status of PolyX construction, as well as describe potential applications of PolyX in physics, chemistry, biology, material science, geoscience and cultural heritage.

Acknowledgements: Authors would like to thank the whole SOLARIS team for work on PolyX. Jakub Szlachetko is acknowledged for many consultations on the beamline project.

References

1. Sowa, K. M., Kujda, M.P. & Korecki, P. Plenoptic X-ray microscopy, *Applied Physics Letters* 116, 014103 (2020).
2. Błachucki, W., Czapla-Masztafiak, J., Sá, J. & Szlachetko, J. A laboratory-based double X-ray spectrometer for simultaneous X-ray emission and X-ray absorption studies. *Journal of Analytical Atomic Spectrometry* 34, 1409-1415 (2019).

SOLABS (XAS-HN): A new SOLARIS beamline for X-ray spectroscopy at low photon energies

Oral presentation
Thursday 10.09.2020
14:30-14:45

H. Lichtenberg^{1*}, J. Hormes^{2,3}, W. Klysubun⁴, J. Göttert¹, A. Maximenko⁵,
K. Morris³, P. Nita⁵, A. Prange¹, J. Szade⁵, L. Wagner¹, M. Zając⁵

¹Hochschule Niederrhein University of Applied Sciences, Krefeld, German

²Institute of Physics, Rheinische Friedrich-Wilhelms-University, Bonn, Germany

³Center for Advanced Microstructures and Devices, Louisiana State University, Baton Rouge, USA

⁴Synchrotron Light Research Institute, Nakhon Ratchasima, Thailand

⁵National Synchrotron Radiation Centre SOLARIS, Jagiellonian University, Kraków, Poland

*e-mail: henning.lichtenberg@hs-niederrhein.de

SOLABS (XAS-HN), a new EXAFS/XANES beamline at NSRC SOLARIS, results from an international collaboration of Niederrhein University of Applied Sciences (Germany), the Synchrotron Light Research Institute (Thailand), Bonn University (Germany) and SOLARIS (Poland). The front end section was installed and commissioned in April-May 2020. Beamline commissioning will take place in spring 2021.

The desired energy range ($\sim 1 - 13$ keV) will be covered by a high vacuum double crystal monochromator (DCM) with 3 sets of crystals (KAP[100] + multilayer, InSb[111] and Ge[220]) which can be changed in less than an hour. In order to minimize absorption of low energy photons the beamline is windowless down to the DCM. A differential ion pump maintains the pressure difference between the storage ring and the DCM, and a thin foil window separates the DCM vacuum from ionization chambers downstream. The straight-forward design of the beamline without additional optical elements and radiation safety hutches, its compact overall dimensions and the easy to handle DCM make SOLABS especially user friendly and attractive for challenging measurements in the low energy X-ray range, i.e. at the K-edges of elements such as P, S, Si, Al and Mg, which are highly relevant for both functional materials and e.g. biological systems, while also covering absorption edges of heavier elements (up to Se K-, Bi L3-, U M-edges). The SOLABS beamline opens tremendous opportunities for both basic and industrial research at SOLARIS.

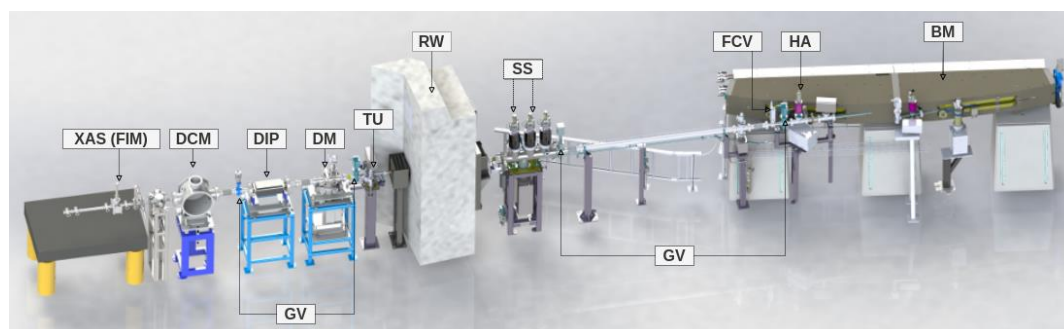


Fig. 1 SOLABS beamline: bending magnet (BM), heat absorber (HA), gate valves (GV), safety shutters (SS), ratchet wall (RW), fast closing valve (FCV) with trigger unit (TU), diagnostic module (DM), differential ion pump (DIP), double crystal monochromator (DCM), ionization chambers and fluorescence detector (XAS (FIM)).

Acknowledgements: The authors would like to thank the Bundesministerium für Bildung und Forschung (03IHS084) and the EU Horizon2020 program (952148-Sylinda) for supporting this project.

BL04ID: a new soft X-ray beamline dedicated for X-ray microscopy at SOLARIS synchrotron

Oral presentation
Thursday 10.09.2020
14:45-15:00

K. Matlak^{1*}, T. Giela¹, A. Mandziak¹, B. Wolanin¹, J. Szade^{1,2}, T. Tyliczszak^{1,3}

¹*SOLARIS National Synchrotron Radiation Centre, Jagiellonian University, Poland.*

²*University of Silesia in Katowice, Poland.*

³*Lawrence Berkeley National Laboratory, USA.*

*e-mail: krzysztof.matlak@uj.edu.pl

The new BL04ID beamline designed at SOLARIS is a classic Plane Grating Monochromator (PGM) design with an Elliptically Polarizing Undulator (EPU) as a high photon flux source ($>10^{12}$ ph/s/0.01%bw). It works in a 100-2000 eV photon energy range, with fully controllable polarization. The beamline can achieve high energy resolution ($E/\Delta E = 3000-15000$) and therefore it is suitable to perform advanced soft X-ray microscopy for materials science, environmental, biological research, etc.

The beamline is made up of two branches and three end stations. The first branch consists of a refurbished Octupole end station and X-ray Photoemission Electron Microscope (X-PEEM) with spatial resolution below 20 nm. This branch is dedicated especially to study of magnetic, chemical, and structural surface and near surface properties under UHV conditions.

The third end station, Scanning Transmission X-ray Microscope (STXM), is placed at the end of the second branch of the beamline. It is a modern microscope designed and built at SOLARIS and allows for chemical analysis with a resolution about 20 nm, limited by available zone plates. A ptychography option with sophisticated cameras will improve a spatial resolution to below 5 nm. This branch is intended to research on chemical and structural properties, in samples which can transmit soft X-ray radiation. The microscope will be equipped with an environmental cell, where samples can be measured in different atmospheres under the pressure from 10^{-7} mbar up to 1100 mbar, variable temperature, or in liquids with full electrochemical control.

The availability of two microscopic methods within the same beamline will allow users to choose the appropriate approach to study their specific case in terms of sample environment, spectroscopy methods, probing depth, etc.

In this presentation, we show the characteristics and features of the beamline and its experimental stations. The current status of their commissioning is reported. Additionally, an overview of the STXM microscope operation modes is briefly presented. Finally, possible research applications are demonstrated, based on results obtained so far by similar facilities.

SOLARIS and MAX IV: A unique example of international collaboration.

Keynote Lecture
Friday 11.09.2020
09:30-10:00

N. Mårtensson*

Department of Physics and Astronomy, Uppsala University Box 516, SE-751 20 Uppsala, Sweden

*e-mail: nils.martensson@physics.uu.se

The Swedish synchrotron radiation laboratory MAX-lab was established in 1986. The first storage ring was a 0.55 GeV facility (MAX I) which a decade later was followed by the 1.5 GeV MAX II facility, one of the first 3rd generation storage rings in the world. The success of MAX-lab was based on innovative accelerator design and the presence of a very strong, national and international, user community.

Already at the end of the 1990s, planning started for a possible next step in the development of the laboratory. This turned into the very ambitious MAX IV project¹. A small 0.7 GeV storage ring (MAX III) was built, which could host a few low energy beamlines. However, MAX III was also built as a test facility for some of the novel design concepts which were the basis for MAX IV. The final MAX IV proposal consisted of two storage rings, a 3 GeV storage ring for harder X-rays and a 1.5 GeV ring for soft X-rays. The 3 GeV ring was the first multibend achromat storage ring to be built¹, taking an important step towards the construction of a diffraction limited storage ring². The reason for building also a 1.5 GeV ring was the very strong spectroscopy community at MAX-lab.

A very interesting opportunity opened up in connection with the MAX IV project. The European Union had provided funding for a storage ring in Krakow, Poland. Due to the limited experience in the field of accelerator physics in Krakow, MAX-lab was contacted in order to find out if MAX-lab could assist in this process. This developed into a very fruitful collaboration between MAX-lab and the Jagiellonian University. A solution developed where the SOLARIS facility in Krakow, should be built as an identical twin to the MAX IV 1.5 GeV storage ring³. Personnel from SOLARIS directly joined the accelerator team at MAX-lab and took part in the design of the new accelerators. SOLARIS team members were also participating in the early commissioning of the MAX IV facility with focus on the LINAC and the 3 GeV ring. Meanwhile, the SOLARIS 1.5 GeV ring was starting up in Krakow. The SOLARIS ring started up in a successful way and the experience from this commissioning was very beneficial for the following start-up of the MAX IV 1.5 GeV ring.

References

1. Martensson, N. & Eriksson, M. The saga of MAX IV, the first multi-bend achromat synchrotron light source. Nucl. Instrum. Methods Phys. Res. A 907, 97-104 (2018).
2. Eriksson, M., van der Veen, J.F. & Quitmann, C. J. Diffraction-limited storage rings - a window to the science of tomorrow. Synchrotron Rad. 21, 837-842 (2014).
3. Wawrzyniak, A.I., Marendziak, A., Kisiel, A., Borowiec, P., Nietubyc, R., Wiechecki, J., Karas, K., Szamota-Leandersson, K., Zajac, M., Bocchetta, C. J. & Stankiewicz, M.J. Solaris a new class of low energy and high brightness light source. Nucl. Instrum. Methods Phys. Res. B 411, 4-11 (2017).

X-ray photoelectron study of polymers surface after modification by extreme ultraviolet radiation

Keynote Lecture
Friday 11.09.2020
10:00-10:30

K. Lawniczak-Jablonska*

Institute of Physics, Polish Academy of Sciences, Al. Lotnikow 32/46, 02-668 Warsaw, Poland

*e-mail: jablo@ifpan.edu.pl

Processes occurring at the interface between the living organism and the lifeless synthetic product determine the success of the medical procedure performed for implants or other medical devices. Controlling and enhancing the biocompatibility of biomaterials remains a challenge in medicine and biomedical engineering. Therefore, scientific effort is focused on effective techniques to modify surface of biomaterials to increase biocompatibility. Preferably, these techniques should change the properties of the surface without affecting the mechanical properties of the bulk material. Conventional techniques, based on photochemical and photophysical processes induced by UV radiation may have undesired effects related to deep penetration of this radiation in polymers¹.

Extreme ultraviolet (EUV) radiation is of particular interest to the modification of biomaterials due to extremely short absorption lengths that limits the modification of their physical and chemical properties to the top layer only. An efficient source of EUV radiation is laser plasma produced as a result of the interaction of nanosecond laser pulses with matter^{2,3}. The ideal tool to analyse the chemical composition of the surface after EUV- modification is X-ray photoelectron spectroscopy (XPS) as well using laboratory as synchrotron source of radiation. The results of XPS investigations of the modified with EUV radiation three polymers: poly (tetrafluoroethylene) (PTFE), poly(vinylidene fluoride) (PVDF) and poly-L-(lactic acid) (PLLA) will be presented as an example of biomaterials study. These polymers were selected due to their wide application in biomedical engineering⁴. Each of three polymers was modified in five variants: gas-free modification, modification in the presence of oxygen, in two time variants (200 and 400 ms) and modification in the presence of nitrogen, with the same time variants. The control sample without modification was also studied. The goal of the performed investigation was to determine the change of chemical composition and other physicochemical properties (morphology, wettability) of the modified polymer surfaces and to correlate the effect of EUV modification with the number and morphology of surface-adhered endothelial cells.

The C, O and where relevant F 1s orbitals were measured for each variant of modification. The content and the chemical binding of elements was estimated and analysed. In Figure 1 the example of C 1s line for control PVDF polymer and after 50 pulses of EUV is presented. PVDF is made from $-\text{[CH}_2\text{-CF}_2\text{]}-$ monomers and two peaks related to C 1s binding with H and F are well separated in control polymer (Fig. 1a). Analysis of the C 1s spectra shows the degradation of the carbon-fluorine bonds (decrease in the number of $-\text{CF}_2-$ bonds) and formation of C-C bonds after heating with 50 pulses of EUV (Fig. b).

The influence of different variants of modification process on the elemental and chemical state of polymers surface will be presented and discussed and finally correlated with process of endothelial cells adhesion. The benefits of using the X-ray spectroscopy to understand the biocompatibility of materials will be highlighted.



Fig. 1 C 1s orbital in unmodified PVDF polymer (a) and after 50 pulses of EUV irradiation (b).

Acknowledgements: This work was part of Adam Lech master thesis supervised by Dr Beata Butruk-Raszeja from Department of Biotechnology and Bioprocess Engineering, Warsaw University of Technology.

References

1. Bäuerle, D. Laser Chemical Processing in Laser Processing and Chemistry (Springer, 2011).
2. Fiedorowicz, H., Bartnik, A., Jarocki, R., Kostecki, J., Krzywiński, J., Mikołajczyk, J., Rakowski, R., Szczurek, A. & Szczurek, M. J. Alloys Compd. 401, 99-103 (2005).
3. Bartnik, A., Fiedorowicz, H., Jarocki, R., Kostecki, J., Szczurek, A. & Szczurek, M. Applied Physics B: Lasers and Optics 96, 727 (2009).
4. Suzuki, S. & Ikada, Y. Polymers for Surgery in Advanced Polymers in Medicine (Ed. Francesco, P) 219–264 (Springer, 2015).

The status and scope of SOLARIS within the European landscape of CERIC-ERIC

Oral Presentation
Friday 11.09.2020
10:00-10:20

C. Rizzuto *

CERIC-ERIC

*e-mail: carlo.rizzuto@ceric-eric.eu

We will briefly present the European approach to build an integrated Research Area capable to compete at world level with all major federal Nations (e.g. China and USA) and, within this, to build an integrated and effective capability of Research Infrastructures (RIs) supporting the whole research community.

CERIC-ERIC is an important player in this context, with its specific scope to close the gap between East and West (as well as between south and North) of the European Area.

A very basic approach is that of Open Access, allowing the use of RIs by all European researchers on an equal footing based solely on quality of the proposed projects. This approach recognizes the reciprocal contributions of users and facilities towards an ever-growing quality and success of research.

CERIC-ERIC has been set-up in the field of RIs dedicated to analysis and synthesis of materials and biomaterials with the aim of overcoming a number of gaps: the gap between different techniques and probes used in material sciences (e.g. photons, neutrons, electrons...), and the gap in the availability of these facilities in smaller Countries and in some parts of Europe.

The basic principle is that of putting together the investments and availability of different RIs, developing joint research projects and allowing, through a single access and international evaluation, the use of complementary techniques to solve the problem of integrated study of materials.

Each Country participating in CERIC has provided a set of techniques and participates in joint projects, while CERIC provides the international independent peer review to stimulate each Government to invest according to the best possible results and to attract the best researchers at world level to stimulate the best exchange of ideas and training.

The participating Countries, and the techniques and fields of research available through CERIC will be briefly presented outlining the role of Poland and Solaris (with its more recent Cryo-EM development), and the opportunities for the Polish Research community to have a free access to a world leading set of facilities.

Observation of the reduction of Ce⁴⁺ to Ce³⁺ in Ce_{0.7}Yb_{0.2}Pd_{0.1}O_{2-δ} catalyst

Oral Presentation
Friday 11.09.2020
11:10-11:30

E. Piskorska-Hommel*, M. J. Winiarski, M. Kurnatowska

*Institute of Low Temperature and Structure Research, Polish Academy of Sciences,
W. Trzebiatowski Institute, Wrocław, Poland*

*e-mail: e.piskorska@intibs.pl

The presence of Pd and Yb dopants in the CeO₂ lattice strongly inhibits the crystal growth of the mixed oxide in elevated temperatures in the reducing ambience¹. The effect of Pd/Yb doping on the CeO₂ properties has been extensively studied in mixed oxide catalysts^{2,3}. The addition of the noble metal to the CeO₂ structure can strongly change its activity and selectivity. Moreover, cerium can be present in a different reduced state in the catalysts. The oxidation state of cerium in such catalysts during the redox reaction has been not studied in detail. Therefore, to study of the cerium ions reduction process in the doubly doped ceria Ce_{0.7}Yb_{0.2}Pd_{0.1}O_{2-δ} lattice *in situ* X-ray absorption near edge structure (XANES) method was applied.

The doubly doped nanocrystalline mixed oxides Ce_{0.7}Yb_{0.2}Pd_{0.1}O_{2-δ} were synthesized with the reversed microemulsion method¹. The nanocrystallites with size 3-5 nm crystallize in fluorite-type. H₂-TPR studies revealed in these catalyst strong hydrogen consumption at low temperatures without significant changes in their structure.

Ce L₃ XANES spectra were collected for the Ce_{0.7}Yb_{0.2}Pd_{0.1}O_{2-δ} catalyst during the reduction conditions, and reference CeO₂ (Ce⁴⁺) and CeAlO₃ (Ce³⁺) samples over the energy range 5.60- 5.9 keV in transmission mode at SAMBA beamline at Soleil synchrotron facility, France.

It was found that the reduction of Ce⁴⁺ to Ce³⁺ starts before the reduction of the noble metal. The redox activity temperature range of Ce in doubly doped ceria is significantly lower than reported by other authors. The explanation of this behavior can be the presence of the oxygen vacancies inherent in the Ce_{0.7}Yb_{0.2}Pd_{0.1}O_{2-δ} sample, which can release the reduction process at the lower temperature.

Acknowledgements: The authors acknowledge the Synchrotron SOLEIL for provision of synchrotron radiation facilities. We would like to thank dr. Andrea Zittolo for assistance in using beamline SAMBA and dr. Emiliano Fonda for the providing of the reference Ce L₃ XANES spectra of CeO₂ and CeAlO₃. This work was financially supported by the National Science Center in Poland (grant 2015/19/D/ST5/00722), supported by the Foundation for Polish Science.

References

1. Kurnatowska, M., Piskorska-Hommel, E., Kraszkiewicz, P. & Winiarski, M. J. *Mat. Chem. Phys.* 229, 49–55 (2019).
2. Kurnatowska, M., Mista, W., Mazur, P. & Kepinski, L. *Appl. Catal. B Environ.* 148, 123–135 (2014).
3. E. Piskorska-Hommel, D. A. Kowalska, P. Kraszkiewicz, M. Kurnatowska, *J. Alloys Compd.* 831, 154703 (2020).

Scanning photoelectron microscopy study of local electronic structure of *p*-type ZnO films doped with nitrogen

Oral Presentation
Friday 11.09.2020
11:30-11:50

E. Guzewicz^{1*}, O. Volnianska¹, I.N. Demchenko², P. Zeller³, M. Amati³,
L. Gregoratti³

¹Institute of Physics, Polish Academy of Sciences, Al. Lotnikow 32/46, PL-02668 Warsaw, Poland

²Dept. Chemistry, University of Warsaw, Pasteura 1, 02-093 Warsaw, Poland

³Elettra – Sincrotrone Trieste S.C.p.A., Trieste, Italy

*e-mail: guzel@ifpan.edu.pl

The problem with *p*-type doping is the main obstacle in application of ZnO in optoelectronics. Our recent CL investigations revealed that *p*-type conductivity might have a complicated microscopic origin, because we found out that the donor-related and the acceptor-related luminescence are placed in different and clearly separated regions¹. This motivated the present scanning photoelectron microscopy (SPEM) study, which was conducted at the Elettra synchrotron facility in Trieste, Italy. The SPEM enables to probe the electronic structure at a submicron scale and thus to obtain the photoemission spectroscopy signal from a single column of growth (Fig. 1a). This unique experiment revealed two types of columns showing different PES spectra in the valence band region.

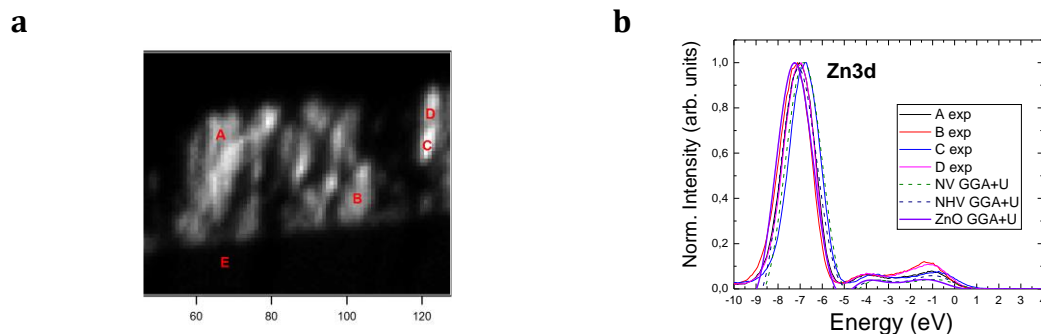


Fig. 1 (a) The SPEM image of the cross-section of $\sim 2\mu\text{m}$ thick ZnO:N film, (b) Comparison of PES spectra (at A, B, C and D points) with calculated density of $d(\text{Zn})$ states x-axis corresponds to the energy relative to the VBM of pure ZnO).

In order to explain differences in the PES spectra, Density Functional Theory calculations using QUANTUM-ESPRESSO code² have been performed. The Hubbard-like term +U describing the on-site Coulomb interactions³ was applied on the $d(\text{Zn})$ and $p(\text{O})$ orbitals. It has been confirmed that hydrogen forms stable complexes with V_{Zn} and $V_{\text{Zn}}\text{-N}_\text{O}$ which can be the origin of *p*-conductivity in grains of ZnO:N. Theoretical calculations indicate that such complex formation might be the origin of differences in the density of states in the valence band region. These results for the first time demonstrate valence band electronic band structure in different grains across the ZnO:N film.

Acknowledgements. The work was supported by the research project No. 2018/31/B/ST3/03576 founded by the National Science Centre (Poland) and by Elettra Sincrotrone Trieste (proposal ID 20180152-Elettra). Calculations were done in ICM UW (grant G16-11).

References

1. E. Guzewicz, E. Przewdziecka, et al., ACS Appl. Mat. Int. **9**, 26143-26150 (2017).
2. P. Giannozzi et al.: *J. Phys.: Condens. Matter.* **21**, 395502 (2009).
3. M. Cococcioni and S. de Gironcoli: *Phys. Rev. B*, **71**, 035105 (2005).

Spectroscopic insight into properties of nanostructured magnetic oxides

Oral Presentation
 Friday 11.09.2020
 11:50-12:10

K. Pitala^{1,2*}, J.M. Ablett³, J. Kuciakowski^{1,2}, K. Maćkosz^{1,2}, K. Kollbek¹, J. Pawlak^{1,2},
 A. Żywczak¹, M. Sikora¹

¹AGH, University of Science and Technology, Academic Centre for Materials and Nanotechnology, Al. Mickiewicza 30, 30-059 Cracow, Poland

²AGH, University of Science and Technology, Faculty of Physics and Applied Computer Science, Al. Mickiewicza 30, 30-059 Cracow, Poland

³Synchrotron SOLEIL, Gif-Sur-Yvette Cedex, France

*e-mail: pitala@agh.edu.pl

Magnetic nanostructures show a high potential for application in fields of spintronics and biotechnology. In order to obtain the best performing devices, the understanding and control of the changes induced into material's properties are required. Influence on the magnetic properties of nanostructured films is mostly exerted by changing the size, dimensionality, symmetry and interface effects. However, ion etching processes involved in preparation of nanostructures may introduce substantial changes into ionic properties of metal oxide surface^{1,2}. We have employed bulk sensitive spectroscopy to shed more light on this problem. We explored local structure and electronic configuration of iron in different types of nanoscale oxides, putting emphasis on how nanostructuring processes affect structural and electronic properties of magnetic oxide films.

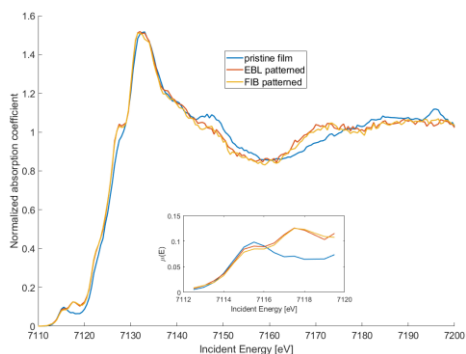


Fig. 1 Fe K-edge HERFD-XAS of pristine magnetite film and nanostructures fabricated using EBL and FIB..

We have studied a set of thin film samples of iron and manganese oxides. The epitaxial layers were grown by means of PLD and nanostructured by means of EBL combined with Ar ion etching and using Ga⁺ FIB. Varied shapes of structures were prepared in order to disentangle the effects of magnetocrystalline and shape anisotropy. Nanocomposites were obtained by magnetron sputtering by adjusting different deposition conditions. Electronic stability and local structure around metal sites was probed using HERFD-XAS³ (Fig. 1). Site selective magnetic response was

determined using RIXS-MCD^{4,5}. Both methods probe K pre-edge structures, which are fingerprints of crystal field symmetry and formal valence of metal ions⁵. They allow to characterize selectively the volume of nanostructures with negligible background counts. Results were analyzed in comparison to soft X-ray XAS and XMCD.

Acknowledgements: Authors would like to thank G. Szwachta for preparation of pristine magnetite samples.

References

1. Hashimoto S. Damage of Metallic Oxides Appeared in XPS Spectral Change after Ion Bombardment. 表面科学 25, 198-204 (2004).
2. de Groot, F., Vankó, G. & Glatzel, P. The 1s x-ray absorption pre-edge structures in transition metal oxides. J. Phys.: Condens. Matter 21 (2009).
3. Sikora, M., Juhin, A. & Weng, T. Strong K-edge Magnetic Circular Dichroism Observed in Photon-in-Photon-out Spectroscopy. Phys. Rev. Lett. 105, 037202 (2010).
4. Ablett, J.M. & Juhin, A., oral presentation during SOLEIL Users' Meeting 2015 (2015).

Poster Session - Thursday 10th September, 15:20-16:30		
Title	Speaker	Page
Crystallization of supercooled liquid metals - X-ray diffraction studies at synchrotron and FEL sources	Jerzy Antonowicz	36
Structural studies of sulfur-containing multicomponent silicate-phosphate glasses	Anna Berezicka	37
CERIC-ERIC the multi-technique research infrastructure for materials research in Central-Eastern Europe	Dariusz Jan Brzosko	38
Comparative study of the luminescence of Ca ₇ ZrAl ₆ O ₁₈ :Eu ceramics under excitation by OPO laser and synchrotron radiation	Dominika Madej	39
The geometry of bioactive Cu(II) complexes determined by XAS and UV-Vis spectroscopies	Aleksandra Drzewiecka-Antonik	40
Ternary Pt/Re/SnO ₂ /C catalyst as a system with outstanding electrocatalytic activity and durability in ethanol oxidation reaction (EOR)	Elżbieta Drzymała	41
Two types of monoclinic deformations of corundum-type trigonal crystal structures of M ₂ O ₃ metal oxides	Piotr Fabrykiewicz	42
Liquid jet sample delivery system for lab-based X-ray spectroscopy and experiments at X-ray free electron lasers	Rafał Fanselow	43
The Photon and Neutron Open Science Cloud for FAIR data	A. Götz	44
VUV photofragmentation of the six-membered heterocyclic molecules containing oxygen	Michał Jurkowski	45
Spectroscopic studies of Nb-doped tricalcium phosphate glass-ceramics prepared by sol-gel method	Wojciech Korzeniewski	46
Correlation of magnetic properties with the electronic structure for magnetocaloric compounds of Mn _{1.1} Fe _{0.9} P _{1-x} (As,Si) _x system	Jerzy Kubacki	47
Superoxide dismutase activity in cyanobacteria grown under different light conditions	Monika Kula-Maximenko	48
Controlled Deposition and Separation of Mn ²⁺ -stearate Single-Molecule Magnets on Surfaces	Magdalena Laskowska & Oleksandr Pastukh	49
Novel nanocomposites: magnetic nanocrystals inside porous silica matrices	Łukasz Laskowski & Andrii Fedorchuk	50
SOLAIR beamline design and example of possible research applications	Danuta Liberda	51

Synchrotron Radiation in Natural Science **20** (2020)

In situ and ex situ structural studies of Fe-doped lithium-manganese oxides for lithium-ion cells	Agnieszka Malinowska	52
Helium recovery and liquefaction system in NCPS SOLARIS	Alexey Maximenko	53
Powder X-ray diffraction study of Cd _{1-x} MnxTe solid solution	Roman Minikayev	54
The emitter evolution universalized model at the cathodic arc	Anatoliy Nedolya	55
fs-XES unravels details of electron dynamics in the Fe-Co assembly	Michał Nowakowski	56
Resonance photoemission study of selected rear earth ions dopants in semiconductor compounds	Bronislaw Orłowski	57
Structure refinement for (Cd,Zn) ₃ As ₂	Wojciech Paszkowicz	58
X-ray diffraction study of mechanochemical synthesis process of Pb _{1-x} CdxTe	Wojciech Paszkowicz	59
Dependence of the degree of tetragonal deformation of the lithium-manganese spinel structure on nonhydrostatic pressure component: Synchrotron powder diffraction study	Paweł Piszora	60
X-ray diffraction study of structure and thermal expansion of Ca ₁₀ M _{0.5} (VO ₄) ₇ (M = Co, Cu)	Houri Sadat Rahimi Mosafer	61
ExPaNDS project	Kat Roarty	62
Direct evidence of uneven dxz and dyz orbital occupation in the superconducting state of iron pnictide	Damian Rybicki	63
Crystallization of glasses with PEEM	Franziska Scheffler	64
AS studies of vanadium oxide thin films	Krystyna Schneider	65-66
XAS studies of RE (RE=Sm, Gd and Dy) doped Bi ₇ REFe ₄ Ti ₃ O ₂₄ compounds	Krystyna Schneider	67-68
Selective magnetometry of nanoparticles in solutions	Marcin Sikora	69
The selected physico-chemical properties and structural studies of two peroxidomolybdates	Adrianna Sławińska	70
Electronic structure investigations of some cresols	Małgorzata Śmiałek-Telega	71
Analysis of physico-chemical properties of nanolayers modified with low-energy Xe ions	Regina Stachura	72
Examination of prospective chemotherapeutics with the use of the X-ray Absorption Spectroscopy	Wiktoria Stańczyk	73
A XAS study of Na _{0.5} Bi _{0.5} TiO ₃ ferroelectric single crystal	Tomasz Straczek	74-75
Spectroscopic studies on sulfur speciation in soil active glasses	Justyna Sułowska	76

An XANES Investigation of the Electronic Structure of ZnO Films implanted by Yb	Yevgen Syryanyy	77
A XAS study of ALD fabricated Fe oxide films	Aleksandra Szkudlarek	78-79
Development of methods and instrumentation for applied X-ray research	Jakub Szlachetko	80
Synchrotron studies on double perovskite cobaltites	Iga Szpunar	81
Revisiting properties of $\text{CaCoSi}_n\text{O}_{2n+2}$. Magnetism and electronic structure.	Magdalena Szubka	82
ARPES studies of transition metal / topological crystalline insulator interface	Bartłomiej Turowski	83
One- and two-photon below threshold cross-sections mechanisms and atomic number and energy dependences	Krzysztof Tyrała	84
Sequence of structural phase transitions in $\text{Pr}_{0.9}\text{Ca}_{0.1}\text{AlO}_{2.95}$	Leonid Vasylechko	85
In situ observation of metal-to-semiconductor transition by high-resolution X-ray spectroscopy techniques	Anna Wach	86
Electronic Properties of Multi-Layer of Graphene Oxide Moderately Annealed in Vacuum obtained using compact laser-plasma based NEXAFS system	Przemysław Wachulak	87
Anisotropy in the Fermi surface of Non-Magnetic semimetal TaAs_2	Ashutosh Wadge	88
Dissociative photo-double-ionization of the isoxazole molecules	Tomasz Wasowicz	89
Tracking changes in electronic structure in real-time during temperature-induced oxidation of titanium	Klaudia Wojtaszek	90
Structural studies of selected PrP peptides – interactions of mutated octarepeat with zinc ions	Joanna Wolak	91
X-ray absorption fine structure study on bioactive Cu(II) complex with thiourea derivative in organic solvents	Anna Wolska	92
Insight into precursor effects in selected superconducting stannides	Paweł Zajdel	93
Interactions between amyloid-beta peptides, human serum albumin and human cystatin C studied by the use of X-ray and light scattering, NMR spectroscopy and bioinformatics	Adriana Żyła	94

Crystallization of supercooled liquid metals - X-ray diffraction studies at synchrotron and FEL sources

Poster Presentation
Thursday 10.09.2020
15:20-16:30

J. Antonowicz^{1*}, P. Zalden², K. Sokołowski-Tinten³, R. Sobierajski⁴

¹ Faculty of Physics, Warsaw University of Technology, Poland

² European XFEL, Germany

³ Faculty of Physics and Center for Nanointegration Duisburg-Essen (CENIDE), University of Duisburg-Essen, Germany

⁴ Institute of Physics Polish Academy of Sciences, Poland

*e-mail: jerzy.antonowicz@pw.edu.pl

Metallic liquids are known to crystallize immediately when cooled below their equilibrium melting point. In particular, the high temperature, sub-melting point crystallization of molten metals remains far too fast to be probed by conventional experimental methods. Here, we propose an experimental approach based on ultrashort pulsed laser annealing to study crystallization of thin metallic films. The essential feature of the approach is ultrafast heating (10^{14} K/s) by femtosecond optical excitation followed by extremely rapid cooling (10^{11} K/s) due to heat dissipation into the film substrate (Fig. 1). We employ X-ray diffraction using synchrotron light to probe crystallization of binary Pd-Si glass-forming alloy which can be configurationally frozen in the partially crystalline state and studied *ex-situ*. To follow an extremely rapid crystallization kinetics of pure, supercooled liquid Pd *in-situ*, during the quench, we apply X-ray free electron laser pulses and pump-probe technique. The proposed technique enables to quantify crystal growth rates reaching 100 m/s.

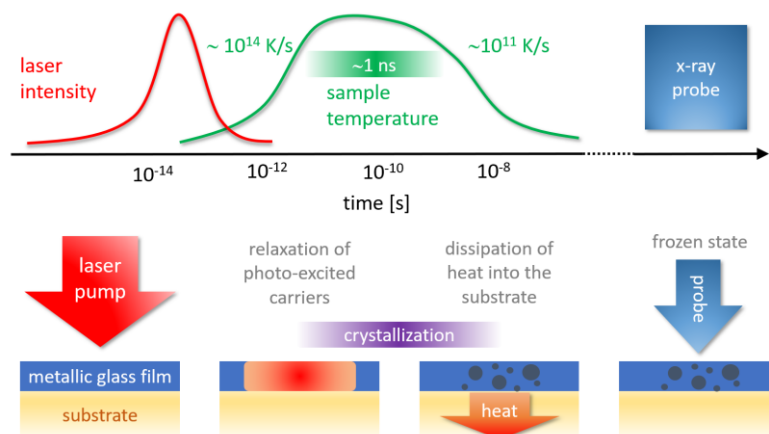


Fig. 1 Schematic concept of an ultrashort pulsed laser annealing approach for resolving crystallization kinetics of a thin film metallic glass using X-ray diffraction at a synchrotron. The cycle is repeated N times to compare the initial state (separate probe event, not indicated in the figure) with that probed after the N cycles.

Acknowledgements: This work was supported by National Science Centre, Poland, grant agreements N° 2017/27/B/ST3/02860 and 2018/02/X/ST3/00197.

Structural studies of sulfur-containing multicomponent silicate-phosphate glasses

Poster Presentation
Thursday 10.09.2020
15:20-16:30

A. Berezicka*, J. Sułowska, M. Szumera

AGH University of Science and Technology, Faculty of Material Science and Ceramics, al.
Mickiewicza 30, 30-059, Cracow, Poland

*e-mail: berezicka@agh.edu.pl

The form and behavior of sulfur in oxide glasses is of interest to multiple research fields, ranging from commercial glass manufacture to radioactive waste vitrification and geology¹. A special type of materials are the bioactive materials, which are able to participate in biological processes of living organisms. Glassy fertilizers from SiO₂-P₂O₅-K₂O-MgO-SO₃ system belong to this group.

The amorphous state of glasses was followed by an X-Ray Diffraction analysis and their chemical composition was verified by an X-Ray Fluorescence technique. In order to control changes in their structure as a result of adding SO₃ to their composition, they were examined using the MIR and Raman spectroscopy techniques.

On this basis, it was shown that obtaining fully amorphous material in the tested system is possible with a maximum SO₃ content of 2 mol%.

Spectroscopic examinations revealed high level of similarity between obtained spectra as regards vibrational modes of silico-oxygen and phospho-oxygen subnetworks. At the same time, presence of all Raman-active spectra for SO₄²⁻ (sulfate) anions was demonstrated for glasses with sulfur content higher than 1 mol% (ν_1 (ν_{as}) at ~ 980 cm⁻¹, ν_2 (δ_s) at ~ 450 cm⁻¹, ν_3 (ν_{as}) at ~ 1080 cm⁻¹ and ν_4 (δ_{as}) at ~ 620 cm⁻¹), with positions of the bands corresponding to those of crystalline sulfate^{2,3}. Obtained results may suggest that sulfur is present in vitreous matrix as isolated tetrahedra, charge-compensated by K⁺ ions, rather than being integrated into silicate-phosphate network.

Acknowledgements: This project was financed by the National Science Centre, Poland, project number 2018/31/D/ST8/03148.

References

1. Vaishnav, S. et al. Neutron Diffraction and Raman Studies of the Incorporation of Sulfate in Silicate Glasses. *J. Phys. Chem. C* 124, 5409-5424 (2020).
2. Bingham, P. A. et al. Modeling the sulfate capacity of simulated radioactive waste borosilicate glasses. *J. Alloys Compd.* 695, 656-667 (2017).
3. Ben Mabrouk, K., Kauffmann, T. H. et al. Raman study of cation effect on sulfate vibration modes in solid state and in aqueous solutions. *J Raman Spectrosc* 44, 1603-1608 (Wiley 2013).

CERIC-ERIC the multi-technique research infrastructure for materials research in Central-Eastern Europe

Poster Presentation
Thursday 10.09.2020
15:20-16:30

D. J. Brzosko*

CERIC-ERIC

*e-mail: dariusz.brzosko@ceric-eric.eu

The scientific problems coming up in this fields have become more and more complex in the recent years and require an ever increasing number of instrumental and analytical techniques and disciplines. Such complexity requires the availability of expertise as well as open access to a wide range of probing techniques and many different complementary instruments. The CERIC-ERIC research infrastructure was developed to face this challenge and to make a wide variety of instruments available through open access.

CERIC stands for Central European Research Infrastructure Consortium and is a distributed research infrastructure unifying several national institutions, under one roof¹. This multinational facility was set up as a European Research Infrastructure Consortium (ERIC). It brings together research facilities from Austria, Croatia, Czech Republic, Hungary, Italy, Poland, Romania, Serbia and Slovenia (Fig 1). Statutory seat is in Trieste, Italy. All partners offer a set of complementary, cutting-edge instrumentation from national institutes for free and open access to excellent researchers all over the world.



Fig. 1 Locations and partners of CERIC-ERIC.

CERIC-ERIC comprises synchrotron radiation, neutron radiation, microscopic techniques, ion-beam analysis methods and NMR. All instruments are available for open access through one single entry point. The selection of proposals and experiment time is done in a peer-review process and based on scientific excellence only. Following the nature of CERIC as a multi-probe facility, the open access operation allows to ask not only one instrument per proposal but to get experiment time granted for several complementary instruments with one proposal.

Comparative study of the luminescence of $\text{Ca}_7\text{ZrAl}_6\text{O}_{18}:\text{Eu}$ ceramics under excitation by OPO laser and synchrotron radiation

Poster Presentation
Thursday 10.09.2020
15:20-16:30

D. Madej*

AGH University of Science and Technology, Faculty of Materials Science and Ceramics, Department of Ceramics and Refractories, al. A. Mickiewicza 30, 30-059 Krakow, Poland

*e-mail: dmadej@agh.edu.pl

Calcium zirconium aluminates is important cement material, which has been studied in recent years. But the use of $\text{Ca}_7\text{ZrAl}_6\text{O}_{18}$ as the luminescent host, up to now, is not reported. Hence, rare earth, Europium (Eu) doped calcium zirconium aluminate, ($\text{Ca}_7\text{ZrAl}_6\text{O}_{18}:\text{Eu}$) was synthesized by the traditional ceramic route. The structural and micro-structural properties of luminescent ceramics were characterized by XRD and SEM-EDS techniques. This work focuses on the comparative study of the luminescence of $\text{Ca}_7\text{ZrAl}_6\text{O}_{18}:\text{Eu}$ ceramics under excitation by OPO laser and synchrotron radiation (planned research).

The room-temperature emission spectra of the Eu-doped $\text{Ca}_7\text{ZrAl}_6\text{O}_{18}$ under different nm excitation are shown in Fig. 1.

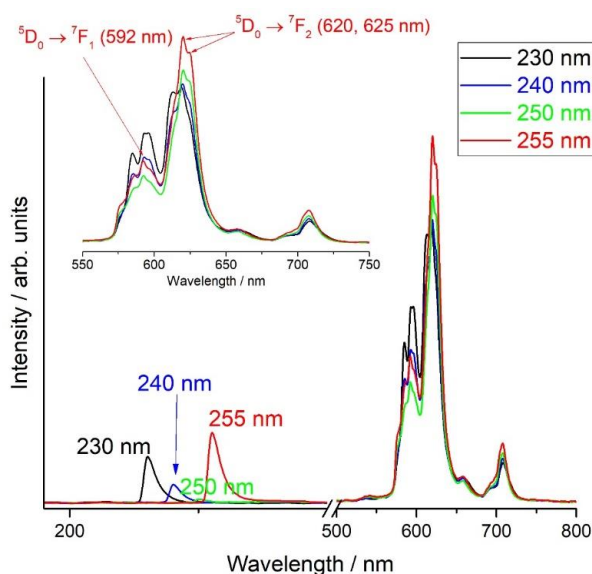


Fig. 1 Luminescence spectra of Eu in as-synthesized $\text{Ca}_7\text{ZrAl}_6\text{O}_{18}:\text{Eu}$ vs. pump wavelength [unpublished preliminary results].

The characteristic emissions of trivalent europium ions Eu^{3+} were clearly observed including the strongest emission peaks at 592 nm for $^5\text{D}_0 \rightarrow ^7\text{F}_1$ spin-allowed transition of Eu^{3+} ion. The emission peak at 617 is due to “spin-forbidden” electric dipole transition arising from the low symmetry position of the Eu^{3+} ion with an inversion centre. The emission peak at ca. 625 nm is also due to the $^5\text{D}_0 \rightarrow ^7\text{F}_2$ transition.

Acknowledgements: This project was financed by the National Science Centre, Poland, project numbers of 2017/26/D/ST8/00012 and 490774.

The geometry of bioactive Cu(II) complexes determined by XAS and UV-Vis spectroscopies

Poster Presentation
Thursday 10.09.2020
15:20-16:30

A. Drzewiecka-Antonik*, P. Rejmak, M. T. Klepka, A. Wolska

¹Institute of Physics, Polish Academy of Sciences, al.Lotników 32/46, 02-668 Warsaw, Poland

*e-mail: adrzew@ifpan.edu.pl

The series of Cu(II) complexes have been synthesized by the reaction of the copper(II) chloride with 1,3-disubstituted thioureas (Figure 1). In each case the complexes, Cu1-Cu9, have an overall neutral charge with two monoanionic ligands. The thioureas coordinate to the copper cation in bidentate fashion via deprotonated N and S atoms according to the ATR-IR and EXAFS spectroscopies. In such four-coordinate complexes the metal cation is a part of two four-membered rings (Cu-S-C-N) which is quite unusual for that element.

UV-Vis studies with molecular modelling have shown that both distorted square planar as well as pseudo-tetrahedral geometries are characteristic for presented complexes. A square planar coordination around Cu(II) is preferred for centrosymmetric complexes with trans arrangements of chelating atoms (two S and two deprotonated N atoms) around the cation. The noncentrosymmetric complexes with *cis-N2S2* arrangement adopted the pseudo-tetrahedral geometry.

Two thiourea complexes, Cu1 and Cu3, with pseudo-tetrahedral geometry have shown significant activity to cancer cell lines SW480 (primary colon cancer) and PC3 (metastatic prostate cancer), being more selective than doxorubicin and cisplatin used as references¹.

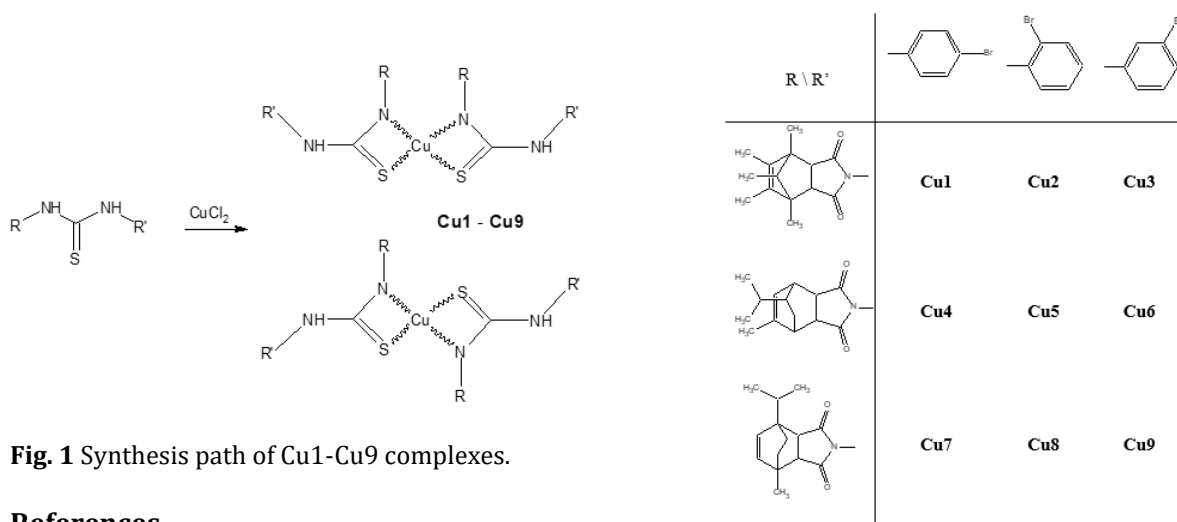


Fig. 1 Synthesis path of Cu1-Cu9 complexes.

References

1. Drzewiecka-Antonik, A., Rejmak, P., Klepka, M.T., Wolska, A., Chrznowska, A. & Struga, M. J. Inorg. Biochem. – under review.

Ternary Pt/Re/SnO₂/C catalyst as a system with outstanding electrocatalytic activity and durability in ethanol oxidation reaction (EOR)

Poster Presentation
Thursday 10.09.2020
15:20-16:30

E. Drzymala*, M. Parlinska-Wojtan

Institute of Nuclear Physics, Polish Academy of Science, 31-342 Kraków, Poland

*e-mail: elzbieta.drzymala@ifj.edu.pl

Currently, the issues related to the production, storage and growing demand for electricity, drives the search for new methods of its production. It is a key topic not only for the quality of human life, but also for the further development of civilization. Fuel cells, especially those using liquid fuels, such as ethanol became a promising and a more and more popular solution of this problem. Unfortunately, in most cases during electrochemical reaction many by-products lowering the efficiency of the device are generated¹. Therefore, the key challenge is to design and develop the appropriate type of catalysts, which could reduce the amounts of unwanted byproducts.

In our work, using intermolecular interactions and electrokinetic potential measurements, we synthesized a ternary Pt/Re/SnO₂/C catalyst for ethanol oxidation reaction (EOR)². The electrostatic interactions between the nanoparticles, building the final ternary nanocatalyst, led to their successful assembly and allowed to create physical contact places between the individual components (Pt, Re and SnO₂ NPs), so important in increasing the performance of the EOR. In our study using the cyclic voltammetry techniques, we demonstrated that the Pt/Re/SnO₂/C catalyst shows over ten times higher activity in the EOR compared to the commercially available platinum catalyst³. Moreover, the value of the onset potential of the EOR for ternary Pt/Re/SnO₂/C catalyst is almost 0.3 V lower compared to the commercially available Pt catalyst, indicating that the reaction starts definitely earlier. Finally, we also showed that the ternary catalyst is characterized by a high stability – after the performed stability tests the catalyst retained 96 % of its electrochemical surface area³.

The synthesized catalysts were studied by scanning transmission electron microscopy (STEM) combined with energy dispersive X-ray spectroscopy (EDS), XPS and cyclic voltammetry (CV) techniques. Investigation of the three component material, characterized already in detail by other techniques, by X-ray absorption spectroscopy methods could provide information explaining their good catalytic properties for EOR. Many catalytic materials change their structures during the electrocatalytic reaction. The restructuring can be induced by both physical and chemical conditions. According to the literature the structures formed under the reaction conditions are responsible for the observed catalytic properties. In this regard, X-ray absorption spectroscopy (XAS) is particularly powerful, as the X-ray absorption near edge structure (XANES) can reveal the oxidation state of the element of interest, and extended X-ray absorption fine structure (EXAFS) is capable of probing the influence from the local coordination environment⁴. Therefore, by utilizing X-ray absorption spectroscopy we would like to investigate the local structure and oxidation state of metal atoms in the catalyst before and after electrochemical tests. Also as plans for the future, we would like to develop and provide in-situ XAS measurements in order to understand the evolution of unique structural motifs in the catalyst under working conditions.

References

1. Yang, G., Namin, L. M., Deskins, N. A. & Teng, X. J. *Catal.* 353, 335–348 (2017).
2. Drzymala E., Gruzal, G., Pajor-Świerzy, A., Depciuch, J., Socha, R., Kowal, A., Warszyński, P. & Parlinska-Wojtan M. J. *Nanoparticle Res.* 20, 144 (2018).
3. Drzymala, E., Gruzal, G., Depciuch, J., Pawlyta, M., Donten, M., Parlinska-Wojtan, M. *Nano Res.* 13, 832–842 (2020).
4. Wenig, Z., Wu, Y., Wang, M. et al. *Nat. Commun.* 9, 1–9(2018).

Two types of monoclinic deformations of corundum-type trigonal crystal structures of M₂O₃ metal oxides

Poster Presentation
Thursday 10.09.2020
15:20-16:30

P. Fabrykiewicz^{1*}, R. Przeniosło¹, I. Sosnowska¹, F. Fauth²

¹Faculty of Physics, University of Warsaw, Pasteura 5, 02-093 Warsaw, Poland

²CELLS-ALBA, BP1413, 08290 Cerdanyola del Vallès, Barcelona, Spain

*e-mail: Piotr.Fabrykiewicz@fuw.edu.pl

Earlier synchrotron radiation powder diffraction (ID-22@ESRF) studies^{1,2} showed that the crystal structure of α -Fe₂O₃ and Cr₂O₃ usually described with the corundum-type trigonal crystal structure (space group R-3c) should be described using the monoclinic space group C2/c. This is connected with the α -Fe₂O₃ and Cr₂O₃ magnetic structures which are incompatible with the threefold rotation axis², however this deformation in α -Fe₂O₃ is present both below and above Néel temperature³.

In this presentation⁴ α -Fe₂O₃ and Cr₂O₃ as well as non-magnetic Ti₂O₃, V₂O₃, Al₂O₃ corundum-type oxides⁵ are studied by synchrotron radiation powder diffraction (MSPD@ALBA-CELLS). The observed angular dependence of the integral breadths is described by two models: (i) the distorted corundum-type structure model described by the space group C2/c and (ii) the Stephens model⁶ of anisotropic Bragg peak broadening. These two models are shown to be equivalent⁴. Examined oxides fall into one of two categories⁴. Ti₂O₃, V₂O₃ and Cr₂O₃ show a 'positive' distortion⁴ which is related to the possible metal-metal bond suggested by Goodenough^{7,8} (the deformation leads to shorter metal-metal distances) whereas Al₂O₃ and α -Fe₂O₃ show a 'negative' distortion⁴ which leads to relatively longer metal-metal distances.

Acknowledgements: We thank Grzegorz Kaproń and Sławomir Ilnicki (Faculty of Geology, University of Warsaw) for help with X-ray diffraction measurements. We thank ALBA-CELLS for provision of beamtime and we thank the Ministry of Science (Poland) for funding.

References

1. Przeniosło, R., Sosnowska, I., Stękiel, M., Wardecki, D. & Fitch, A. Monoclinic deformation of the crystal lattice of hematite α -Fe₂O₃. *Physica B* 449, 72–76 (2014).
2. Stękiel, M., Przeniosło, R., Sosnowska, I., Fitch, A., Jasiński, J., Lussier, J. & Bieringer, M. Lack of a threefold rotation axis in α -Fe₂O₃ and α -Cr₂O₃ crystals. *Acta Cryst.* B71, 203–208 (2015).
3. Fabrykiewicz, P., Stękiel, M., Sosnowska, I. & Przeniosło, R. Deformations of the α -Fe₂O₃ rhombohedral lattice across the Néel temperature. *Acta Cryst.* B73, 27–32 (2017).
4. Fabrykiewicz, P., Przeniosło, R., Sosnowska, I. & Fauth, F. Positive and negative monoclinic deformation of corundum-type trigonal crystal structures of M₂O₃ metal oxides. *Acta Cryst.* B74, 660–672 (2018).
5. Prewitt, C., Shannon, R., Rogers, D. & Sleight, A. C rare earth oxide-corundum transition and crystal chemistry of oxides having the corundum structure. *Inorg. Chem.* 8, 1985–1993 (1969).
6. Stephens, P. Phenomenological model of anisotropic peak broadening in powder diffraction. *J. Appl. Cryst.* 32, 281–289 (1999).
7. Goodenough, J. *Magnetism and the Chemical Bond*. (John Wiley and Sons, 1963).
8. Goodenough, J. Transition-metal oxides with metallic conductivity. *Bull. Soc. Chim. Fr.* 4, 1200–1205 (1965).

Liquid jet sample delivery system for lab-based X-ray spectroscopy and experiments at X-ray free electron lasers

Poster Presentation
Thursday 10.09.2020
15:20-16:30

R. Faselow^{1,2}, W. Błachucki¹, A. Wach¹, J. Czapla-Masztafiak¹, W. M. Kwiatek¹, J. Szlachetko^{1,*}.

¹ Institute of Nuclear Physics, Polish Academy of Sciences, 31-342 Kraków, Poland.

² Faculty of Chemistry, Jagiellonian University, Gronostajowa 2, 30-387 Kraków, Poland.

*e-mail: jakub.szlachetko@ifj.edu.pl

This work reports a newly developed sample delivery system for X-ray spectroscopy analysis of materials in liquid environment. Proposed approach provides also characterization of specimen to be analyzed in its native conditions without its time-consuming preparation procedure.

The built prototype sample delivery system is capable of forming a liquid jet of thickness ranging from 0.5 mm to 3 mm. Micro gear pump was used to ensure constant flow of the fluid in a closed circuit which reduces the amount of sample necessary for the measurement and allows long-time operation of the system. The jet system was tested at the Institute of Nuclear Physics PAN using lab-based X-ray spectrometer¹. A suspension of zinc oxide (ZnO) nanoparticles in distilled water was used as a sample which was injected to the system. The X-ray absorption spectroscopy (XAS) was used to collect the Zn K-edge spectra in transmission mode. Zn K-edge XAS spectra were acquired for different Zn concentrations. The obtained spectra were of high quality, comparable to the ones achieved using synchrotron source and allowed determination of optimal jet thickness for a given Zn concentration.

The presented setup will be used for in-situ X-ray study on various nanomaterial suspensions by means of the available laboratory X-ray spectroscopy setups as well as in time-resolved experiments at X-ray free electron lasers.

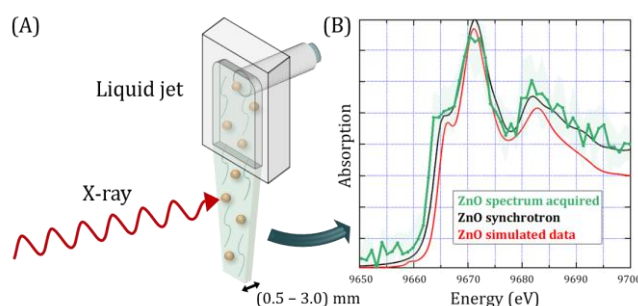


Fig. 1. (A) Schematic representation of the liquid jet formation. (B) Comparison between the acquired Zn K-edge XAS spectrum with synchrotron-measured and simulated data².

Acknowledgements: This work was supported by the National Science Centre (Poland) under grant numbers 2016/21/D/ST4/00378, 2019/03/X/ST3/00035 and 2017/27/B/ST2/01890.

References

1. Błachucki, W., Czapla-Masztafiak, J., Sá, J. & Szlachetko, J. A laboratory-based double X-ray spectrometer for simultaneous X-ray emission and X-ray absorption studies. *J. Anal. At. Spectrom.* 34, 1409–1415 (2019).
2. Penfold, T. J. *et al.* Revealing hole trapping in zinc oxide nanoparticles by time-resolved X-ray spectroscopy. *Nat. Commun.* 9, 1–9 (2018).

The Photon and Neutron Open Science Cloud for FAIR data

A. Götz^{1*}, D. Roccella²

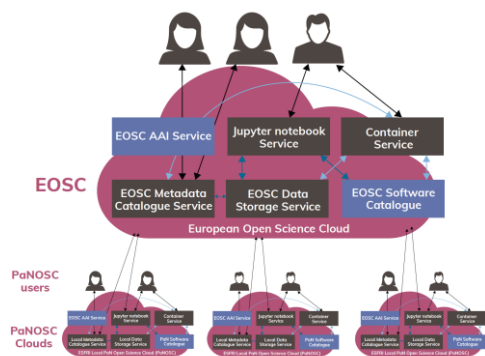
Poster Presentation
Thursday 10.09.2020
15:20-16:30

¹The European Synchrotron, ESRF

²Central European Research Infrastructure Consortium, CERIC-ERIC

*e-mail: andy.gotz@esrf.fr

The Photon and Neutron Open Science Cloud (PaNOSC) is a cluster which proposes to align the efforts of the existing and new photon and neutron sources to link up to the EOSC (European Open Science Cloud). Photon and Neutron (PaN) sources produce petabytes of scientific data that in order to be available to everyone, have to comply with the principles of being Findable, Accessible, Interoperable and Reproducible (FAIR). At the same time, scientific publishing has been evolving to make scientific data part of publications. The presentation will introduce the PaNOSC project (<https://www.panosc.eu>), aimed at providing scientific data management tools, policies and services for enabling FAIR and Open Science in 6 Photon and Neutron research facilities: ESRF, ILL, European XFEL, ELI, ESS and CERIC-ERIC, with its partner facility SOLARIS, in collaboration with the e-infrastructures EGI and GÉANT. The outputs of PaNOSC will benefit the whole community of researchers using photon and neutron sources.



PaNOSC objectives include:

- Full FAIR compliance of PaN scientific data;
- Innovative data service services at RIs and as part of the EOSC;
- Support in shaping EOSC services for users needs;
- Sharing best practices for open data policies;
- Increase RIs' impact by encouraging data reuse;
- Collaboration with EOSC projects to share outcomes.

Fig. 1 EOSC + PaNOSC Clouds

In addition to presenting the benefits that the PaNOSC project will bring for the scientific community, the talk will give an overview of the updated FAIR Data Policy framework for research data, developed in collaboration with most of the PaN sources in Europe and its implementation in CERIC. Special emphasis will be put in the collection of feedback from the community.

Having an open access data policy with data in well-defined formats has many benefits:

- It makes previously measured data available for further analysis without having to repeat the experiment.
- It promotes data use, cross-disciplinary research and machine learning.
- Raw data becomes open to scrutiny by other researchers, ensuring scientific integrity and experiments' reproducibility.
- Scientists can mine data in previously unknown ways or reapply new methods to existing data.

References

1. Götz, A.; Perrin, J.-F.; Fangohr, H.; Salvat, D.; Gliksohn, F.; Markvardsen, A.; McBirnie, A.; Gonzalez-Beltran, A.; Taylor, J.; Matthews, B., *PaNOSC Research Data Policy Framework* (Zenodo, 2020).
2. Götz, A., *PaNOSC position paper on the EOSC* (Zenodo, 2020).

VUV photofragmentation of the six-membered heterocyclic molecules containing oxygen

Poster Presentation
Thursday 10.09.2020
15:20-16:30

M. Jurkowski¹, A. Kivimäki^{2,3}, R. Richter⁴, T. J. Wasowicz^{1*}

¹Department of Physics of Electronic Phenomena, Gdansk University of Technology,
ul. G. Narutowicza 11/12, 80-233 Gdansk, Poland

²Nano and Molecular Systems Research Unit, University of Oulu, 90014 Oulu, Finland

³MAX IV Laboratory, Lund University, 22100 Lund, Sweden

⁴Elettra-Sincrotrone Trieste, 34149 Trieste, Italy

*e-mail: tomasz.wasowicz1@pg.edu.pl

Cancer is a significant public health concern worldwide, which results in millions of deaths each year. The standard cure routine for cancer is surgery, and nowadays, radiotherapy or a hadrontherapy. Depending on the type of cancer, patients may undergo additional treatment, including targeted therapy. A combination of radio- or hadron-therapy with proper drug treatment can inhibit the proliferation of cancer cells and thus can significantly improve survival rates. This is because the interaction of radiation on those drugs can lead to their fragmentation, which additionally increases the number of reactive species that interact with the adjacent medium. For example, anthracyclines, a class of drugs build on tetrahydropyran ring, are broad-spectrum antitumor agents that induce, among other things, indirect damage to DNA via reactions involving reactive oxygen species.

It is, therefore, vital to understand how different types of ionizing radiation produce damage to the biologically active compounds. Valuable details on these molecular mechanisms may be obtained by investigating the mechanisms of the excitation, relaxation, and fragmentation of the structural units of these substances or their prototypes. The heterocyclic molecules containing oxygen atoms (e.g., 3,4-dihydro-2H-pyran (C₅H₈O) and tetrahydro-2H-pyran (C₅H₁₀O)) are of particular relevance to studies of the radiation damage due to the fact, that they are the structural units of the biologically active substances that play a significant role not only in medicine but also in many different fields of chemistry and biology. C₅H₈O has a non-aromatic ring with five carbon atoms and one oxygen atom. It contains one double bond. By removing the double bond by two more hydrogen atoms, we get a saturated six-membered ring of tetrahydro-2H-pyran. We believe that the small change in the bond rearrangement may provide access to new chemically reactive entities with potentially interesting properties. Thus, in the present communication, we present results on the photoionization and fragmentation of C₅H₈O and C₅H₁₀O molecules. The experiments were carried out at the GasPhase beamline at the Elettra-Sincrotrone radiation facility exploiting the VUV excitation and the ion time-of-flight spectrometry. Numerous well-resolved cations were identified in the mass spectra of both molecules. Possible ionic fragmentation channels yielding particular ions will be discussed.

Acknowledgements: We are grateful to the Elettra-Sincrotrone Trieste for providing beamtime no. 20190430. The research leading to this result has been supported by the project CALIPSOplus under Grant Agreement 730872 from the EU Framework Programme for Research and Innovation HORIZON 2020.

Spectroscopic studies of Nb-doped tricalcium phosphate glass-ceramics prepared by sol-gel method

Poster Presentation
Thursday 10.09.2020
15:20-16:30

W. Korzeniewski^{1*}, A. Witkowska¹, M. Manecki²

¹Department of Solid State Physics, Gdansk University of Technology,
Gabriela Narutowicza 11/12, 80-233 Gdańsk, Poland

²Department of Mineralogy, Petrography and Geochemistry, AGH University of Science and
Technology, al. Adama Mickiewicza 30, 30-059 Kraków, Poland

*e-mail: wojciech.korzeniewski@pg.edu.pl

Calcium-phosphate based glasses and glass-ceramics play a crucial role in the tissue engineering development. Apart from their high biocompatibility and excellent ability to undergo varying degrees of resorbability¹, they exhibit relatively high bioactivity and due to that they are commonly used as bone and dental implants. A substantial research effort is devoted to improve calcium-phosphate materials physico-chemical properties by tuning their degree of crystallinity and doping them with metal ions is one of the mostly researched strategies. The results found in the literature show that synthesized CaO-P₂O₅-Nb₂O₅ compounds exhibit a good biocompatibility, very low cytotoxicity in respect to calcium-phosphate doped with other metals and additionally can enhance human osteoblast function^{2,3}. As of today structure of these materials is not thoroughly described. Therefore, the detailed structural investigation by means of spectroscopic studies, i.e. FTIR spectroscopy, Raman spectroscopy, XAFS spectroscopy, XPS and EDX, together with SEM imaging, XRD and BET surface area measurements, was realized to shed light on the relationship between materials structure and the presence of dopant.

In this work, we show the results obtained for bioactive glass-ceramics, prepared via simple sol-gel method, with Ca/(P+Nb) molar ratio equal to 1.5 and with relative Nb contents of 0 mol% and 10 mol% of P. XRD patterns analysis shows that samples consist of tricalcium phosphate and hydroxyapatite phase. Raman spectra analysis confirms the incorporation of Nb into the material structure. Moreover, niobium doping leads to an increase in degree of crystallinity and crystallite size of the sample. Stoichiometry of the ceramics is as intended. Additionally, there is a greater proportion of carbonate groups in the doped material than in the undoped one (FTIR, Raman spectroscopy), and all samples exhibit calcium deficiency on the surface (XPS). XAFS analysis shows presence of octahedral coordination of niobium ions, with average oxidation state around +4.5 and XPS analysis indicates that on the sample surface the contribution of Nb⁺⁵ ions is greater than Nb⁺⁴ ions. Additionally it can be concluded, that Nb accumulates on materials surface.

Acknowledgements: We gratefully acknowledge the support of the SLL ELETTRA in providing synchrotron radiation facilities (XAS F11.1 station) for 20160241 experiment.

References

1. Layrotte, P., Ito, A. and Tateishi, T. Sol-gel Synthesis of Amorphous Calcium Phosphate and Sintering into Microporous Hydroxyapatite Bioceramics. *J. Am. Ceram. Soc.* 81, 1421–1428 (1998).
2. Obata, A. et al. Effects of Niobium Ions Released from Calcium Phosphate Invert Glasses Containing Nb₂O₅ on Osteoblast-Like Cell Functions. *ACS Appl. Mater. Interfaces* 4, 5684–5690 (2012).
3. Capanema, N. S. V. et al. Niobium-Doped Hydroxyapatite Bioceramics: Synthesis, Characterization and In Vitro Cytocompatibility. *Materials* 8, 4191–4209 (2015)

Correlation of magnetic properties with the electronic structure for magnetocaloric compounds of $\text{Mn}_{1.1}\text{Fe}_{0.9}\text{P}_{1-x}(\text{As},\text{Si})_x$ system

Poster Presentation
Thursday 10.09.2020
15:20-16:30

J. Kubacki^{1*}, J. Goraus¹, J. Szade^{1,2}

¹A. Chełkowski Institute of Physics, 75 Pułku Piechoty 1, 41-500 Chorzów, University of Silesia

² SOLARIS National Synchrotron Radiation Center, Czerwone Maki 98, 30-392 Kraków

*e-mail: jerzy.kubacki@us.edu.pl

Magnetic refrigeration which is based on the magnetocaloric effect (MCE) has emerged as a serious alternative to conventional refrigeration. Recently, the group of compounds $(\text{Mn,Fe})_2\text{P}_{1-x}\text{As}_x$ has been found to exhibit the giant magnetocaloric effect which is related to the first-order phase transition, and is tunable around room temperature¹. The P/As ratio appeared to be an interesting method to tune the basic properties for any application such as Curie temperature and thermal hysteresis width². In order to understand the effect of substitution we performed the extended studies of the electronic structure, crystal structure and magnetism for the selected group of solid compounds $\text{Mn}_{1.1}\text{Fe}_{0.9}\text{P}_{1-x}\text{As}_x$ ($0.4 < x < 0.55$). The substitution of silicon by arsenic has strong influence on the value of the magnetocaloric effect and the phase transition temperature. Despite the standard method of determination of the magnetic entropy changes from the magnetic measurements in conjunction with the Maxwell relations we measured the direct adiabatic temperature change which reached the high value of 4 K at the field of 1.7 T for $x=0.5$ and Si substituted by As. Knowledge of a detailed electronic structure and impact of the silicon on the density of states in the valence band of examined compounds can be related with their magnetic properties. The impact of the silicon substitution is clearly visible in the shape of the valence band. The lower intensity of the valence band shape was found at about 5 eV for silicon substituted sample. The observed exchange splitting of 2p states of manganese indicated on existence of magnetic moments of d electrons and correlated with changes in the valence band measurements. The specific magnetic moments of iron and manganese were deduced from splitting of Mn3s and Fe3s levels³. Our calculation of the total density of states DOS reflects very well the shape of the valence band obtained for the 1486 eV x-ray beam. To study the evolution of the electronic states and magnetism of the metallic and metalloid atoms across the first-order ferromagnetic transition of $\text{Mn}_{1.1}\text{Fe}_{0.9}\text{P}_{0.6}\text{As}_{0.4}$ and $\text{Mn}_{1.1}\text{Fe}_{0.9}\text{P}_{0.5}\text{As}_{0.4}\text{Si}_{0.1}$ compounds, we planning to perform of x-ray absorption (XAS) and magnetic circular dichroism (XMCD) measurements at the L edges of P, Mn, and Fe.

References

1. Shen, B. G., Sun, J. R., Hu, F. X., Zhang, H. W. & Cheng, Z. H., Recent Progress in Exploring Magnetocaloric Materials. *Advanced Materials* 21, 4545-4564 (2009).
2. Tegus, O., Bruck, E., Buschow K. H. J., & de Boer, F. R., Transition-metal-based magnetic refrigerants for room-temperature applications. *Nature* 415, 150-152 (2002).
3. Kubacki, J., Balin, K., Kulpa, M., Hawełek, Ł., Włodarczyk, P., Zackiewicz, P., Kowalczyk, M., Polak M. & Szade, J., Magnetic moments and exchange splitting in Mn3s and Mn2p core levels of magnetocaloric $\text{Mn}_{1.1}\text{Fe}_{0.9}\text{P}_{0.6}\text{As}_{0.4}$ and $\text{Mn}_{1.1}\text{Fe}_{0.9}\text{P}_{0.5}\text{As}_{0.4}\text{Si}_{0.1}$ compounds. *Physica B: Condensed Matter* 549, 127-132 (2018).

Superoxide dismutase activity in cyanobacteria grown under different light conditions

Poster Presentation
Thursday 10.09.2020
15:20-16:30

M. Kula–Maximenko*, K. J. Zieliński, I. Ślesak

The Franciszek Górski Institute of Plant Physiology, Polish Academy of Sciences, Niezapominajek 21, 30-239 Kraków, Poland

*e-mail: m.kula@ifr-pan.edu.pl

Superoxide dismutase (SOD, EC 1.15.1.1) belongs to the group of metalloproteins that remove one form of the so-called reactive oxygen species (ROS), i.e. superoxide anion radical ($O_2^{\cdot-}$). Superoxide anion radical is produced via the univalent reduction of molecular oxygen and is a by-product of aerobic metabolism. $O_2^{\cdot-}$ can be transformed into other more toxic for cellular metabolism ROS such as hydrogen peroxide (H_2O_2) and hydroxyl radical ($OH\cdot$). For this reason, scavenging of $O_2^{\cdot-}$ by SOD is the first line of defence against overproduction of harmful ROS. SOD occurs in four different classes depending on the presence of metal ions in the active site of the enzyme: manganese- (MnSOD), iron- (FeSOD), copper/zinc- (Cu/ZnSOD), and nickel-containing superoxide dismutase (NiSOD).

MnSOD, FeSOD and Cu/ZnSOD have been identified in plants, algae and cyanobacteria. There is little knowledge about the occurrence and activity of SOD under different light conditions in various cyanobacteria. Therefore, three cyanobacteria species *Gloeobacter violaceus*, *Synechocystis* PCC 6803 and *Geitlerinema* sp. were cultured under white light (WL), blue-red (BR), BR and far-red (BR+FR), BR and UVA (BR+UVA), and BR and green (BR+G) light emitted by light-emitting diodes (LEDs). We hypothesized that type of irradiation will modify SOD activity in analyzed cyanobacteria. In all cyanobacterial species, forms that belong to FeSOD and MnSOD family were identified. The obtained results showed also that colour of light used for cyanobacteria culture distinctly affect the activity of various SOD forms. However, methods used for SOD identification were insufficient for the correct detection of potentially new SOD or SOD-like proteins that were observed in *G. violaceus* cultured under BR+FR light conditions. Application of the X-ray fluorescence microscopy (XFM) and X-ray absorption spectroscopy (XANES and EXAFS) technique would allow to identify new classes of SOD in cyanobacteria and to obtain information about the oxidation state and local structure of metals (Fe and Mn) in SOD. A complex approach of the combination of techniques using synchrotron radiation and methods used in biochemistry will enable a better understanding of the light adaptation process and photoprotection mechanisms of organisms performing oxygenic photosynthesis.

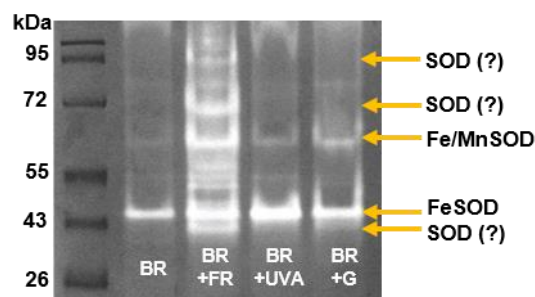


Fig. 1 The identification of SOD in *G. violaceus* culture under different light conditions (BR -blue-red, BR+FR - BR and far-red, BR+UVA - BR and UVA, and BR+G - BR and green LED).

Controlled Deposition and Separation of Mn₁₂-stearate Single-Molecule Magnets on Surfaces

Poster Presentation
Thursday 10.09.2020
15:20-16:30

M. Laskowska*, O. Pastukh

Institute of Nuclear Physics Polish Academy of Sciences, PL-31342 Krakow, Poland

*e-mail: Magdalena.laskowska@ifj.edu.pl

The present work is devoted to controlled deposition and separation of Mn₁₂-stearate single-molecule magnets ([Mn₁₂O₁₂(CH₃(CH₂)₁₆CO₂)₁₁(CH₃CO₂)₅(H₂O)₄]·2CH₃COOH) on various surfaces by chemical immobilization. The Mn₁₂-stearate was prepared in accordance with the procedure described in the literature¹. This derivative of Mn₁₂, in contrast to the commonly used Mn₁₂-acetate, is resistant against water catalyzed reduction and soluble in most organic solvents. The use of anchoring groups and spacer units, in this case, provides controlled separation of molecules^{2,3}. In order to check the effect of separation and the correctness of deposition procedure, samples containing four different concentrations of Mn₁₂-st molecules were prepared and compared with the bulk Mn₁₂-st. All materials have been examined by means of transmission electron microscopy, vibrational spectroscopy and squid magnetometry. The obtained results confirmed the successful deposition of Mn₁₂-st molecules on the surface. Additionally, a correlation between the test results and the concentration of molecules on the surface was observed. A more detailed analysis of the arrangement of molecules on the surface and their interaction with the surface and with neighbour molecules would be possible by means of methods offered by the PEEM/XAS beamline.

Acknowledgements: This work has been supported by the resources of the National Science Centre (Grant-No:2017/26/E/ST5/00162).

References

1. Park, C.-D. & Jung, D.-Y. Soluble Single-Molecule Magnet: Mn₁₂-stearate. *Bull. Korean Chem. Soc.* 22(6), 611-515 (2001).
2. Laskowska, M., Pastukh, O., Kuźma, D. & Laskowski, Ł. How to Control the Distribution of Anchored, Mn₁₂-Stearate, Single-Molecule Magnets. *Nanomaterials* 9, 1730-1739 (2019).
3. Laskowski, Ł., Kityk, I., Konieczny, P., Pastukh, O., Schabikowski, M. & Laskowska, M. The Separation of the Mn₁₂ Single-Molecule Magnets onto Spherical Silica Nanoparticles. *Nanomaterials* 9, 764-768 (2019).

Novel nanocomposites: magnetic nanocrystals inside porous silica matrices

Poster Presentation
Thursday 10.09.2020
15:20-16:30

Ł. Laskowski*, A. Fedorchuk

Institute of Nuclear Physics Polish Academy of Sciences, PL-31342 Krakow, Poland

*e-mail: lukasz.laskowski@ifj.edu.pl

According to the Eric Drexler's postulates (Creation Methods, 1984), the essence of the nanotechnology is to plan the synthesis process in such a way that the atoms connect themselves in the form to create material with expected properties. This process should be preceded by precise needs analysis which should define expected physical and chemical properties of the material. Next step is to design a molecular structure of a compound to meet expected properties. What left is to plan a synthesis to obtain the assumed molecular structure. It sounds simple, but in most cases, it is difficult but not impossible.

Needs analysis indicated that high-density magnetic memory would be very much desirable by contemporary computer systems. Working with mesoporous silica, we noticed that its channel regularity could be considered as possible placement of the magnetic units. Our idea is to fill in these channels with a permanent magnet material and use them as memory units. The base of this structure will have a form of the thin film that is made of mesoporous silica with perpendicular regular pores. These pores, also called channels, will have attached magnetic crystallites with the ability to change its magnetization when information bits need to be changed (see: Fig. 1). Reading information will, of course, be possible in the same way.

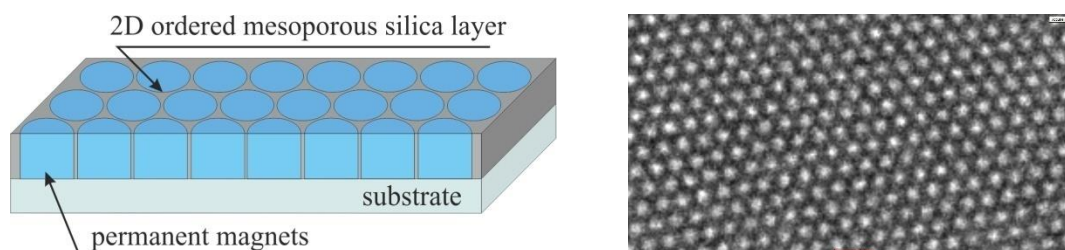


Fig. 1 The structure of the proposed thin-film layout of permanent magnetic units (left) and the structure of porous silica thin film (right).

In this work, we present the attempt to the fabrication of such a structure. The applied procedure assume treating the silica channels as nanoreactors, where nanocrystals are created as a result of thermal decomposition of internal functional units. The method was demonstrated by the example of a few metals pyrophosphates. In the next step, we assume fabrication of the magnetite nanocrystals in an ordered matrix. When ready, we plan to investigate our structure by means of X-ray Magnetic Circular Dichroism (XMCD).

Acknowledgements: This work has been supported by the resources of the National Science Centre (Grant-No:2017/26/E/ST5/00162).

SOLAIR beamline design and example of possible research applications

Poster Presentation
Thursday 10.09.2020
15:20-16:30

D. Liberda¹, T. P. Wrobel^{1*}, A. I. Wawrzyniak¹, A. Marendziak¹, P. Nowak¹,
M. Zajac¹, K. Malek², W. M. Kwiatek³, P. Dumas⁴, M. Stankiewicz¹

¹ *Solaris National Synchrotron Radiation Centre, Jagiellonian University, Czerwone Maki 98, 30-392 Krakow, Poland*

² *Faculty of Chemistry, Jagiellonian University in Krakow, Gronostajowa 2, 30-387 Krakow, Poland*

³ *Institute of Nuclear Physics Polish Academy of Sciences, PL-31342, Krakow, Poland.*

⁴ *SMIS beamline, SOLEIL synchrotron, L'orme des Merisiers, Gif sur Yvette, France*

*e-mail: tomek.wrobel@uj.edu.pl

SOLAIR beamline which is now under construction at SOLARIS will enable extraction of wide spectral range (from near to far) of infrared radiation (IR). Banding magnet will be the source of synchrotron radiation and the extraction of infrared radiation will be ensured by the first flat mirror placed in the dipole chamber of the magnet. IR beam reflected from the first mirror will be extracted outside from the storage ring, simultaneously correcting chromatic aberrations, with a specially designed system of five mirrors with different shapes and sizes. One of the end stations which will be available for the synchrotron users will be equipped with an FT-IR microscope with a Focal Plane Array detector. This equipment configuration will allow for sample imaging with IR radiation and therefore recognition of sample chemical composition distribution. An example of the research which can be performed with the FT-IR imaging system is an esophagus tissue biopsies histopathological classification done with the aim of improving of histopathologist work¹. Properly preprocessed data acquired with the FT-IR imaging system for 80 esophagus biopsies with application of machine learning algorithm allowed creating a model which classified patients as cancer or healthy with very high AUC metric in the range of 0.96 to 1.

References

1. Liberda, D., Hermes, M., Koziol, P., Stone, N. & Wrobel, T. P. Translation of an esophagus histopathological FT-IR imaging model to a fast quantum cascade laser modality. *J. Biophotonics* 13, 1–9 (2020).

***In situ* and *ex situ* structural studies of Fe-doped lithium-manganese oxides for lithium-ion cells**

Poster Presentation
Thursday 10.09.2020
15:20-16:30

M. Michalska^{1,2}, A. Malinowska^{1*}, A. Grabias¹, R. Diduszko¹, E. Wierzbicka¹

¹Lukasiewicz Research Network – Institute of Electronic Materials Technology, Wólczyńska 133, 01-919 Warsaw, Poland

²Department of Chemistry, VŠB-Technical University of Ostrava, 17. listopadu 15/2172, 708 00 Ostrava-Poruba, Czech Republic

*e-mail: agnieszka.malinowska@itme.edu.pl

Lithium manganese oxide LiMn_2O_4 (LMO) with spinel structure is one of the most promising materials for a positive electrode in lithium-ion batteries. Inexpensive, non-toxic and environmentally friendly LMO is a candidate to replace lithium cobalt oxide, which is currently the most widely used material in commercial batteries ¹⁻⁵.

The present work is a preliminary investigation on modification of a method of synthesis of undoped and Fe-doped LMO electrode materials for lithium-ion cells. The LMO powders were synthesized by the sol-gel technique with a use of various chelating compounds. Then the powder were annealed under different conditions.

Structural studies were performed using *ex situ* and *in situ* high-temperature X-ray powder diffraction (XRD) as well as transmission Mössbauer spectroscopy.

The effect of annealing temperature (25-700°C) and annealing atmosphere (air vs. nitrogen) on the structure, morphology and phase composition of the powder samples was studied in detail. Additionally, the structure of the powders obtained by annealing in a furnace during a standard technological procedure was compared with the powders prepared during in-situ high temperature XRD measurements performed in air. A good correlation was observed as concerns phase composition of the samples prepared by the two thermal procedures applied. Analysis of the results allowed the determination of structural and phase transformations related to LMO synthesis, occurring during annealing. Furthermore, a presence of iron dopant in the LMO structure was revealed. Depending on the annealing atmosphere and Fe content in the sample, a single Fe-doped LMO or two spinel phases of Fe-doped LMO and $\text{Li}(\text{Fe},\text{Mn})_5\text{O}_8$ were observed.

References

1. Nitta, N., Wu, F., Lee, J. T. & Yushin, G. Li-ion battery materials: present and future. *Materials Today* 18, 252-264 (2015).
2. Huggins, R. A. *Advanced Batteries, Materials Science Aspects*. Springer (2009).
3. Talik, E., Lipińska, L., Zajdel, P., Załóg, A., Michalska, M. & Guzik, A. Electronic structure and magnetic properties of $\text{LiMn}_{1.5}\text{M}_{0.5}\text{O}_4$ (M = Al, Mg, Ni, Fe) and $\text{LiMn}_2\text{O}_4/\text{TiO}_2$ nanocrystalline electrode materials. *Journal of Solid State Chemistry* 206, 257-264 (2013).
4. Michalska, M., Lipińska, L., Diduszko, R., Mazurkiewicz, M., Małolepszy, A., Stobinski, L. & Kurzydłowski, K. J. Chemical syntheses of nanocrystalline lithium manganese oxide spinel. *Physica Status Solidi C* 8 No. 7-8, 2538-2541 (2011).
5. Talik, E., Załóg, A., Skrzypek, D., Guzik, A., Zajdel, P., Michalska, M. & Lipińska, L. LiMn_2O_4 nanocrystalline electrode materials. *Crystal Research and Technology* 47 No. 3, 351-362 (2012).

Helium recovery and liquefaction system in NCPS SOLARIS

Poster Presentation
Thursday 10.09.2020
15:20-16:30

A. Maximenko*, P. Nita, M. Zając, A. Mandziak, M. Rosmus, N. Olszowska,
M. Szczepanik-Ciba, T. Wróbel, T. Giela, M. Kozak, J. Szade

National Synchrotron Radiation Center SOLARIS, Jagiellonian University, Kraków, Poland

*e-mail: alexey.maximenko@uj.edu.pl

Nowadays SOLARIS operates two beamlines (PEEM/XAS) and UARPES, however, next two beamlines will be commissioned soon (PHELIX and XMCD) and four lines more (SOLCRYS, SOLABS, SOLAIR and POLYX) are under construction and will be commissioned in 2021-2023. Each of the above-described SOLARIS synchrotron beamlines, except the POLYX beamline, uses or will use liquid helium (LHe) during experiments in a wide temperature range, especially for ultra-low (around 10 K) measurements, which are of great interest to scientists all over the world and are necessary to provide some of the measurements. LHe is used as a cryogenic liquid for samples cooling, which allows to increase the resolution of the measurements, protect samples (especially biological) against strong synchrotron radiation, and investigate change of the physical properties in the samples (e.g. by inducing a phase transition). Also, helium is used to cool down radiation detectors (e.g. infrared Mercury-Cadmium-Telluride detectors) and insertion devices (e.g. superconducting wigglers) for their proper operation. The evaporated helium gas, that results from the thermal exchange between LHe and cooled samples or components of the beamline, may either be released to the atmosphere or be collected and liquified for reuse. Helium is a non-renewable resource and cannot be replaced with another gas for many of the above-mentioned applications. Therefore, its recovery is part of the sustainable development policy of Poland. Moreover, for academic research centers, in particular, for synchrotrons, where LHe consumption is high, its recovery is the only way to reduce the costs and mitigate the scarcity and risk of uncertain LHe delivery.

The preliminary analysis of the SOLARIS liquid helium consumption shows that the total demand, when all the mentioned beamlines are commissioned, can reach around 410 liters/day (in the case of maximum loading of the beamlines with the measurements at ultra-low temperatures) and the average annual consumption will be around 130 liters/day. Based on the evaluated average demand for LHe, the price of LHe and assuming that SOLARIS beamlines will operate for 8 months (34 weeks) it was decided to install helium recovery and liquefaction system (HRLS) in SOLARIS, which will reduce cost up to 80-85%. The HRLS will collect evaporated helium gas, purify it and return it to a liquid state for reuse. Thus, the working process of the HRLS will include three stages: recovery, purification and condensation.

In 2021 the SOLARIS experimental hall will be extended and enlarged. A dedicated room for HRLS will be built as a part of the investment. The parameters of the room will allow to install the parts of HRLS in a functional manner considering the dimensions and the service space of the parts. Thereby, infrastructure in SOLARIS is prepared for the installation of the HRLS. The installation will be financed partly from the SOLARIS own funds, but the main part of financing will be obtained from external sources. For this purpose SOLARIS prepared and sent an application for financing of a large research infrastructure to the Polish Ministry of Science and Higher Education.

Powder X-ray diffraction study of $\text{Cd}_{1-x}\text{Mn}_x\text{Te}$ solid solution

R. Minikayev*, D. Kochanowska, A. Mycielski, W. Paszkowicz

Poster Presentation
Thursday 10.09.2020
15:20-16:30

Institute of Physics of the Polish Academy of Sciences, al. Lotników 32/46, 02-668, Warsaw, Poland

*e-mail: minik@ifpan.edu.pl

The $\text{Cd}_{1-x}\text{Mn}_x\text{Te}$ crystals belong to the II-VI based dilute magnetic semiconductors. These materials arouse the investigators interest due to their pronounced magnetic and magneto-optical properties and because of new possible application in spintronic devices¹ and X and gamma ray detectors^{2,3}.

Despite the fact that at ambient conditions $\text{Cd}_{1-x}\text{Mn}_x\text{Te}$ have a well-known crystallographic structure⁴ the knowledge of some of its crystallographic characteristics are limited.

The $\text{Cd}_{1-x}\text{Mn}_x\text{Te}$ crystal with Mn concentration $0 \leq x \leq 0.4$ were obtained by using the low pressure Bridgman method. Carefully performed powder x-ray diffraction measurements were analyzed by Rietveld method⁵. Based on these results the lattice parameters variations as well as the Mn - concentration dependence of Debye-Waller factor data, $B(x)$, will be presented and discussed on the background of existing data.

Acknowledgements: This work was in part supported by National Science Centre, Poland [Grant No. UMO-2014/13/B/ST3/04393]. Growth of crystals was partially supported by the National Centre for Research and Development, Poland [Grant No. TECHMATSTRATEG1/346720 /8/NCBR/2017].

References

1. Mycielski, A., Szadkowski, A., Kaliszek, W. & Witkowska, B. Proc. SPIE Int. Soc. Opt. Eng. 4412, 38-45 (2001).
2. Mycielski, A., Burger, A., Sowinska, M., Groza, M., Szadkowski, A., Wojnar, P., Witkowska, B., Kaliszek, W. & Siffert, P. Phys. Stat. sol. (c) 2, 1578-1585 (2005).
3. Roy, U. N., Okobiah, O. K., Camarda, G. S., Cui, Y., Gul, R., Hossain, A., Yang, G., Egarievwe, S. U. & James, R. B. AIP Advances 8, 105012(1-6) (2018).
4. Sondermann, U. Journal of Magnetism and Magnetic Materials 2, 216-222 (1975).
5. Rietveld, H. M. J. Appl. Cryst. 2, 65-71 (1969).

The emitter evolution universalized model at the cathodic arc

I. Titov¹, A. Nedolya^{2*}

Poster Presentation
Thursday 10.09.2020
15:20-16:30

¹*UAD-Systems, 84 Olexandrivska str., 69002 Zaporizhzhia, Ukraine*

²*AVN Lab, 20 Avtozavodska str., 152, 69118 Zaporizhzhia, Ukraine*

*e-mail: avnedolya@hotmail.com

We proposed the universalized model of the emitter evaporation at the cathode arc deposition of metals and their compounds where the emitter shape as an ellipsoid of rotation considered. The numerical simulation and calculation were carried out by the finite element method for the thermal distribution determination by the emitter at various current densities. The model contains the equation of thermal conductivity with initial and boundary conditions, the final solution of which is given in dimensionless coordinates.

Using the model, we calculate the temperature near the tip of the cathode emitter in established processes and fast-flowing processes (Fig. 1) at the beginning of the arc. By the simple mathematical transformations, the model can be used for the different shape of the emitter.

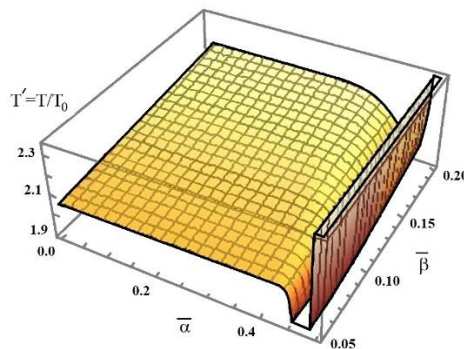


Fig. 1 The temperature near the emitter tip for fast-moving processes (in dimensionless coordinates).

The model can be used to optimize cathodic-arc processes in case of deposition the refractory and superconducting films on the surface of parts of synchrotrons, free-electron lasers and other accelerators¹.

References

1. Lorkiewicz, J., Nietubyc, R., Diduszko, R., Sekutowicz, J., & Kosinska, A. Coating in ultra-high vacuum cathodic-arc and processing of Pb films on Nb substrate as steps in preparation of Nb-Pb photocathodes for radio-frequency, superconducting e – guns. *Vacuum*. 179, 109524 (2020).

fs-XES unravels details of electron dynamics in the Fe-Co assembly

Poster Presentation
Thursday 10.09.2020
15:20-16:30

M. Nowakowski*, M. Huber, M. Bauer

Department Chemie, Universität Paderborn, 33098 Paderborn, Germany

*e-mail: michal.nowakowski@uni-paderborn.de

The pulse duration at X-Ray Free-Electron Laser (XFEL) ranges from a few fs up to picosecond values¹. This enables us to study for example charge and spin dynamics in excited states with fs time resolution². The NHC-carbenes are promising candidates to develop cheap, base metal light-harvesting systems for energy conversion purposes. The Fe(II)-NHC light-harvesting system is designed to prolong the lifetime of electron-donating MLCT upon excitation by the UV-VIS light. The excited electron can be further transported to a catalyst system in ps timescale within the photosensitizer-catalyst assembly.

We conducted a “two-color” Fe and Co K α X-Ray emission spectroscopy pump-probe experiment with the use of the FXE instrument at the XFEL, Schenefeld, Germany. The X-Ray beam energy was set to 9.3 keV while the optical pump laser was set to a wavelength of ~400 nm. Data was collected using a dispersive von Hamos setup with a 2D Jungfrau detector. We present the first results of electron kinetics of the excited Fe(II)-NHC photosensitizer. In the first 15 ps after excitation, the dynamics can be described by a three-component decay process dominated by the MLCT \rightarrow MC transition. Additionally, a relative temporal relation between Fe K α and Co K α is presented in Fe-Co dyad, which sets up the upper limit on the electron transfer speed.

Understanding the first ~15 ps of the deexcitation cascade in photosystem is crucial in electron and charge transfer systems. Obtained data shows a catalytic potential of Fe-Co systems for future uses.

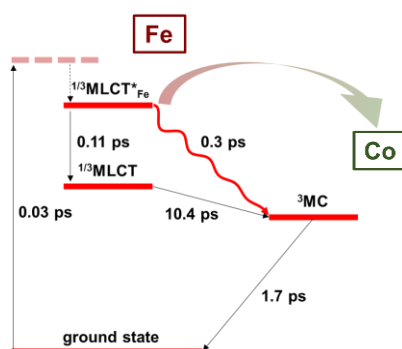


Fig. 1 Electron decay dynamics in the Fe-Co dyad.

Acknowledgements: Authors would like to thank to the rest of the team: Wojciech Gawęda, Dmitry Khakhulin, Tae Kyu Choi, Frederico Alves Lima, Angel Rodriguez-Fernandez, Aleksandr Kalinko, Jakob Staube, Natalia Pierunek, Ahmet Kertem, Jacek Kubicki and Christian Bressler.

References

1. Ding, Y. et al. Femtosecond X-ray pulse characterization in free-electron lasers using a cross-correlation technique. *Phys. Rev. Lett.* 109, 1–5 (2012).
2. Barrett, J. & Malati, M. A. Coordination Complexes. *Fundam. Inorg. Chem.* 509, 203–256 (2013).

Resonance photoemission study of selected rear earth ions dopants in semiconductor compounds

Poster Presentation
Thursday 10.09.2020
15:20-16:30

B. A. Orlowski*, E. Guziewicz, B. J. Kowalski

Institute of Physics, Polish Academy of Sciences, Aleja Lotnikow 32/46, PL-02668 Warsaw, Poland

*e-mail: orb@ifpan.edu.pl

The presented results concern contribution of Rare Earth (RE) impurity 4f electrons to the valence band of selected semiconductor compounds with different valence of anions^{1,2}. Application of synchrotron radiation with continuous spectrum allows us to acquire Fano type resonant photoemission spectra in the energy range of $h\nu = 130-170$ eV corresponding to RE 4d \rightarrow 4f optical transition.

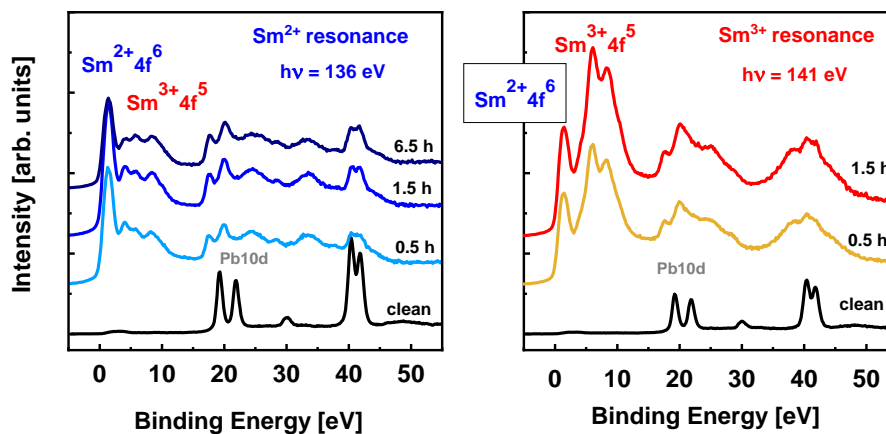


Fig 1. A comparison of resonant photoemission spectra of $\text{Pb}_{0.97}\text{Ge}_{0.03}\text{Te}$ with a deposited Sm layer of 7ML taken for $h\nu=136$ eV (resonant energy for Sm^{2+}) and $h\nu=141$ eV (resonant for Sm^{3+}) after annealing of the sample during the time of 0.5, 1.5 and 6.5 h.

RE atoms deposited on the surface of CdTe, ZnO, GaN or PbGeTe occur as a mixture of RE^{2+} and RE^{3+} ions. The resonant photoemission spectra acquired after subsequent stages of the substrate/RE layer system annealing (Fig. 1) enable us to follow formation of a solid solution subsurface layer, due to diffusion of RE atoms into the substrate. We observe conversion between RE^{3+} and RE^{2+} ions when the ion environment changes from that of RE metal layer to the environment of the solid solution formed in the substrate subsurface layer.

References

1. Orlowski, B. A., Guziewicz, E., Reszka, E. A., Pietrzyk, M. A. & Kowalski, B. J. & Johnson, R.L., Fano resonance photoemission study of Sm on $\text{Pb}_{0.97}\text{Ge}_{0.03}\text{Te}$ crystal. *Rad. Phys. Chem.* 175, 108080-108082 (2020).
2. Guziewicz, E., Orlowski, B. A., Kowalski, B. J., Kowalik, I. A., Reszka, A., Wachnicki, L., Gieraltowska, S. Godlewski, M. & Johnson, R.L. Gd and Sm on clean semiconductor surfaces-Resonant Photoemission study. *Appl. Surf. Sc.* 282, 326-334 (2013).

Structure refinement for $(\text{Cd,Zn})_3\text{As}_2$

W. Paszkowicz^{1*}, M. Wołczyrz², K. Graszka¹, P. Skupiński¹, G. Grabecki¹

Poster Presentation
Thursday 10.09.2020
15:20-16:30

¹ Institute of Physics, PAS, Aleja Lotników 32/46, PL-02-668 Warsaw, Poland

² Institute of Low Temperature and Structure Research, PAS, ul. Okólna 2, PL-50-422 Wrocław, Poland

*e-mail: paszk@ifpan.edu.pl

Cadmium–zinc arsenide, $(\text{Cd}_{1-x}\text{Zn}_x)_3\text{As}_2$, is an alloy system of inverted gap semiconductor, Cd_3As_2 and direct-gap semiconductor, Zn_3As_2 . Its basic electronic and optical properties have been determined in¹. The interest in $(\text{Cd}_{1-x}\text{Zn}_x)_3\text{As}_2$ has been renewed after discovery of Dirac semimetal character of Cd_3As_2 ² and expected topological phase transition to the open-gap semiconductor for some x ³. The $(\text{Cd}_{1-x}\text{Zn}_x)_3\text{As}_2$ system includes a number of phases of relatively complex structure. The Cd-rich α phase crystallizes in a tetragonal structure ($I4_1/acd$ space group) with 160 atoms in the unit cell. It changes into a $P4_2/nmc$ (α'') structure for higher x . In the range between $x=0.45$ and $x=0.80$, another tetragonal structure, $I4_1/amd$ (α''') is reported. From $x=0.85$ to $x=0.97$, there is again a $P4_2/nmc$ structure, and for $x>0.97$ the solid solution crystallizes in $I4_1/acd$ space group.

Crystals $(\text{Cd}_{1-x}\text{Zn}_x)_3\text{As}_2$ were grown by horizontal Bridgman method. The X-ray powder diffraction measurements were performed using the X'pert MPD diffractometer equipped with a Johansson monochromator and a strip detector. The structures of the crystals was refined by the Rietveld method, employing the Fullprof2k,v.5.30⁴ software). Single crystal diffraction measurements were performed on an Oxford Diffraction Xcalibur diffractometer, employing the graphite-monochromated $\text{MoK}\alpha$ ($\lambda = 0.71073 \text{ \AA}$) radiation. Data collection and reduction were performed using CrysAlis CCD and CrysAlis RED programs (Rigaku Oxford Diffraction, 2015)⁵. The crystal structures were refined by full-matrix least-squares methods on F^2 using the SHELX-2014 crystallographic software package⁶. Phase analysis confirmed the expected structure ($I4_1/amd$ space group) as well as the phase purity of the material. The obtained results are in line with those of ref.⁷ for a crystal of a much higher Zn content, $x=0.74$.

Acknowledgements: This work was in part supported by National Science Centre (Poland) through Grant No. UMO-2014/13/B/ST3/04393.

References

1. Turner, W. J., Fischer, A. S. & Reese, W. E., Physical properties of several II-V semiconductors. *Phys. Rev.* 121, 759–767 (1961).
2. Borisenko, S., Gibson, Q., Evtushinsky, D., Zabolotnyy, V., Büchner, B. & Cava, R. J. Experimental realization of a three-dimensional Dirac semimetal. *Phys. Rev. Lett.* 113, 027603 (2014).
3. Nishihaya, S., Uchida, M., Nakazawa, Y., Akiba, K., Kriener, M., Kozuka, Y., Miyake, A., Taguchi, Y., Tokunaga, M. & Kawasaki, M. Negative magnetoresistance suppressed through a topological phase transition in $(\text{Cd}_{1-x}\text{Zn}_x)_3\text{As}_2$ thin films. *Phys. Rev. B* 97, 245103 (2018).
4. Rodríguez-Carvajal, J. Recent advances in magnetic structure determination by neutron powder diffraction. *Physica B: Cond. Matt.* 192, 55–69 (1993).
5. Rigaku Oxford Diffraction, CrysAlisPro Software System, Version 1.171, (Rigaku Corporation, Oxford, UK, 2015).
6. Sheldrick, G. M. Crystal structure refinement with SHELXL. *Acta Cryst.* C71, 3–8 (2015).
7. Volodina, G. F., Zakhvalinskii, V. S. & Kravtsov, V. K. Crystal structure of α''' - $(\text{Zn}_{1-x}\text{Cd}_x)_3\text{As}_2$ ($x = 0.26$). *Crystallogr. Rep.* 58, 563–567 (2013).

X-ray diffraction study of mechanochemical synthesis process of $\text{Pb}_{1-x}\text{Cd}_x\text{Te}$

Poster Presentation
Thursday 10.09.2020
15:20-16:30

W. Paszkowicz^{1*}, R. Minikayev¹, T. Rygier², A. Królicka¹, D. Oleszak², T. Story¹

¹Institute of Physics PAS, Aleja Lotników 32/46, PL-02-668 Warsaw, Poland

²Warsaw Univ. of Technology, Faculty of Materials Science and Engineering, PL-02-507 Warsaw, Poland

*e-mail: paszk@ifpsn.edu.pl

Mechanochemical synthesis is a valuable way to producing various materials¹, in particular it has been successfully applied for elaboration of various chalcogenides, as reviewed in². For chalcogenides and other semiconductors, a number of synthesis pathways have been applied. The elements, binary oxides and other inorganic compounds, organic compounds and chalcogen hydrates have been used as reactants leading to mechanochemically synthesized nanocrystalline semiconductors such as binary PbTe, PbSe, PbS, SnSe, CdS, and ZnTe, pseudobinary (Pb,Cr)Te, (Pb,Cd)S, (Cd,Zn)S, ternary CuInSe₂, CuInS₂, and Cu₂SnS₃, as well as many others. For each reaction, the reaction parameters are determined experimentally; a continuous analysis of the progress is now possible thanks to opportunity of use of hard X-rays at dedicated synchrotron radiation facilities (for an example of experimental setting suitable for the *in situ* studies of mechanochemical reaction see³).

PbTe is a well known thermoelectric material. Its properties can be improved by alloying with CdTe. As CdTe is insoluble in PbTe, suitable methods must be used to achieve a (metastable) solid solution. For example, single crystals of such solution, with size of about 1 cm³, can be produced by the physical vapor transport method⁴. The present study is devoted to mechanochemical synthesis of (Pb,Cd)Te from PbTe and CdTe reactants. Synthesis of semiconductor materials requires a high energy reaction option. Fritsch Pulverisette-5 and Retsch PM-100 planetary ball mills were alternatively used. The X-ray diffraction served for characterization of the synthesized materials. The measurements were performed using an X'pert MPD diffractometer equipped with a Johansson monochromator and a strip detector. The structures of the crystals was refined by the Rietveld method (Fullprof2k,v.5.30)⁴ software. In this study, we show that the reaction between PbTe and CdTe, monitored by the lattice parameter of the product, takes place, and that it is possible to produce a (Pb,Cd)Te material with up to about 3 at% of CdTe, the composition depending on the mechanochemical process parameters.

Acknowledgements: This work was in part supported by National Science Centre (Poland) through Grant No. UMO-2014/13/B/ST3/04393.

References

1. James, S. L., Adams, C. J., Bolm, C., Braga, D., Collier, P., Frišćić, T., Grepioni, F., Harris, K. D. M., Hyett, G., Jones, W., Krebs, A., Mack Maini, J.L., Orpen, A. G., Parkin, I. P., Shearouse, W. C., Steed, J. W. & Waddell, D. G. Mechanochemistry: Opportunities for new and cleaner synthesis. *Chem. Soc. Rev.* 41, 413-447 (2012).
2. Baláž, P., Baláž, M., Achimovičová, M., Bujňáková, Z. & Dutková, E. Chalcogenide mechanochemistry in materials science: Insight into synthesis and applications (a review). *J. Mater. Sci.* 52, 11851-11890 (2017).
3. Ban, V., Sadikin, Y., Lange, M., Tumanov, N., Filinchuk, Y., Černý, R. & Casati, N. Innovative *in situ* ball mill for X-ray diffraction. *Anal. Chem.* 89, 13176-13181 (2017).
4. Szot, M., Szczerbakow, A., Dybko, K., Kowalczyk, L., Smajek, Domukhovski, V., Łusakowska, E., Dziawa, P., Mycielski, A., Story, T., Bukała, M., Galicka, M., Sankowski, P., Buczek, R. & Kacman, P. Experimental and theoretical analysis of PbTe-CdTe solid solution grown by physical vapour transport method. *Acta Phys. Polon. A* 116, 959-961 (2009).

Dependence of the degree of tetragonal deformation of the lithium-manganese spinel structure on nonhydrostatic pressure component: Synchrotron powder diffraction study

Poster Presentation
Thursday 10.09.2020
15:20-16:30

P. Piszora*, J. Darul

Department of Materials Chemistry, Faculty of Chemistry, Adam Mickiewicz University,
Uniwersytetu Poznańskiego 8, 61-614 Poznań, Poland

*e-mail: pawel@amu.edu.pl

A strong relationship can be observed between the non-hydrostatic pressure component and the degree of tetragonal deformation of the spinel structure. Phase transitions considered to be pressure induced are often in fact strain induced phase transitions.

Structural properties of $\text{Li}_{0.95}\text{Mn}_{2.05}\text{O}_4$ under pressure and at elevated temperature were examined up to 12 GPa by powder X-ray diffraction using DAC on the MSPD-BL04 beam line of the ALBA synchrotron.¹ Synchrotron X-ray diffraction experiments were performed using polydimethylsiloxane oil as the pressure transmitting medium (PTM). Increase in the c/a' distortion parameter (Figure 1) in the pressure range up to about 5 GPa is in good agreement with the known from literature decreasing of hydrostaticity in the applied PTM. This effect is not observed for isothermal compression at 380 K. Sensitivity to the hydrostaticity of the pressure transmitting medium allows the design of spinel materials with new interesting properties.

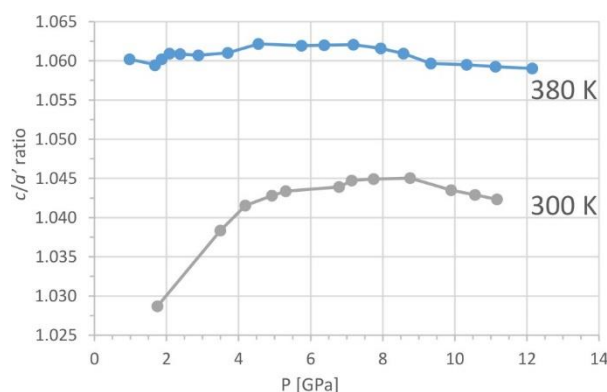


Fig. 1 Axial ratio in the high pressure tetragonal phase at 300 K and 380 K.

Acknowledgements: The experiments were performed at the MSPD-BL04 beamline at ALBA Synchrotron with the collaboration of ALBA staff.

References

1. Fauth, F., Peral, I., Popescu, C. & Knapp, M. The new material science powder diffraction beamline at ALBA synchrotron. Powder Diffr. 28, S360 –S370 (2013).

X-ray diffraction study of structure and thermal expansion of $\text{Ca}_{10}\text{M}_{0.5}(\text{VO}_4)_7$ ($\text{M} = \text{Co}, \text{Cu}$)

Poster Presentation
Thursday 10.09.2020
15:20-16:30

H. S. Rahimi Mosafer*, W. Paszkowicz, R. Minikayev, M. Kozłowski, R. Diduszko, M. Berkowski

Institute of Physics, Polish Academy of Sciences, Al. Lotników 32/46, PL-02-668 Warsaw, Poland

*e-mail: rahimi@ifpan.edu.pl

Calcium orthovanadate and orthophosphate $\text{Ca}_3(\text{XO}_4)_2$, $\text{X} = \text{P}$ or V , is known to crystallize in R3c space group. By substitution of alkali or rare earth at Ca sites, synthetic materials related to those of whitlockite group minerals are obtained. In particular, europium and copper doped calcium vanadates are competitor for the application as inorganic yellow pigments¹. Pure and Nd-doped $\text{Ca}_{10}\text{Li}(\text{VO}_4)_7$ single crystal are supposed to be suitable as non-linear optics material². $\text{Yb}^{3+}:\text{Ca}_9\text{Gd}(\text{VO}_4)_7$ crystal can be regarded as a potential candidate for ultrashort pulse laser material³.

In this study, we investigate the structural properties of $\text{Ca}_{10}\text{M}_{0.5}(\text{VO}_4)_7$, where M are cobalt and copper, at room temperature and high temperature. The insight of the structural properties of these materials, not available until now, is important for their understanding and characterization.

Solid solution of above named new materials, were synthesized by solid state reaction. Copper (Cobalt) and vanadium oxide with calcium carbonate mixed in stoichiometric proportion and formed into pellets. Powder diffraction measurements were performed at Philips X'Pert Pro Alpha1 diffractometer with Bragg-Brentano geometry. Scanning electron microscopy (SEM) was performed for morphological analysis.

Phase analysis of $\text{Ca}_{10}\text{M}_{0.5}(\text{VO}_4)_7$ has shown that samples crystallize in R3c group. Diffraction peaks are assigned to those of other whitlockite-type materials. Due to a difference of the ionic radii, the lattice parameters decrease by substitution of M [$\text{M}=\text{Cu}, \text{Co}$]. The starting model for refinement of these material is $\text{Ca}_{1.5}\text{Sr}_{1.5}(\text{VO}_4)_7$ ⁴. At the final step, we refined 80 parameters. Rietveld analysis allows for analysis of the site occupancy preferences of the transition metal atoms.

High temperature measurements were performed for both samples. The diffraction patterns indicate that the structure is stable within the investigated temperature range. Thermal expansion coefficient is determined for samples as function of temperature.

References

1. Pogosova, M. A., Azarmi, F., Eliseev, A. A. & Kazin, P. E. Dyes and Pigments Eu and Cu co-substituted calcium vanadate d The crystal structure, luminescence and color. *Dye. Pigment.* 148, 219–223 (2018).
2. Kosmyna, M. B. *et al.* $\text{Ca}_{10}\text{Li}(\text{VO}_4)_7:\text{Nd}^{3+}$, a promising laser material: Growth, structure and spectral characteristics of a Czochralski-grown single crystal. *J. Cryst. Growth* 445, 101–107 (2016).
3. Zheng, F. *et al.* $\text{Yb}:\text{Ca}_9\text{Gd}(\text{VO}_4)_7$, a potential ultrafast pulse laser crystal with promising spectral properties. *J. Lumin.* 221, 117085 (2020).
4. Belik, A. A., Stefanovich, S. Y. & Lazoryak, B. I. Polar-to-centrosymmetric phase transition in $\text{Ca}_{1.5}\text{Sr}_{1.5}(\text{VO}_4)_2$ and the polar phase structure. *Mater. Res. Bull.* 36, 1873–1880 (2001).

ExPaNDS project

K. Roarty*

Poster Presentation
Thursday 10.09.2020
15:20-16:30

Diamond Light Source Ltd, Harwell Science and Innovation Campus, Didcot, Oxfordshire OX11 0DE, UK

*e-mail: k.roarty@diamond.ac.uk

ExPaNDS is the European Open Science Cloud (EOSC) Photon and Neutron Data Service. Our ambitious ExPaNDS project is a collaboration between 10 national Photon and Neutron Research Infrastructures (PaN RIs) as well as EGI. The project aims to deliver standardised, interoperable, and integrated data sources and data analysis services for Photon and Neutron facilities. ExPaNDS, alongside the Photon and Neutron Open Science Cloud (PaNOSC) are European H2020 projects who are working towards the development of the European Open Science Cloud (EOSC). The Photon and Neutron Research Infrastructures (PaN RIs) containing free electron laser, synchrotron light and neutron sources are generating petabytes of research data each year and such vast amounts of data can be hard to share. Researchers around the globe use the data to advance knowledge across a variety of societal challenges. These challenges can be found in energy, transport, healthcare, food safety, and sustainable living to list only a few.

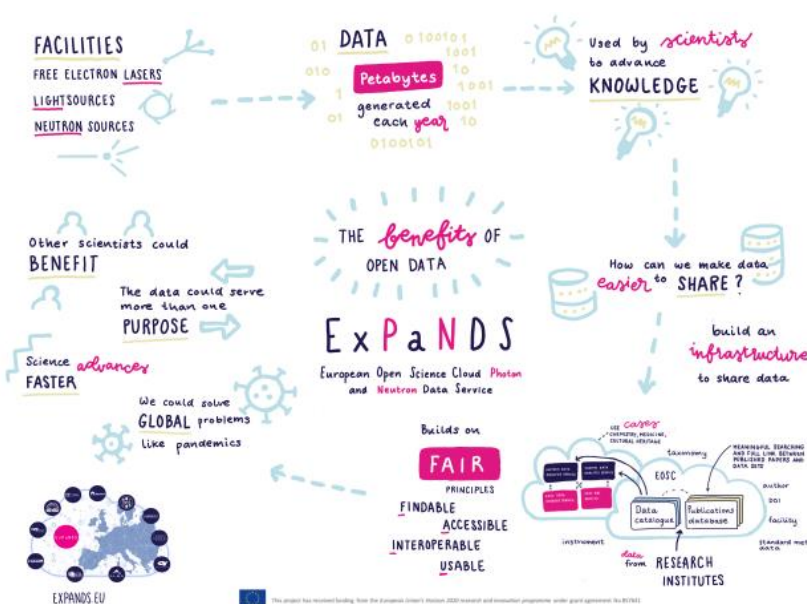


Fig. 1 The benefits of Open Data.

Accessible, Interoperable and Reusable (FAIR). Fostering FAIR Data Practices will allow other facilities and their users to benefit from the valuable data produced thanks to our light and neutron sources to help combat 21st century global problems. By reusing data, it is possible to plan experiments and simulations that will produce more than was originally imagined.

ExPaNDS and PaNOSC see EOSC as an opportunity to generalise the adoption of FAIR data practices at our PaN RIs that will enable data sharing, the reuse across a wider community and the provisioning of services for remote data analysis. We will map all relevant data catalogues to ensure that our scientific research communities have access to both the raw data collected that is linked to the experiments at their facility, and the relevant peer review articles produced as a direct result of their usage.

The goal of our projects and the EOSC is to make data from publicly funded research in Europe Findable,

Direct evidence of uneven d_{xz} and d_{yz} orbital occupation in the superconducting state of iron pnictide

Poster Presentation
Thursday 10.09.2020
15:20-16:30

D. Rybicki^{1*}, M. Sikora², J. Stępień², Ł. Gondek¹, K. Goc¹, T. Strączek¹,
M. Jurczyszyn², C. Kapusta¹, Z. Bukowski³, M. Babij³, M. Matusiak^{3,4}, M. Zając⁵

¹AGH University of Science and Technology, Faculty of Physics and Applied Computer Science, Department of Solid State Physics, al. A. Mickiewicza 30, 30-059 Kraków, Poland

²AGH University of Science and Technology, Academic Centre for Materials and Nanotechnology, al. A. Mickiewicza 30, 30-059 Kraków, Poland

³Institute of Low Temperature and Structure Research, Polish Academy of Sciences, Okólna 2, 50-422 Wrocław, Poland

⁴International Research Centre MagTop, Institute of Physics, Polish Academy of Sciences, Al. Lotników 32/46, PL-02668 Warszawa, Poland

⁵National Synchrotron Radiation Centre SOLARIS, Jagiellonian University, Czerwone Maki 98, 30-392 Kraków, Poland

*e-mail: ryba@agh.edu.pl

The origin of nematicity and its relation to superconductivity in iron pnictide high-temperature superconductors remains unclear. One of its possible sources is the uneven occupation of Fe d_{xz} and d_{yz} orbitals. Here, by using X-ray linear dichroism technique we show that such an imbalance is present in $\text{Eu}(\text{Fe}_{1-x}\text{Co}_x)_2\text{As}_2$ single crystals deep in the tetragonal phase and also in the superconducting state, where we find that d_{xz} orbital has a higher occupation as indicated by XLD magnitude of 1.5%. Our result shows the importance of orbital polarization in the theoretical description of nematicity and superconductivity, particularly for determination of the superconducting gap symmetry, which is affected by orbital fluctuations.

Crystallization of glasses with PEEM

F. Scheffler^{1*}, C. Tielemann^{2*}, R. Busch³, M. Kober¹, R. Müller², D. Brauer¹

Poster Presentation
Thursday 10.09.2020
15:20-16:30

¹Friedrich-Schiller-University Jena, Otto-Schott-Institute for Materials Research, Fraunhofer Str. 6, 07743 Jena, Germany

²Bundesanstalt fuer Materialforschung und -pruefung, D-12200 Berlin, Germany.

³Fraunhofer-Gesellschaft zur Förderung der angewandten Forschung, 80686 München Germany

*e-mail: Franzi.Scheffler@uni-jena.de; christopher.tielemann@bam.de

With given time and temperature, every glass crystallizes eventually. A heat treated glass that formed crystals under controlled conditions, can be a glass ceramic (Fig. 1). Such glass ceramics combine properties of glasses and ceramics and are for example used as cooktops (e.g. CERAN®). For full controlment, it is needed to fully understand the crystallization processes. These processes are, amongst other things, highly dependent on the mobility of elements within the glass during heat treatment and the reorganization of atomic bonds during crystallization. This reorganization, which is often accompanied by a change in coordination number of certain elements, is easily observable in bulk glass samples during heat treatment with XAS. Our plan was to monitor these reorganization processes in situ at the imminent surface during heat treatment with PEEM to get time- and spatial-resolved data. However, it was not that simple. Here we would like to discuss the difficulties that appeared, how we overcome some of them and which are still problematic.

First of all, we had to face the problem that the samples were outgassing extensively, which was unexpected for the observed glass systems. The second was the coating. We chose a thin C-coating that worked fine with XAS, but with PEEM the layer was too thin to conduct enough electrons and too thick to get sufficient signal. Another issue was that heat treated glass becomes viscous, so the surface became uneven (Fig. 2). During crystallization, topography is created due to crystal growth. Initially we thought that this might be the biggest issue to overcome, but compared to the others this was neglectable. As a result, in-situ monitoring of glass crystallization during heat-treatment with PEEM is challenging. Already crystallized samples (different time steps, spatially-resolved) seem manageable. The important points here are, that the samples need to be outgassed prior to the measurement and that no coating works best, because at elevated temperatures the glasses become conductive themselves.

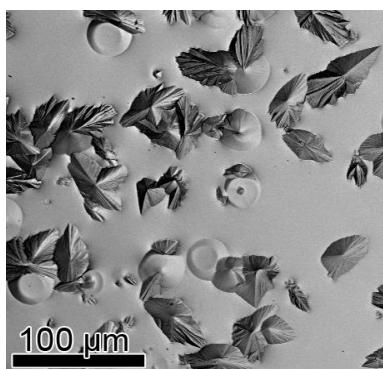


Fig. 1 This is a 2BaO-TiO₂-2.75SiO₂-Fresnoite glass ceramic. The matrix is the residual glass and the crystals are made of Ba₂TiSi₂O₈. Note the topography that is created during crystallization.



Fig. 2 This glass slide was completely even. It got a wavy surface during heat treatment.

Acknowledgements: Authors would like to thank Dr. Marcin Zajęc, Dr. Tomasz Giela and Dr. Ewa Madej from Synchrotron Solaris, Krakow for beamline optical design optimization and support during the design period.

XAS studies of vanadium oxide thin films

K. Schneider^{1*}, P. Nowak¹, K. Goc², T. Strączek², K. Raszka², M. Rękas³, J. Stępień⁴, C. Kapusta²

Poster Presentation
Thursday 10.09.2020
15:20-16:30

¹AGH-University of Science and Technology, Faculty of Computer Science, Electronics and Telecommunications, al. Mickiewicza 30, 30-050 Krakow, Poland

²AGH-University of Science and Technology, Faculty of Physics and Applied Computer Science, al. Mickiewicza 30, 30-059 Krakow, Poland

³AGH-University of Science and Technology, Faculty of Materials Science and Ceramics, al. Mickiewicza 30, 30-059 Krakow, Poland

⁴National Synchrotron Radiation Centre SOLARIS, Jagiellonian University, Czerwone Maki 98, 30-392 Kraków, Poland

*e-mail: kryschna@agh.edu.pl

Vanadium oxides are used in many technological applications, including electrical and optical switching devices, light detectors, thermal and chemical sensors, write-erase media, and in heterogeneous catalysis^{1,2}. Among them, V₂O₅ is the most popular one. This is a wide-band-gap, n-type semiconductor material that exhibits particularly useful properties stemming from the fact that the electric charge is transported via polarons, as reported for bulk single-crystals and amorphous V₂O₅ layers. The surface properties of V₂O₅ in ceramic and thin film forms make it an attractive candidate for many practical applications, including catalyst materials and gas sensors. The most typical application of V₂O₅ as a heterogeneous catalyst is the fabrication of sulfuric acid, where it catalyses the oxidation of sulfur dioxide to sulfur trioxide by air.

In this study thin films of 200 nm of VO_x RF magnetron sputtered on the SiO₂ glass and Si substrates were studied with X-ray Absorption Spectroscopy in the XANES range of the Oxygen K and Vanadium L_{2,3} edges. The measurements were carried out at the PEEM/XAS beamline of Solaris National Synchrotron Radiation Centre, Poland. The total electron yield (TEY) detection mode was used. The spectra were collected at several temperatures between room temperature and 300°C. Selected spectra of the VO_x films on the SiO₂ glass are shown in Fig. 1, together with those of reference Vanadium oxides taken at room temperature. The room temperature Vanadium L_{2,3} white lines (peaks at 525 eV and 518 eV, respectively) of the VO_x thin film show the closest similarity to those of V₂O₅ powder, whereas the spectrum at 300°C is the closest to that of V₂O₃ powder reference. Cooling the sample down to room temperature and its exposure to air does not modify it noticeably. A similar behavior can be seen at the Oxygen K-edge spectrum (530 – 545 eV), Fig. 1 and reflects occurrence of deoxygenation and the corresponding change of the oxide stoichiometry from close to V₂O₅, towards V₂O₃.

The linear dichroism in the XAS spectra of the samples studied was also measured. In the presentation its results will be shown along with a detailed interpretation of the XAS spectral features and their relation to the temperature driven surface modification of the films studied. The results obtained will be discussed in terms of their relation to the sensor performance of the VO_x thin films and a possibility of the occurrence of the metal – insulator transition in them.

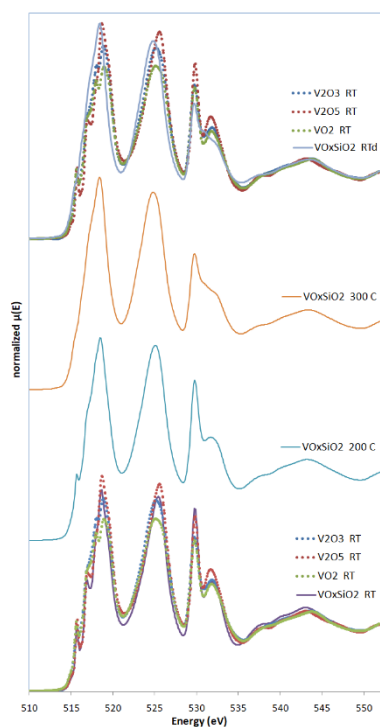


Fig. 1 The O:K and V:L_{2,3} XANES spectra of the VO_x thin film on the SiO₂ substrate at selected temperatures together with room temperature spectra of reference oxides.

Acknowledgements: This work was supported by the National Science Centre of the Republic of Poland under Grant No. 2016/23/B/ST8/00163. Experiment was performed owing to the collaboration of SOLARIS Staff.

References

1. Schneider, K., Lubecka, M. & Czapl, A. Sensors and Actuators. B. Chemical 236, 970 (2016).
2. Schneider, K. & Maziarz, W. Sensors 18, 4177. 2 (2018).

XAS studies of RE (RE=Sm, Gd and Dy) doped Bi₇REFe₄Ti₃O₂₄ compounds

Poster Presentation
 Thursday 10.09.2020
 15:20-16:30

J. Polnar¹, K. Goc², T. Strączek², A. Figura², K. Schneider^{3*},
 M.M. Bućko¹, J. Lis¹, C. Kapusta²

¹AGH-University of Science and Technology, Faculty of Materials Science and Ceramics,
al. Mickiewicza 30, 30-059 Krakow, Poland

²AGH-University of Science and Technology, Faculty of Physics and Applied Computer Science,
al. Mickiewicza 30, 30-059 Krakow, Poland

³AGH-University of Science and Technology, Faculty of Computer Science, Electronics and
Telecommunications, al. Mickiewicza 30, 30-050 Krakow, Poland

*e-mail: kryschna@agh.edu.pl

Bismuth layer-structured oxide compounds, with perovskite blocks sandwiched between (Bi₂O₂)²⁺ layers known as Aurivillius phases¹, belong to one of the few groups of single phase multiferroics. Some compounds in the Bi₄Ti₃O₁₂-BiFeO₃ system with the general formula Bi_{m+1}Fe_{m-3}Ti₃O_{3m+3} are considered as the most interesting electroceramic materials due to their possible applications, that include electrically controlled microwave devices, ferromagnetic resonance devices, magnetically controlled electro-optic broadband magnetic field sensors, and ME memory devices². In our previous studies some series of compounds of the Bi_{m+1}Fe_{m-3}Ti₃O_{3m+3} family were studied^{3,4}.

In the present study four compounds of the m=7 sub-group: Bi₈Fe₄Ti₃O₂₄ (BFT7), Bi₇SmFe₄Ti₃O₂₄ (BSFT7), Bi₇GdFe₄Ti₃O₂₄ (BGFT7) and Bi₇DyFe₄Ti₃O₂₄ (BDFT7) were synthesized and characterized. In order to determine the influence of Rare Earth elements doping on their electronic properties the X-ray Absorption Spectroscopy study in the XANES range of the Oxygen K, Titanium L_{2,3} and Iron L_{2,3} edges was performed. The measurements were carried out at the PEEM/XAS beamline of Solaris National Synchrotron Radiation Centre, Poland. The total electron yield (TEY) detection mode was used and the spectra were collected at room temperature. The spectra are shown in Figs 1, 2 and 3 for O:K, Ti:L_{2,3} and Fe:L_{2,3} edges, respectively. At the O:K edge spectra a noticeable difference between the BSFT7 and the other materials is visible as additional peaks at 540 and 552 eV. It is worth noting that the Ti spectra show a much higher overall intensity for the pristine BFT7 material. A similar, although weaker, effect is observed for the Fe spectra.

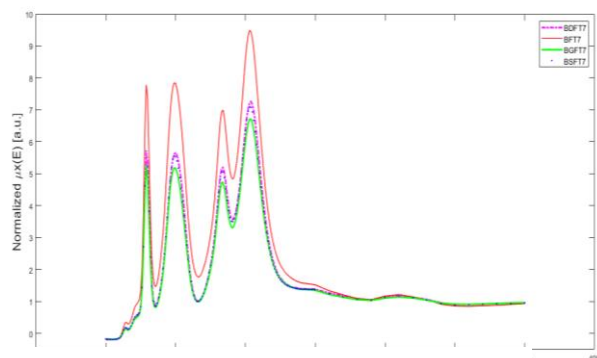


Fig. 1 The O:K edge XANES spectra.

In the presentation these results will be analysed in details, in particular with respect to the XAS spectral features and the corresponding electronic properties of the materials. Their relation to the multiferroic properties will be discussed.

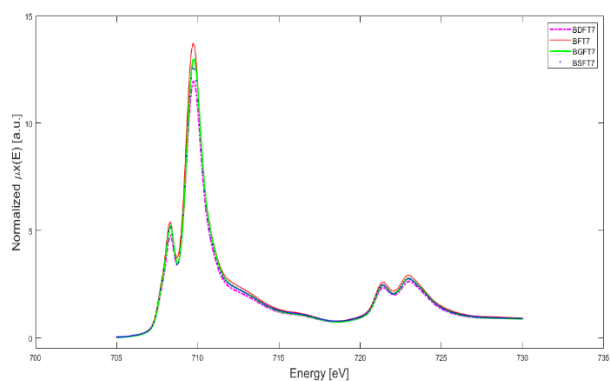


Fig. 2 The Ti:L_{2,3} edge XANES spectra.

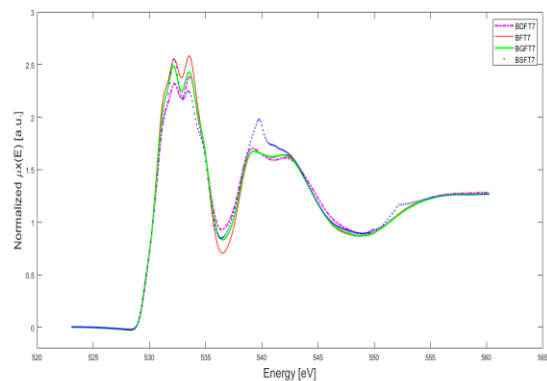


Fig. 3 The Fe:L_{2,3} edge XANES spectra.

Acknowledgements: Experiment was performed owing to the collaboration of SOLARIS Staff.

References

1. Aurivillius, B. *Arki. Kemi.* 1, 463 (1949).
2. Boullay, Ph., Troiliard, G. & Mercurio, D. J. *Solid State Chem.* 164, 252 (2002).
3. Zientara, D., Bućko, M. M. & Polnar, J. *Adv. Sci. Tech.* 67, 164 (2010).
4. Jartych, E., Pikula, T., Mazurek, M., Lisinska-Czekaj, A., Czekaj, D., Gaska, K., Przewoźnik, J., Kapusta, C. & Surowiec, Z. J. *Magn. Mater.* 342, 27 (2013).

Selective magnetometry of nanoparticles in solutions

Poster Presentation
Thursday 10.09.2020
15:20-16:30

J. Kuciakowski^{1,2}, A. Kmita¹, D. Lachowicz¹, M. Wytrwał-Sarna¹, K. Pitala^{1,2},
S. Lafuerza³, D. Koziej⁴, A. Juhin⁵, M. Sikora^{1*}

¹AGH University of Science and Technology, Academic Centre for Materials and Nanotechnology,
Al. Mickiewicza 30, 30-059 Krakow, Poland

²AGH University of Science and Technology, Faculty of Physics and Applied Computer Science,
Al. Mickiewicza 30, 30-059 Krakow, Poland

³European Synchrotron Radiation Facility, CS40220, 38043 Grenoble Cedex 9, France

⁴Institute of Nanostructure- and Solid State Physics, Center for Hybrid Nanostructures,
University of Hamburg, Luruper Chaussee 149, 22607 Hamburg, Germany

⁵Institut de Minéralogie, de Physique des Matériaux et de Cosmochimie (IMPMC), Sorbonne
Université, UMR CNRS 7590, Muséum National d'Histoire Naturelle, 4 Place Jussieu, 75005 Paris,
France

*e-mail: marcin.sikora@agh.edu.pl

Properties of magnetic nanoparticles (MNP) in solutions are routinely determined using volume magnetometry. Quantitative analysis of such measurements is often questioned by uncertainty in diameter (mean and distribution), concentration and chemical composition.

Here we discuss the possibility of application of 1s2p RIXS-MCD (magnetic circular dichroism in resonant inelastic x-ray scattering) for selective characterization of magnetic properties of iron oxide MNP in solution. RIXS-MCD is a photon-in photon-out spectroscopy probe. When probed with circularly polarized light at 1s excitation (K edge) and collecting 2p emission, it reaches the same final states as L-edge XMCD and similar magnetic contrast, but using hard X-ray photons. As such it is well suited for element and site selective volume magnetic measurements. In addition, (i) it simultaneously probe the K pre-edge structures sensitive to local coordination and charge, (ii) it is free from non-resonant background, which makes it well suited for selective probing of magnetic properties of nanoparticles.

We have applied RIXS-MCD to determine selective magnetization profiles of iron oxide nanoparticles dispersed in water solution. Measurements were performed at room temperature on spinel iron oxide, cobalt ferrite and zinc ferrite MNP with mean diameter of 5-10nm. Analysis of the spectral shape and magnetic contrast produced by this experiment enables an assessment of the site distribution and magnetic state of metal ions in the spinel phase. The dependence of the strongest feature of 1s2p RIXS-MCD, which is ascribed to tetrahedral Fe(III), was probed versus external magnetic field in the full magnetization loop. Comparison of the RIXS-MCD derived magnetization profiles with that of volume magnetization collected from the same solutions by means of VSM method shows a significant difference. Selective profiles are free from the negative slope component observed in volume magnetization at large field, which is associated with a strong diamagnetic contribution of the solvent. However, upon separation of superparamagnetic signal of particles from the diamagnetic signal of carrier liquid a good agreement is achieved.

The selective magnetization profile of particles as derived from the field dependence of dichroism empowers an estimation of particle size distribution. Furthermore, the new proposed methodology discriminates sizes that are below the detection limits of X-ray and light scattering probes and that are difficult to spot in TEM.

The selected physico-chemical properties and structural studies of two peroxidomolybdates.

Poster Presentation
Thursday 10.09.2020
15:20-16:30

A. Sławińska^{1*}, P. Serda², M. Oszajca², K. Pamin¹, W. Łasocha^{1,2}

¹Jerzy Haber Institute of Catalysis and Surface Chemistry, Polish Academy of Sciences, Krakow, POLAND;

²Faculty of Chemistry, Jagiellonian University, Gronostajowa 2, 30-387 Krakow, POLAND

*e-mail: slawinska@ikifp.edu.pl

Peroxidomolybdate are a subgroup of polyoxometalates(POMs). Such compounds with transition metals (Mo, W, V ect.) are important in the processes of catalytic oxidation of alcohols and sulfides, epoxidation, effluent treatment, pyrotechnics, hydrometallurgy and medicine¹. Hitherto, our group obtained a new compounds with pyridinocarboxylic acid (nicotinic acid N-oxide², picolinic acid N-oxide² and isonicotinic acid N-oxide³. Currently, we are working on obtaining a new organic-inorganic hybrid peroxidomolybdates with dicarboxylicpyridine acid.

This study presents crystal structure and selected physico-chemical properties of the newest two oxidoperoxidocompounds with isonicotinic acid N-oxide. The first compound is potassium salt: $K_2C_6H_4MoNO_8 \cdot H_2O$ (denoted as K-isoO) and the second ammonium salt: $(NH_4)_2(C_6H_4MoNO_8)_2 \cdot 2H_2O$ (NH₄-isoO). The structural study of compounds were investigated using powder X-ray diffraction (K-isoO) or single crystal (NH₄-isoO) techniques. To characterize compounds were examined with the use of XRPD versus temperature method, IR spectroscopy and catalytic activity studies³.

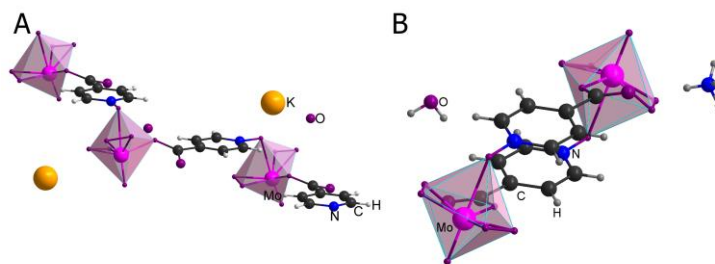


Fig. 1 Building blocks of K-isoO(A) and PMA-isoO(B).

Acknowledgements: AS acknowledges the fellowship with the project POWR.03.02.00-00-I013/16.

References

1. Szymańska, A., Nitek, W., Mucha, D., Karcz, R., Pamin, K., Połtowicz, J. & W. Łasocha, Structural studies and physico-chemical properties of new oxidoperoxomolybdenum complexes with nicotinic acid, *Polyhedron* 60, 39–46 (2013).
2. Sławińska, A., Serda, P., Pamin, K., Połtowicz, J. & Łasocha, W., Synthesis, crystal structure and selected properties of a group of new peroxomolybdates, *Polyhedron* 121, 191–198 (2017).
3. Sławińska, A., Serda, P., Oszajca, M., Pamin, K., Połtowicz, J. & Łasocha W. Synthesis, crystal structure and selected properties of two new peroxidomolybdates. *Polyhedron* 183, 0–6 (2020).

Electronic structure investigations of some cresols

Poster Presentation
Thursday 10.09.2020
15:20-16:30

M. A. Śmiałek^{1*}, D. Duflot², N. C. Jones³, S. V. Hoffmann³, N. J. Mason⁴,
P. Limão-Vieira⁵

¹Department of Control and Power Engineering, Faculty of Ocean Engineering and Ship Technology, Gdańsk University of Technology, Gabriela Narutowicza 11/12, 80-233 Gdańsk, Poland

²Univ. Lille, UMR 8523–Physique des Lasers Atomes et Molécules, F-59000 Lille, France

³ISA, Department of Physics and Astronomy, Aarhus University, Ny Munkegade 120, DK-8000 Aarhus C, Denmark

⁴School of Physical Sciences, University of Kent at Canterbury CT2 7NH, United Kingdom

⁵Laboratório de Colisões Atômicas e Moleculares, CEFITEC, Departamento de Física, Faculdade de Ciências e Tecnologia, Universidade NOVA de Lisboa, 2829-516 Caparica, Portugal

*e-mail: smialek@pg.edu.pl

The o-, m- and p-cresol isomers, also known as methylphenols or hydroxytoluenes, are toxic compounds widely used throughout industry as raw materials or in their chlorinated and nitrated forms to yield compounds with herbicidal and insecticidal properties. In other fields of application, o-cresol is used in the synthesis of epoxy resins, precursors of dye intermediates, pharmaceuticals and adducts for various synthetic purposes. They are also the basis of fragrance and flavour substances as well as disinfectants, preservatives, explosives and light-resistant antioxidants and dyes. Mixtures of cresols are used as lubricant additives, fire-resistant hydraulic fluids, and plastic additives. They are also formed by biotic and abiotic transformation of pesticides in agriculture. From there they readily contribute to the pollution of ground waters and the atmosphere. In the atmosphere in the presence of NO_x radicals, the degradation of these compounds in the troposphere contributes substantially to the ozone and photooxidant burden and also the formation of secondary organic aerosol. Cresol isomers have been reported to account for 15–42% of the products from the OH+toluene reaction with the level of about 20%. Thus obtaining a detailed information on the electronic structure throughout the photoabsorption measurements of these compounds is desired.

We support our experimental results with theoretical calculations thus obtaining a full description of the target molecule as in many previous studies of such targets. In the measured spectra it was also possible to detect the influence of the respective positions of the methyl and hydroxyl groups on the aromatic ring, making the spectra either resembling the ones of phenol or of toluene.

Here we present a comparison between the previously obtained data of phenol and toluene and the newly measured spectra of all three isomers supported by theoretical calculations.

Analysis of physico-chemical properties of nanolayers modified with low-energy Xe ions

Poster Presentation
Thursday 10.09.2020
15:20-16:30

R. Stachura^{1*}, A. Kubala-Kukuś^{1,2}, D. Banaś^{1,2}, I. Stabrawa^{1,2}, K. Szary^{1,2},
P. Jagodziński¹, G. Aquilanti³, I. Božičević Mihalić^{3,4}, J. Braziewicz^{1,2},
M. Pajek¹, J. Semaniak¹

¹Institute of Physics, Jan Kochanowski University, Uniwersytecka 7, 25-406 Kielce, Poland

²Holycross Cancer Center, Artwińskiego 3, 25-734 Kielce, Poland

³Elettra - Sincrotrone Trieste, s.s. 14, km 163.5 in Area Science Park, 34149 Basovizza, Trieste, Italy

⁴Rudjer Boskovic Institute, Bijenicka cesta 54, 10000 Zagreb, Croatia

*e-mail: regina.stachura@phd.ujk.edu.pl

Modification of metal, semiconductor and insulator surfaces by ion irradiation is of great importance for developing new technologies for manufacturing a small functional electronics system with nanometer dimensions. Due to the exhausting potential of currently used technologies, extensive research is carried out around the world to develop a new, repeatable and effective technologies for modifications of various material properties. One from such promising future technologies, which gives possibility for obtaining novel physico-chemical properties of materials, not achievable by any other material processing methods, is modification of materials surfaces by irradiation with low-energy (slow) highly charged ions (HCI)^{1,2}.

The main aim of this study is to determine the changes in morphology and physico-chemical properties of nanolayers caused by irradiation by low-energy Xe ions in highly charged states. In order to investigate the changes of nanolayer properties, as a result of the HCI irradiation, in dependence of their thicknesses and energies, surface sensitive X-ray spectroscopy methods can be applied. Before the irradiation process, the properties of nanolayers were measured by classical and grazing incidence X-ray diffraction (XRD and GIXRD) and classical X-ray reflectometry (XRR) carried out on the X'Pert Pro MPD [2]. The nanolayers were implanted with low-energy highly ionized Xe^{q+} ions at the Kielce EBIS facility (Jan Kochanowski University, Kielce, Poland). The SR-XRR measurements were performed at Elettra Synchrotron X-ray fluorescence beamline, using synchrotron X-ray beam with energy 6.0 keV^{3,4}.

In the presented studies X-ray reflectometry was used for characterization of morphology (density, thickness and roughness) of TiO₂ nanolayers, deposited on the substrate Si not implanted and implanted with Xe^{q+} ions. The first experimental results for TiO₂ nanolayers implanted with different charge states of the Xe^{q+} ions showed that thicknesses fitted from XRR curves by Direct and Fourier methods agree within the experimental uncertainty with declared values. As expected, it was found that the measured density of TiO₂ nanolayers (3.2 ± 0.3 g / cm³) is much lower than the bulk density of TiO₂ (3.78 g / cm³ - anatase, 4.23 g / cm³ - rutile).

Finally, the results obtained for irradiated samples suggest possible amorphization and smoothening of the TiO₂ nanolayers surface as a function of HCI potential energy⁴.

References

1. I. Stabrawa et al. Nucl. Instrum. Methods Phys. Res. B 408, 235 (2017).
2. I. Stabrawa et al. Thin Solid Films 671, 103 (2019).
3. D. Banaś, et al. Nucl. Instrum. Methods Phys. Res. B 354, 125-128 (2015).
4. R. Stachura et al. Acta Physica Polonica A 137, 38-43 (2020).

Examination of prospective chemotherapeutics with the use of the X-ray Absorption Spectroscopy

Poster Presentation
Thursday 10.09.2020
15:20-16:30

W. Stańczyk*, J. Czapla-Masztafiak, J. Szlachetko, W. Błachucki, A. Wach,
W.M. Kwiatek

Institute of Nuclear Physics Polish Academy of Sciences, PL-31342 Krakow, Poland

*e-mail: wiktoria.stanczyk@ifj.edu.pl

Platinum compounds, like cisplatin, are still widely used in a cancer treatment, despite the fact that some tumors do not respond to the treatment with their application. This led scientists to look for alternatives, including compounds with other metals. Copper complexes are one of those who are in the centre of interest, because they exhibit cytotoxic properties by inducing the cleavage of DNA and an apoptosis of cells¹. They could also overcome problems with which platinum drugs cannot deal.

Within this report, we demonstrate applicability of synchrotron and laboratory X-ray Absorption Spectroscopy (XAS) experiments² to study Cu-based materials. Unoccupied electronic structure of Cu(1,10-phenanthroline)Cl₂ compound is examined and the obtained results are supported with density of states calculations to determine the atomic contributions of ligands to Cu electronic states. Because of specific molecular geometry, the Cu(1,10-phenanthroline)Cl₂ complex is regarded as a potential candidate to coordinate to nitrogenous bases and in a consequence to break DNA at specific sites. The fundamental understanding of the electronic properties of this compound is thus crucial for any future application studies.

Acknowledgements: Authors acknowledge National Science Centre, Poland (NCN) for partial support under grant no. 2016/21/D/ST4/00378.

References

1. Barone, G., Terenzi, A., Lauria, A., Almerico, A. M., Leal, J. M., Busto, N., & Garcia, B. DNA-binding of nickel (II), copper (II) and zinc (II) complexes: Structure–affinity relationships. *Coordination Chemistry Reviews*, 257(19-20), 2848-2862 (2013).
2. Błachucki, W., Czapla-Masztafiak, J., Sá, J. & Szlachetko, J. A laboratory-based double X-ray spectrometer for simultaneous X-ray emission and X-ray absorption studies. *Journal of Analytical Atomic Spectrometry* 34, 1409 (2019).

A XAS study of $\text{Na}_{0.5}\text{Bi}_{0.5}\text{TiO}_3$ ferroelectric single crystal

Poster Presentation
Thursday 10.09.2020
15:20-16:30

D. Sitko¹, T. Strączek^{2*}, K. Goc², D. Pietruch², K. Schneider³, M. Dziubaniuk⁴,
M. Rękas⁴, Cz. Kapusta²

¹Pedagogical University, Institute of Physics, ul. Podchorążych 2, 30-084 Krakow, Poland

²AGH-University of Science and Technology, Faculty of Physics and Applied Computer Science, al. Mickiewicza 30, 30-059 Krakow, Poland

³AGH-University of Science and Technology, Faculty of Computer Science, Electronics and Telecommunications, al. Mickiewicza 30, 30-050 Krakow, Poland

⁴AGH-University of Science and Technology, Faculty of Materials Science and Ceramics, al. Mickiewicza 30, 30-059 Krakow, Poland

*e-mail: Tomasz.Straczek@fis.agh.edu.pl

$\text{Na}_{0.5}\text{Bi}_{0.5}\text{TiO}_3$ (NBT) is a complex $A'_{0.5}A''_{0.5}\text{TiO}_3$ perovskite exhibiting a random occupation of the A-site by the Na^{1+} and Bi^{3+} ions. Therefore, its properties, e.g. dielectric and phase transitions process, present diffuse character. On the other hand this structural disorder is responsible for excellent applied properties of this compounds. It may also be a reason of difficulties in definitive determination of symmetry of the low-temperature ferroelectric phase. Most of earlier studies pointed to the rhombohedral (R), rhombohedral with regions of tetragonal (T) symmetry, while some, more sensitive to local nanoscale order investigations, to the monoclinic (M) or monoclinic-rhombohedral coexistence (M-R) ones. Remembering these doubts, many researchers denote symmetry of the ferroelectric phase as rhombohedral R, similarly to that in¹.

Single crystals of NBT were grown by the Czochralski method, as described in². Powder reagents Na_2CO_3 (99.95%), Bi_2O_3 (99.95%) and TiO_2 (99.95%) were weighed in stoichiometric ratio and homogenized in agate mortar for 24 h with using of ethanol. Then the milled powders were dried and calcined at 800°C for 2h and at 1000°C for 4h. The calcined material was placed in a Pt crucible. The crystal growth was carried out at 1300°C. Slightly yellowish transparent cube shaped single crystals of 1.5 cm in size and resistivity of order of $10^{12} \Omega\text{cm}$ were obtained.

In the present work, the X-ray Absorption Spectroscopy study in the XANES range of the Oxygen K, and Titanium $L_{2,3}$ edges was performed at room temperature and 242°C. The latter is above the transition to the low temperature rhombohedral ferroelectric phase, which occurs at 220°C². The aim of the study was to determine possible changes in the electronic structure occurring at the transition. The measurements were carried out at the PEEM/XAS beamline of Solaris National Synchrotron Radiation Centre, Poland. The total electron yield (TEY) detection mode was used and the measurements were made with linearly polarized light in two geometries, providing the direction of the electric field vector of the exciting X-rays in the plane perpendicular to the c-axis of the crystal or at 60 degrees to this plane. The examples of the spectra obtained are shown in Figs 1, 2 for the $\text{Ti}:L_{2,3}$ XANES range at room temperature and 242°C.

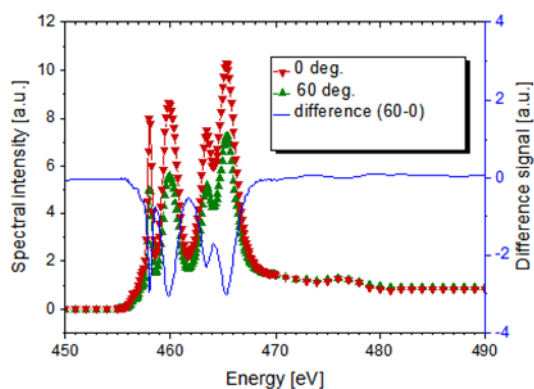


Fig. 1 The Ti: $L_{2,3}$ edge XANES spectra of the NBT sample at room temperature along with their difference.

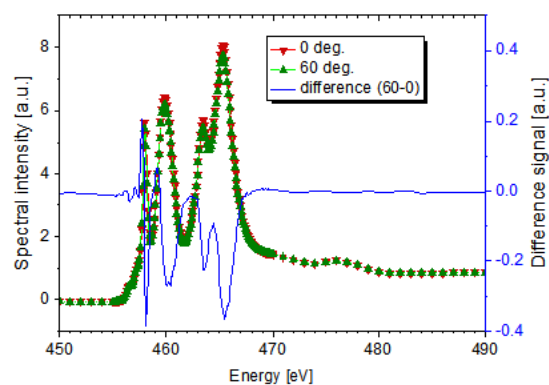


Fig. 1 The Ti: $L_{2,3}$ edge XANES spectra of the NBT sample at 242°C along with their difference.

The spectra show double-peak structures of the L_3 and L_2 edges at 458-460 eV and 463-466 eV, respectively. The difference of the spectra taken at 60 deg and 0 deg. reveals a significant dichroic effect in the rhombohedral ferroelectric phase (room temperature), whereas it is an order of magnitude smaller at 242°C, above the transition. A similar tendency is observed in the O:K XANES spectra. In the presentation the results obtained will be analysed in details, with respect to the XAS spectral features, in connection with local atomic environments and their modifications upon phase transition. Their relation to the ferroelectric properties of the material will be discussed.

Acknowledgements: Experiment was performed owing to the collaboration of SOLARIS Staff.

References

1. Aktas, O., Duclere, J. R., Quignon, S., Trolliard, S.G. & Salje, E. K. H. *Appl. Phys. Lett.* 113, 032901 (2018).
2. Suchanicz, J. & Kruzina, T.V. *Mat. Sci. Eng.* B178, 889 (2013).

Spectroscopic studies on sulfur speciation in soil active glasses

J. Sułowska*, A. Berezicka, M. Szumera

Poster Presentation
Thursday 10.09.2020
15:20-16:30

AGH University of Science and Technology, Faculty of Material Science and Ceramics,
al. Mickiewicza 30, 30-059 Kraków, Poland

*e-mail: sulowska@agh.edu.pl

Sulfur is one of the elements having the most important biochemical and physiological functions in the plant. Sulfur, apart from playing the role of essential component for growth and development of plants, has also an impact on increasing their resistance to various kinds of pathogens. However, proecological activities leading to sulfur emission reductions in the industry, conducted in recent years, as well as the increasing use of high-grade fertilizers led to the situation that in many soils sulfur is running out. The applied fertilizers that introduce sulfur to the soil are characterized by a large solubility in water, causing an easy leaching of this element from the upper layers of soil, which results in a low concentration of sulfate sulfur that can be absorbed by plants.

Thus, was conceived the idea of design of glassy materials containing sulfur as potential mineral fertilizers. But it's not that straightforward. First, because sulfur in oxide glasses may be present at different states of oxidation (S^{6+} , S^{4+} , S^0 , and S^{2-})¹ and, from the viewpoint of the agricultural practice the sulfur is absorbed by plant roots from the soil solution as the SO_4^{2-} anion mainly, therefore, it is essential that the structure of the designed glassy fertilizers would contain oxysulfur species as much as possible. Second, the developed glasses have a silicate-phosphate matrix, which has a limited capacity to receive sulfur.

X-Ray Absorption Spectroscopy especially is the best way to characterize the sulfur oxidation states and its environments in the structure of glasses^{1,2}. Sulfur K-absorption edges are especially sensitive to different sulfur valences, where edge energies increase with increasing valence^{2,3}. Because of difficult access to this method during the Meeting we would like to focus on discussing the results of spectroscopic studies on sulfur speciation in the silicate-phosphate glasses with a particular emphasis on Raman Spectroscopy and Magic Angle Spinning Nuclear Magnetic Resonance results on the basis of which certain but not all degree of sulfur oxidation present in the structure of the glasses can be determined.

Acknowledgements: This project was financed by the National Science Centre, Poland, project number 2018/31/D/ST8/03148.

References

1. Hirashima, H., Yoshida, T. & Brückner, R. Redox equilibria and constitution of polyvalent ions in oxide melts and glasses. *Glastechn. Ber. Glass Sci. Technol.* 68, 283-292 (1988).
2. McKeown, D. A., Muller, I. S., Gan, H., Pegg, I. L. & Stolte, W. C., Determination of sulfur environments in borosilicate waste glasses using X-ray absorption near-edge spectroscopy. *J. Non-Cryst. Solids* 333, 74-84 (2004).
3. Paris, E., Giuli, G. & Carroll, M. R., The valence and speciation of sulfur in glasses by X-Ray Absorption Spectroscopy. *The Canadian Mineralogist* 39, 331-9 (2001).

An XANES Investigation of the Electronic Structure of ZnO Films implanted by Yb

Poster Presentation
Thursday 10.09.2020
15:20-16:30

Y. Syryanyy^{1*}, M. Zając², E. Guzewicz³, R. Ratajczak¹, I.N. Demchenko⁴

¹National Centre for Nuclear Research, A. Soltana 7, 05-400, Otwock-Swierk, Poland

²Solaris National Synchrotron Radiation Centre, ul. Czerwone Maki 98, 30-392 Kraków

³Institute of Physics, Polish Academy of Sciences, Lotnikow Alley 32/46, 02-668, Warsaw, Poland

⁴University of Warsaw, Department of Chemistry, Pasteura 1 Str., 02-093, Warsaw, Poland

*e-mail: Yevgen.Syryanyy@ncbj.gov.pl

The electronic structure of ZnO:Yb epitaxial layers grown on GaN/sapphire substrates was studied using X-ray absorption spectroscopy at the Zn L_3 , O K and Yb M_5 edges at Solaris light source. Knowing that the ZnO crystallizes in an anisotropic wurtzite structure, the linear polarization of synchrotron radiation was exploited to estimate the influence of the crystal structure anisotropy on the distribution of the local density of states at the site of Zn and O. The calculated partial density of states describes the observed anisotropy in the measured spectra. Influence of the core-hole effect on the analyzed absorption spectra was verified.

Acknowledgements: These research took place at the National Synchrotron Radiation Centre SOLARIS, at the PEEM/XAS beamline. The experiment was performed thanks to collaboration of the SOLARIS Team. The work was partially supported by the Interdisciplinary Centre for Mathematical and Computational Modelling (ICM) at University of Warsaw, Poland, grant ID G59-20. The samples growth was co-financed by international project supported by the Polish Ministry of Science and Higher Education (3846/HZDR/2018/0) and Helmholtz-Zentrum Dresden-Rossendorf (17000941-ST).

A XAS study of ALD fabricated Fe oxide films

Poster Presentation
 Thursday 10.09.2020
 15:20-16:30

A. Szkudlarek^{1*}, T. Strączek², K. Goc², K. Schneider³, L. Ruśkiewicz², J. Stępień¹, I. Utke⁴, C. Kapusta²

¹AGH University of Science and Technology, Academic Centre for Materials and Nanotechnology, al. Mickiewicza 30, 30-059 Kraków, Poland

²AGH-University of Science and Technology, Faculty of Physics and Applied Computer Science, al. Mickiewicza 30, 30-059 Krakow, Poland

³AGH-University of Science and Technology, Faculty of Computer Science, Electronics and Telecommunications, al. Mickiewicza 30, 30-050 Krakow, Poland

⁴Empa - Swiss Federal Laboratories for Materials Science and Technology, Laboratory for Mechanics of Materials and Nanostructures, Feuerwerkerstrasse 39, CH - 3602 Thun, Switzerland

*e-mail: aleszkud@agh.edu.pl

Thin films of hematite are recently widely investigated materials due to their peculiar optical properties which are attractive for applications e.g. in photoelectrochemical cells¹ or lithium-ion batteries². In order to use the material as an anode in solar energy conversion the thin films made of it should have the thickness of the order of tens of nm. Such films can be fabricated using Atomic Layer Deposition (ALD). In this method the precursor gases are injected simultaneously into the reaction chamber and chemisorbed onto the surface. By alternating the gases, the thin films are grown layer by layer. Among various physical and chemical deposition techniques, it is a unique one, which allows to coat conformally 3D nanostructured surfaces. Whereas the protocols are well established for other materials such as ZnO, TiO₂, Al₂O₃, only few studies exist for Fe₂O₃.

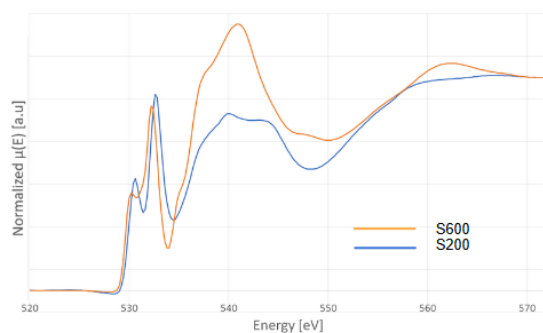


Fig. 1 .The O:K edge XANES spectra of the S200 and S600 samples.

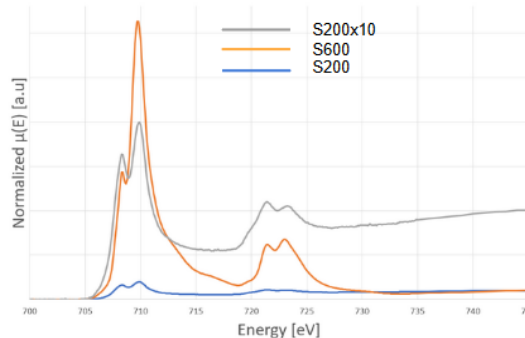


Fig. 2 The Fe:L_{2,3} XANES spectra of the S200 and S600 samples.

In this work we have been depositing the films using ferrocene and oxygen as precursor gases. The two investigated samples, deposited with different number of cycles (200 and 600) were characterized with X-ray diffraction and Moessbauer spectroscopy, which show a mixture of magnetite and maghemite phases for the thicker sample, S600 (600 deposition cycles). For the thinner sample, S200 (200 deposition cycles) which exhibit very weak and broadened diffraction lines possible coexistence of maghemite and hematite is found. In order to get a deeper insight into the nature of the Fe oxides in these thin films the X-ray Absorption Spectroscopy study in the XANES range of the Oxygen K and Iron L_{2,3} edges has been carried out. The measurements were performed at the PEEM/XAS beamline of Solaris National

Synchrotron Radiation Centre, Poland. The total electron yield (TEY) detection mode was used and the spectra were collected at room temperature. The spectra are shown in Fig. 1 for the O:K edge and Fig. 2 for the Fe:L_{2,3} edges. In the poster the analysis of the spectral details will be presented in relation to those of the spectra of reference Fe oxides: magnetite, maghemite and hematite. The results obtained and the differences observed between the thinner and the thicker sample will be discussed in terms of their relation to the substrate impact. Conclusions on the possible way of tuning of the ALD fabrication procedure to obtain hematite films will be drawn.

Acknowledgements: This work was supported by the Polish National Science Centre NCN (2015/17/D/ST3/00968) Experiment was performed owing to the collaboration of SOLARIS Staff.

References

1. Bora, D. K., Braun, A. & Constable, E. C. "In rust we trust". Hematite – the prospective inorganic backbone for artificial photosynthesis. *Energy Environ. Sci.* 6, 407-425 (2013).
2. Lv, X., Deng, J., Wang, J., Zhong, J. & Sun, X. Carbon-coated α -Fe₂O₃ nanostructures for efficient anode of Li-ion battery. *J. Mater. Chem. A* 3, 5183-5188 (2015).

Development of methods and instrumentation for applied X-ray research

Poster Presentation
Thursday 10.09.2020
15:20-16:30

J. Szlachetko*, W. Błachucki, J. Czapla-Masztafiak, A. Wach, R. Fanselow, K. Tyrała, W. Stańczyk, K. Wojtaszek and W. Kwiatek*

Institute of Nuclear Physics, Polish Academy of Sciences, 31-342 Kraków, Poland

*e-mail: jakub.szlachetko@ifj.edu.pl, wojciech.kwiatek@ifj.edu.pl

The Department of Applied Spectroscopy (NZ53) at the Institute of Nuclear Physics of the Polish Academy of Sciences aims at exploring diverse X-ray methods to study material's electronic structure. The research is performed with laboratory setups, synchrotrons and X-ray free electron lasers, and is oriented in three main research activities. First, we are studying changes taking place in biological systems at the cellular and molecular level and specifically looking towards DNA damage-repair mechanisms and interactions of metal-centered molecules with DNA. Secondly, we are looking on changes in the electronic structure of atoms during chemical transformations of molecules and disordered systems with main focus on performing research on chemical processes in real time. Finally, we are also investigating fundamental interactions of X-rays with matter, such as non-linear processes and mechanisms leading to sequential and multiple ionizations of atoms. Research with X-ray free electron lasers includes also developments of new methods and experimental schemes for femto-second X-ray research. In the poster, we will present our recent activities and developments in laboratory as well as results obtained at synchrotrons and XFELs. Several examples will be shown, where application of X-rays was crucial to specifically approach the project and to answer important scientific questions.

Acknowledgements: This work was supported by the National Science Centre (Poland) under the grants of numbers 2017/27/B/ST2/01890, 2016/21/D/ST4/00378, 2019/03/X/ST3/00035, 2015/18/E/ST3/00444, 2019/03/X/ST3/00035 and 2019/03/X/ST2/00949.

References

1. Błachucki, W., Czapla-Masztafiak, J., Sá, J. & Szlachetko J. A laboratory-based double X-ray spectrometer for simultaneous X-ray emission and X-ray absorption studies. *J Anal At Spectrom* 34, 1409 (2019).
2. Kayser, Y. et al. Core-level nonlinear spectroscopy triggered by stochastic X-ray pulses. *Nat. Commun.* 10, 4761 (2019).
3. Wojtaszek, K. et al. The influence of nitrogen doping on the electronic structure of the valence and conduction band in TiO₂. *J Synchrotron Radiat* 26, 145-151 (2019).
4. Tyrała, K. et al. Cross-section determination for one- and two-photon absorption of cobalt at hard-x-ray energies. *Phys Rev A* 99, 052509 (2019).
5. Smolentsev G. et al. Taking a snapshot of the triplet excited state of an OLED organometallic luminophore using X-rays. *Nat. Commun.* 11, 2131 (2020).
6. Wach A. et al. In situ Observation of Charge Transfer and Crystal Field Formation with High- Energy Resolution X-ray Spectroscopy during Temperature Programmed Oxidation. *Phys. Chem. Chem. Phys.* 22, 14731-14735 (2020).

Synchrotron studies on double perovskite cobaltites

I. Szpunar*, A. Witkowska, S. Wachowski, M. Gazda, A. Mielewczyk-Gryń

Poster Presentation
Thursday 10.09.2020
15:20-16:30

Department of Solid State Physics, Faculty of Applied Physics and Mathematics, Gdansk University of Technology, Gdansk, Poland

*e-mail: iga.lewandowska@pg.edu.pl

Double perovskite cobaltites, with general formula $\text{BaLnCo}_2\text{O}_{6-\delta}$ (Ln = lanthanide), have gained much attraction due to their varied magnetic and electrical properties and many potential applications. In this group ferromagnets, antiferromagnets or even spin glasses may be found¹. A large variety of properties results from the variable nature of cobalt, which can be on +2, +3, and +4 oxidation state. What is more, cobalt can be differently coordinated in the structure and exhibit different spin states. The multitude of variable cobalt parameters makes it difficult to analyze and tailor the properties of these materials.

This work aims at the detailed description of the fundamental physical properties of $\text{BaA}_{1-x}\text{A}^{\text{II}}_x\text{Co}_2\text{O}_{6-\delta}$ (A = La, Pr, Nd, Gd). X-ray absorption spectroscopy (XAS) was used to determine the the spin state of cobalt and lanthanide (Fig. 1). This study was supported by structural characterization by the means of Synchrotron Radiation Powder X-ray Diffraction (SR-PXD). The average cobalt oxidation state was determined by the means of iodometric titration. The combination of those techniques enabled the determination of all cobalt features.

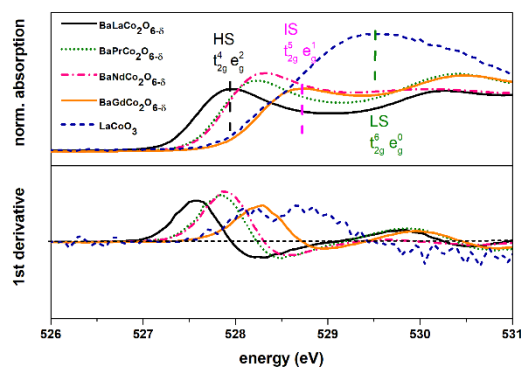


Fig. 1 X-ray absorption spectra of oxygen K-edge in the Co 3d bands region. For comparison low spin (LaCoO_3) reference sample is included.

Acknowledgements: Authors would like to acknowledge CERIC-ERIC Consortium for the access to MCX beamline at Elettra Sinchrotrone Trieste (proposal no 20187079), Solaris National Radiation Centre Poland for access to the XAS/PEEM beamline (proposal no 181MS001). The research has been supported by the National Science Centre Poland (2016/22/Z/ST5/00691) through the M-ERA.NET Joint Call 2016.

References

1. Nakajima, T., Ichihara, M. & Ueda, Y. New A-site ordered perovskite cobaltite $\text{LaBaCo}_2\text{O}_6$: Synthesis, structure, physical property and cation order-disorder effect. *J. Phys. Soc. Japan* 74, 1572–1577 (2005).

Revisiting properties of $\text{CaCoSi}_n\text{O}_{2n+2}$. Magnetism and electronic structure.

Poster Presentation
Thursday 10.09.2020
15:20-16:30

M. Szubka^{1*}, P. Zajdel¹, M. Fijałkowski¹, E. Talik¹, A. Balerna², M. Cestelli-Guidi²,
M. Romani², J. Łażewski³, P.T. Jochym³

¹Institute of Physics, University of Silesia, ul. 75 Pułku Piechoty 1, PL-41-500, Chorzów, Poland

²INFN-Laboratori Nazionali di Frascati, Via E. Fermi 40, Frascati, I-00044, Italy

³Institute of Nuclear Physics, PAS, ul. Radzikowskiego 152, PL-31-342, Kraków, Poland

*e-mail: magdalena.szubka@us.edu.pl

In a public space¹ there are several reports of materials with general stoichiometry $\text{CaCoSi}_n\text{O}_{2n+2}$. For $n=2$ it is a known pyroxene $\text{CaCoSi}_2\text{O}_6$ ^{2,3}. However, not much is known about materials with $n=3$ and $n=4$, which seem to be analogous to known pigments $\text{CaCuSi}_n\text{O}_{2n+2}$.

In this study several attempts were carried out to synthesize those phantom materials and it was found that they do not exist as a single phase. A quantitative XRD analysis revealed that their stoichiometry is correct but the formula should be written as $\text{CaCoSi}_2\text{O}_6 + (n-2)\text{SiO}_2$. Similar qualitative conclusions were drawn from investigation of magnetic (DC magnetometry) and electronic properties including XPS and Si K edge XANES. Additionally we have carried out DFT ab initio calculations to obtain electronic signature from band structure of $\text{CaCoSi}_2\text{O}_6$.

The apparent influence of the excess of SiO_2 on magnetic properties of this "series" can be understood in terms of presence of secondary phases like $\text{Ca}_2\text{CoSi}_2\text{O}_7$, which form when the starting materials are not homogenized properly. Addition of surplus SiO_2 suppresses their formation leaving clear signature from $\text{CaCoSi}_2\text{O}_6$, which also can be synthesized from stoichiometric mixture using proper techniques.

Acknowledgements: The research leading to these results received funding from the European Community Horizon 2020 research and innovation program under the grant agreement N. 730872 project CALIPSOPlus

References

1. German Patent <http://www.freepatentsonline.com/DE10121871.html> (2002).
2. Mantovani, L., Tribaudino, M., Dondi, M. & Zanelli, C. Synthesis and color performance of $\text{CaCoSi}_2\text{O}_6$ pyroxene, a new ceramic colorant. *Dyes Pigm.* 120, 118-125 (2015).
3. Durand, G., Vilminot, S., Rabu, P., Derory, A., Lambour J. P. & Ressouche, E. Synthesis, structure, and magnetic properties of CaMSi_2O_6 (M = Co, Ni) compounds and their solid solutions. *Journal of Solid State Chem.* 124, 374-380 (1996).

ARPES studies of transition metal / topological crystalline insulator interface

Poster Presentation
Thursday 10.09.2020
15:20-16:30

B. Turowski^{1*}, O. Caha², N. Olszowska³, J. Kołodziej³, T. Wojtowicz¹,
G. Springholz⁴, V.V. Volobuev¹

¹International Research Centre MagTop, Institute of Physics, Polish Academy of Sciences, Aleja Lotników 32/46, PL-02668 Warsaw, Poland

²Masaryk University, Kotlářská 2, 61137 Brno, Czech Republic

³National Synchrotron Radiation Centre SOLARIS, Jagiellonian University, Czerwone Maki 98, PL-30392 Kraków, Poland

⁴Institute of Semiconductor and Solid State Physics, Johannes Kepler University Linz, Altenbergerstr. 69, A-4040 Linz, Austria

*e-mail: turowski@ifpan.edu.pl

Topological insulator / magnetic material heterostructures are considered to be efficient materials for charge-spin interconversion¹. However, the important question how an adjacent material with uncompensated magnetic moments affects topological surface states (TSS) remains relatively unexplored. In this work, we studied band structure on transition metal (TM) / topological crystalline insulator (TCI) interface by angular resolved photoemission spectroscopy (ARPES).

TCI $\text{Pb}_{1-x}\text{Sn}_x\text{Se}$ epilayers were prepared by MBE on (111) BaF_2 and (001) KCl substrates. The evolution of ARPES spectra was investigated as a function of thickness of deposited Mn and Fe TMs (Fig. 1,2).

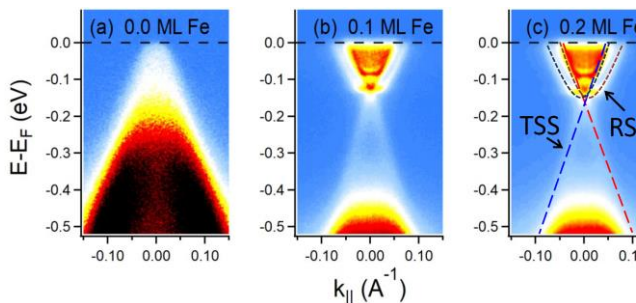


Fig. 1 Evolution of ARPES spectra of (111) $\text{Pb}_{0.75}\text{Sn}_{0.25}\text{Se}$ epilayer as a function of submonolayer Fe deposition.

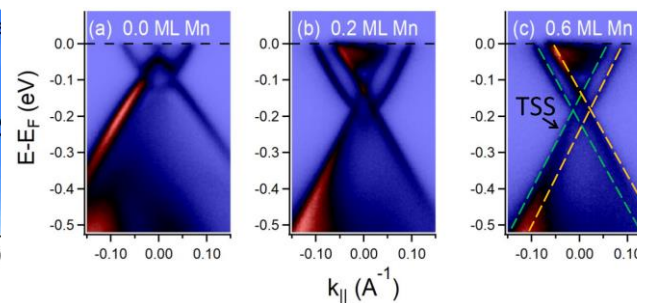


Fig. 2 Evolution of ARPES spectra of (001) $\text{Pb}_{0.76}\text{Sn}_{0.26}\text{Se}$ epilayer as a function of submonolayer Mn deposition.

Despite theoretical predictions, no band gap opening was observed². However, formation of Rashba splitted surface states (RSS) was detected in conduction band for (111) oriented samples. Estimated Rashba parameter α_R can be tuned over a wide range from 0 to $1.5 \text{ eV}\cdot\text{\AA}$ as a function of deposited TM. For (001) oriented films, decrease of separation in k -space between Dirac points of the double Dirac cone was observed. The reasons of band structure modification with TM deposition will be discussed.

Acknowledgements: The work is supported by the Foundation for Polish Science through the IRA Programme co-financed by EU within SG OP. We thank NSRC SOLARIS for beamtime allocation.

References

1. Han W., Otani Y. C. & Maekawa S. Quantum materials for spin and charge conversion. npj Quantum Mater. 3, 1-16 (2018).
2. Reja, S., Fertig, H. A., et al. Surface magnetism in topological crystalline insulators. Physical Review B 96, 201111 (2017).

One- and two-photon below threshold cross-sections mechanisms and atomic number and energy dependences

Poster Presentation
Thursday 10.09.2020
15:20-16:30

K. Tyrała*, J. Czapla-Masztafiak, A. Wach, K. Wojtaszek, W. Błachucki,
W. M. Kwiatek, J. Szlachetko

Institute of Nuclear Physics Polish Academy of Sciences, 31-342 Krakow, Poland

*e-mail: krzysztof.tyrala@ifj.edu.pl

Below threshold one-photon scattering is an inelastic process that involves core-shell electron excitation with incident photon energy lower than the ionization threshold of given element. This effect was observed for the first time in 1974 and explained shortly after^{1,2}. The mechanism of this phenomenon is mediated by the intermediate virtual state, making possible the electron excitation above Fermi level with the expense of the X-ray fluorescence photon energy. The physical properties of the virtual state are important due to the connection with sequential two-photon absorption process (TPA) that exploits the same intermediate state. Taking this into consideration, the relations between the cross-sections for both processes can be investigated which make possible to estimate the TPA cross-sections based on the one-photon data³.

For many years the off-resonant excitations at below threshold energies were observed by use of monochromatized radiation from X-ray tubes^{1,4,5} or synchrotrons⁶⁻¹⁰. Yet, the cross-sections values were determined so far only for a few elements, usually by means of low energy resolution measurements. Herein we report the comprehensive studies on the cross-section values for below edge ionization energies of various elements. Based on the obtained results, we will discuss cross-sections dependences on energy and atomic number for both, one and two-photon absorption mechanisms.

Acknowledgments: This work was partially supported by National Science Centre, Poland (NCN) under grant no. 2017/27/B/ST2/01890

References

1. Sparks, C. J. Phys. Rev. Lett. 33, 65 (1974).
2. Bannet, Y. B. & Freund, I. 34, (1974).
3. Szlachetko, J., et al. Sci. Rep. 6, 33292 (2016).
4. Hamalainen, K., et al. J. Phys.: Condens. Matter 1, 5955 (1989).
5. Suortti, P. Phys. Status Solidi 91, 657 (2018).
6. Sánchez, H. J., Valentinuzzi, M. C. & Pérez, C. J. Phys. B At. Mol. Opt. Phys. 39, 4317 (2006).
7. Briand J. P. et al. Phys. Rev. Lett. 46, 1625 (1981).
8. Manninen, S., Suortti, P., Cooper, M. J., Chomilier, J. & Loupías G. Phys. Rev. B 34, 8351 (1986).
9. Szlachetko, J. et al. Phys. Rev. Lett. 97, 73001 (2006).
10. Tyrała, K. et al. Phys. Rev. A, 99, 052509 (2019).

Sequence of structural phase transitions in $\text{Pr}_{0.9}\text{Ca}_{0.1}\text{AlO}_{2.95}$

L. Vasylechko*, V. Hreb

Poster Presentation
Thursday 10.09.2020
15:20-16:30

Lviv Polytechnic National University, Lviv, Ukraine

*e-mail: Leonid.O.Vasylechko@lpnu.ua

Calcium doped praseodymium orthoaluminate $\text{Pr}_{0.9}\text{Ca}_{0.1}\text{AlO}_{2.95}$ was prepared from stoichiometric amounts of constituent oxides Pr_6O_{11} , Al_2O_3 , and calcium carbonate CaCO_3 by solid-state reaction technique. According to *in situ* low-temperature X-ray synchrotron powder diffraction examinations (HASYLAB/DESY, B2 beamline), $\text{Pr}_{0.9}\text{Ca}_{0.1}\text{AlO}_{2.95}$ undergoes reversible discontinuous structural phase transitions from rhombohedral $R\text{-}3c$ to the orthorhombic $Imma$ structure at 210 K and from orthorhombic to monoclinic $I2/m$ structure at 130 K. Analysis of high-temperature behavior of $\text{Pr}_{0.9}\text{Ca}_{0.1}\text{AlO}_{2.95}$ revealed that rhombohedral $R\text{-}3c$ structure persists at least up to 1173 K. From extrapolation of c/a parameter ratio of the rhombohedral phase a second-order phase transition to the cubic perovskite structure is predicted in $\text{Pr}_{0.9}\text{Ca}_{0.1}\text{AlO}_{2.95}$ at around 1490 K, which is *ca* 280 K lower comparing with the “pure” PrAlO_3 ¹. Evolution of unit cell dimensions of $\text{Pr}_{0.9}\text{Ca}_{0.1}\text{AlO}_{2.95}$ in the temperature range of 10–1173 K is shown in Fig. 1.

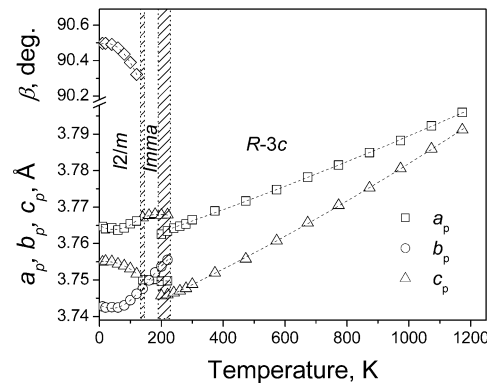


Fig. 1 Temperature dependencies of normalized lattice parameters of $\text{Pr}_{0.9}\text{Ca}_{0.1}\text{AlO}_{2.95}$. The monoclinic (M), orthorhombic (O) and rhombohedral (Rh) lattice parameters are normalized to the perovskite cell (P) as follow: $a_p = a_m/\sqrt{2}$, $b_p = b_m/2$, $c_p = c_m/\sqrt{2}$; $a_p = a_o/\sqrt{2}$, $b_p = b_o/2$, $c_p = c_o/\sqrt{2}$; $a_p = a_r/\sqrt{2}$, $c_p = c_r/\sqrt{12}$. $a_p = a_r/\sqrt{2}$, $c_p = c_r/\sqrt{12}$.

Acknowledgements: The work was supported in parts by the Ministry of Education and Sciences of Ukraine under the Project N 0118U000264 (DB/Feryt) and ICDD Gant-in-Aid program. Authors would like to thank D. Trots and A. Berghäuser for kind assistance and support during the synchrotron diffraction experiments.

References

1. Vasylechko, L., Senyshyn, A. & Bismayer, U. Perovskite-type aluminates and gallates. in: Handbook on the physics and chemistry of rare earths, Vol. 39 (eds. Gschneidner, K. A., Jr., Bünzli, J.-C. G., Pecharsky, V. K.) 113–295 (North-Holland-Elsevier, 2009).

In situ observation of metal-to-semiconductor transition by high-resolution X-ray spectroscopy techniques

Poster Presentation
Thursday 10.09.2020
15:20-16:30

A. Wach*, W. Błachucki, J. Czapla-Masztafiak, W. M. Kwiatek, J. Szlachetko

Institute of Nuclear Physics Polish Academy of Sciences, Krakow, Poland

*e-mail: anna.wach@ifj.edu.pl

The tungsten-based materials due to their large variety of compositions, crystal structures, physical and chemical properties are relevant for many technological applications such as optoelectronics, catalysis, sensors, energy conversion and storage^{1,2}. Their functional properties originate from the outer d-valence electrons and thereby are very sensitive to the electronic band structure of central transition metal. Thus, knowledge about the electronic structure of tungsten element, especially orbital contribution and relative energy position of the highest occupied (valence band) and the lowest unoccupied states (conduction band) is crucial for design of innovative and efficient tungsten-based materials.

In the present study, we demonstrate the capability of the high-energy resolution X-ray spectroscopy to investigate electronic structure of metallic tungsten and tungsten (VI) oxide. The occupied (valence band) and the unoccupied (conduction band) electronic states were probed by a combination of valence-to-core X-ray emission (v2c-XES) and high-resolution X-ray absorption (HR-XAS) techniques, respectively³. Moreover, the process of unoccupied electronic states reconfiguration during the transition from metallic W to semiconductor WO₃ was studied under in situ conditions by time-resolved RXES spectroscopy⁴. Application of the high energy resolution schemes allowed us to follow splitting of the tungsten 5d states into the t_{2g} and e_g orbitals by the crystal field of the surrounding oxygen atoms. Based on the time-resolved studies, it was possible to determine the charge transfer between the metallic centre and bonding oxygen atoms during thermal oxidation of metal.

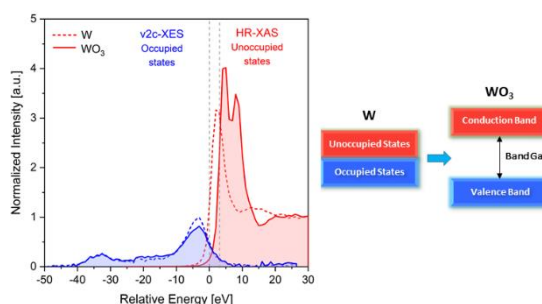


Fig. 1 Comparison of X-ray emission and X-ray absorption spectra collected for W and WO₃ samples.

Acknowledgements: Authors would like to acknowledge the National Science Centre, Poland (NCN) for partial support under grants no. 2015/18/E/ST3/00444 and 2019/03/X/ST3/00035.

References

1. Wang, S., Fan, W., Liu, Z., Yu, A. & Jiang, X. H, J. Mater. Chem. C 6, 191 (2018).
2. Zhu, T., Chong, M.N. & Chan E.S., ChemSusChem 7, 2974 (2014).
3. Wach, A., Sá, J. & Szlachetko, J., J. Synchrotron Rad. 27, 689 (2020).
4. Wach, A., Błachucki, W., Czapla-Masztafiak, J., Abreu Fernandes, D.L., Banaś, D., Wojtaszek, K., Tyrala, K., Kwiatek, W.M., Sá, J. & Szlachetko, J., Phys.Chem.Chem.Phys. 22, 14731 (2020).

Electronic Properties of Multi-Layer of Graphene Oxide Moderately Annealed in Vacuum obtained using compact laser-plasma based NEXAFS system

Poster Presentation
Thursday 10.09.2020
15:20-16:30

T. Fok^{1‡}, K. A. Janulewicz^{1‡}, P. Wachulak^{1*}, B. Nasiłkowska¹, A. Bartnik¹,
J. Kostecki¹, M. Djas², K. Ławniczak-Jabłońska³, P. Kuzmiuk³, B. Budner¹,
H. Fiedorowicz¹

¹ Institute of Optoelectronics, Military University of Technology, 2 Kaliskiego Str., 00-908 Warsaw, Poland

² Institute of Electronic Materials Technology, 133 Wólczyńska Str., 01-919 Warsaw,

³ Institute of Physics, Polish Academy of Sciences, Al. Lotników 32/46, 02-668 Warsaw, Poland

‡ - These authors contributed equally.

* e-mail: wachulak@gmail.com

This contribution will discuss the NEXAFS and EXAFS spectroscopy systems developed recently at the Institute of Optoelectronics of the Military University of Technology, which are based on laser-plasma compact sources of soft X-ray radiation (SXR, wavelength of 0.1-10nm) with a double stream gas puff target. The characterization of these systems and their applications for the examination of exemplary organic and inorganic samples will be presented, as well as the combination of spectroscopic technique with scanning microscopy, i.e. spectromicroscopy.

In particular, we will discuss the experiment concerning the influence of the annealing temperature of graphene oxide (GO) on its physicochemical changes, measured by a combination of NEXAFS and the analysis of data from the XPS¹. The fact, that there are still serious discrepancies concerning dependency of the GO electronic structure on the production technique and the used precursor material, is the main reasons for undertaking such investigation, and will be presented in this paper. The striking similarity of some of the GO NEXAFS spectrum features to those present in the spectrum of the crystalline graphite is surprising and in contradictions to other features typical for GO suggesting some sort of the sample "graphitization".

References

1. Fok, T., Janulewicz, K.A., Wachulak, P., Nasiłkowska, B., Kostecki, J., Djas, M., Ławniczak-Jabłońska, K., Kuzmiuk, P., Budner, B., Bartnik, A., Fiedorowicz, H., Electronic Properties of Multi-Layer Graphene Oxide Moderately Annealed in Vacuum, in preparation (2020).

Anisotropy in the Fermi surface of Non-Magnetic semimetal TaAs₂

Poster Presentation
Thursday 10.09.2020
15:20-16:30

A. Wadge^{1*}, G. Grabecki², K. Dybko^{1,2}, B. J. Kowalski², N. Olszowska³, J. Kołodziej³,
P. Iwanowski^{1,2}, A. Hruban², A. Wiśniewski^{1,2}

¹International Research Centre MagTop, Institute of Physics, Polish Academy of Sciences, Aleja
Lotnikow 32/46, PL-02668 Warsaw, Poland

²Institute of Physics, Polish Academy of Sciences, Aleja Lotnikow 32/46, PL-02668 Warsaw, Poland

³National Synchrotron Radiation Centre SOLARIS, Jagiellonian University, Czerwone Maki 98, PL-
30392 Kraków, Poland

*e-mail: wadge@magtop.ifpan.edu.pl

Conducting materials with extremely large magnetoresistance are interesting from the point of view of applications in various magneto-electronic devices. Recently, it was found that non-magnetic semimetal, TaAs₂, exhibits non-saturated magnetoresistance as large as 10⁵, in the magnetic field range up to 9 T. This is a result of nearly compensated electron-hole character of the conductance of this system¹. We have confirmed this by using mobility spectrum analysis (Fig. 1 a) which is very useful tool for studies of various multi-carrier conducting systems². Additionally, we observe multi-carrier Shubnikov-De Haas (SdH) oscillations whose periods shows pronounced band anisotropy (Fig. 1 b). The band anisotropy is reflected in the preliminary results of ARPES studies of our TaAs₂ crystals (Fig. 1 c), and the more detailed studies are underway.

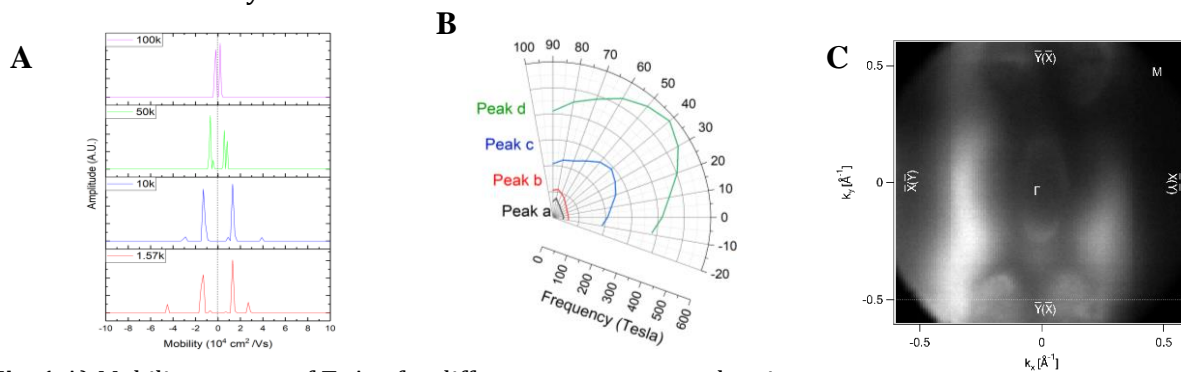


Fig. 1 A) Mobility spectra of TaAs₂ for different temperatures showing up to 6 types of conducting carriers in the material. Positive mobility values indicate electrons, negative-holes. B) Polar plot showing anisotropy of the four different SdH oscillation periods C) ARPES image obtained on (1 0 -1) TaAs₂ surface, freshly cleaved in ultra-high vacuum.

Acknowledgements: The research was partially supported by the Foundation for Polish Science through the IRA Program co-financed by the European Union within SGOP.

References

1. Butcher, T.A., Hornung, J., Förster, T., Uhlarz, M., Klotz, J., Sheikin, I., Wosnitza, J. and Kaczorowski, D., Fermi surface investigation of the semimetal TaAs 2. *Physical Review B*, 99(24), p.24511 (2019).
2. Grabecki, G., Dąbrowski, A., Iwanowski, P., Hruban, A., Kowalski, B.J., Olszowska, N., Kołodziej, J., Chojnacki, M., Dybko, K., Łusakowski, A. and Wojtowicz, T., Conductance spectra of (Nb, Pb, In)/NbP superconductor/Weyl semimetal junctions. *Physical Review B*, 101(8), p.085113 (2020).

Dissociative photo-double-ionization of the isoxazole molecules

Poster Presentation
Thursday 10.09.2020
15:20-16:30

T. J. Wasowicz^{1*}, A. Kivimäki^{2,3}, R. Richter⁴

¹Department of Physics of Electronic Phenomena, Gdansk University of Technology,
ul. G. Narutowicza 11/12, 80-233 Gdansk, Poland

²Nano and Molecular Systems Research Unit, University of Oulu, 90014 Oulu, Finland

³MAX IV Laboratory, Lund University, 22100 Lund, Sweden

⁴Elettra-Sincrotrone Trieste, 34149 Trieste, Italy

*e-mail: tomasz.wasowicz1@pg.edu.pl

The five-membered heterocyclic rings are incorporated into a wide variety of structures that play a vital role in many biochemical processes. In particular, the isoxazole molecule appears in many bioactive compounds due to its unique ring structure that consists of one oxygen atom and one nitrogen atom at adjacent positions. The unique atomic composition and bond arrangement of isoxazole imply its specific electronic properties that may be probed by diverse spectroscopic techniques, including those utilizing synchrotron radiation. In particular, the photoelectron-photoion coincidence (PEPICO) technique provides detailed information about the presence of specific bonds, the reactivity of these molecules, as well as their electronic structure and decomposition mechanisms.

Therefore in the present communication, we present results on the photo-double-ionization and fragmentation of isoxazole molecule. The experiments were carried out at the CiPo beamline at the Elettra-Sincrotrone radiation facility exploiting the VUV excitation and the ion time-of-flight spectrometry combined with the PEPICO technique. The dissociative processes where only one electron is emitted are quite well known¹. However, double ionization is a more complex mechanism producing the doubly charged parent ion after the emission of two correlated electrons. These doubly charged ions are usually very reactive objects that can dissociate into the ionic fragments. PEPICO method gives the coincidence maps plotted as the arrival time of the first ion and that of the second one, with respect to the instance of detection of one of the photoelectrons (see Fig. 1a). As a result, the pairs of correlated ions show up as areas with a higher density of points. The calculation of the coincidence events in these “islands” gives information about the particular fragmentation channel (see Fig. 1b).

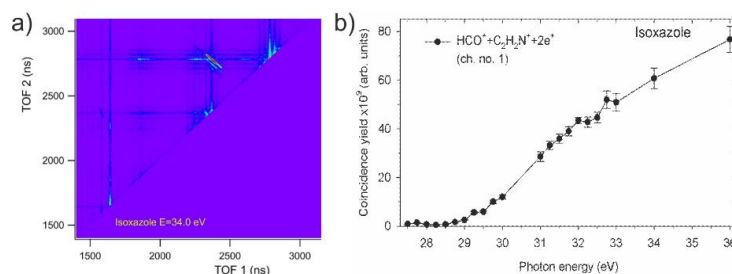


Fig. 1 a) The coincidence map of isoxazole. b) Coincidence yield of the major fragmentation channel.

Acknowledgements: We are grateful to the Elettra-Sincrotrone Trieste for providing beamtime no. 20165364. Staying of TJW in Elettra was financially supported by COST Action CM1204 XLIC (COST-STSM-CM1204-36527).

References

1. Wasowicz, T. J. et al. Int. J. Mass Spectrom. 449, 116276 (2020).

Tracking changes in electronic structure in real-time during temperature-induced oxidation of titanium

Poster Presentation
Thursday 10.09.2020
15:20-16:30

K. Wojtaszek*, A. Wach, W. Błachucki, K. Tyrała, J. Czapla-Masztafiak,
W. M. Kwiatek J. Szlachetko

Institute of Nuclear Physics Polish Academy of Sciences, 31-342 Krakow, Poland

*e-mail: klaudia.wojtasze@ifj.edu.pl

Thanks to the unique possibility to probe the highest occupied and the lowest unoccupied states in matter X-ray emission spectroscopy (XES) and X-ray absorption spectroscopy (XAS) are becoming increasingly used methods to study the formation of band structures in semiconductor and photocatalytic materials. In particular, rapid chemical processes that occur during the process of photocatalyst formation, can be studied using synchrotron radiation sources.

In the present study, a combination of valence-to-core XES and XAS spectra was used to determine changes in the electronic structure during temperature-induced oxidation of titanium at ambient atmosphere and range of temperatures (30°C - 800°C)¹. In situ measurements for Ti K edge were performed at the SuperXAS beamline at the Swiss Light Source Synchrotron (Villigen, Switzerland) using custom-made cell designed for thermal studies under different atmospheres². Analysis of the obtained data allowed to track formation of the band gap, determine oxidation state of titanium at various stages and observe the mechanism of crystalline form formation. The experimental data were compared with theoretical calculations of the DOS performed with the FEFF9.0 program. Finally, our studies were aimed at understanding the kinetics of the anatase-to-rutile transformation which is of great importance for TiO₂ applications.

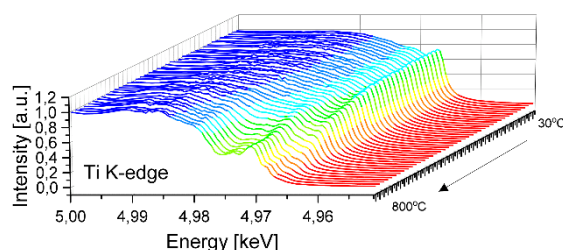


Fig. 1 XAS signal evolution during temperature-induced oxidation of metallic titanium from 30°C to 800°C.

Acknowledgements: Authors would like to acknowledge National Science Centre, Poland (NCN) for partial support under grant no. 2015/18/E/ST3/00444.

References

1. Wojtaszek, K., Wach, A., Czapla-Masztafiak, J., Tyrała, K., Sa, J., Ozer, Y., Garlisi, C., Palmisano, G. & Szlachetko, J. The influence of nitrogen doping on the electronic structure of the valence and conduction band in TiO₂. *J. Synchrotron Rad.* 26, 145–151(2019).
2. Wojtaszek, K., Tyrała, K. & Wach, A., Custom-Made Cell Designed for Thermal Studies and In Situ X-Ray Spectroscopy Experiments. *Acta Phys. Pol.* 137, 54-58 (2020).

Structural studies of selected PrP peptides – interactions of mutated octarepeat with zinc ions

Poster Presentation
Thursday 10.09.2020
15:20-16:30

J. Wolak^{1*}, M. Taube¹, A. Szymańska³, M. Kozak^{1,2}

¹Faculty of Physics, Adam Mickiewicz University in Poznań, Poland

²Faculty of Chemistry, University of Gdańsk, Gdańsk, Poland

³NCPS Solaris, Jagiellonian University, Kraków, Poland

*e-mail: joanna.wolak@amu.edu.pl

Human prion protein (PrP^C) is a glycosylated membrane protein, occurring physiologically in nervous system. This protein, in its pathologically misfolded form, also known as scrapie-form (PrP^{Sc}), is involved in the development of “prion-like” neurodegenerative diseases (transmissible encephalopathies)¹. Previous studies show that divalent cations, like Cu²⁺, Zn²⁺, cause significant structural changes of PrP^C molecule, and induce its aggregation^{2,3}. A specific octarepeat sequence, containing four histidine residues and located in N-terminal domain of PrP, exhibits a strong ability to coordinate some divalent ions^{2,4}.

The aim of our study was to examine the ability of the prion protein fragment (PrP58-93), containing native octarepeat sequence or its subsequent point mutants with histidine residues substituted by alanine, to form complexes with zinc ions. The structure of these systems was analysed using small angle X-ray scattering (SAXS) and circular dichroism spectroscopy (CD). Experimental structural parameters were compared with theoretical models obtained by the molecular dynamics simulation and the modelling. Moreover, the influence of zinc ions on the conformation of studied prion peptide (PrP58-93) and its mutants was examined by using CD spectroscopy.

Acknowledgements: This work was supported in part by the research grant (2014/15/B/ST4/04839) from the National Science Centre (Poland).

References

1. Lee, I. Y. et al. Complete Genomic Sequence and Analysis of the Prion Protein Gene Region from Three Mammalian Species. *Genome Res.* 8, 1022–1037 (1998).
2. Viles, J. H. et al. Copper binding to the prion protein: Structural implications of four identical cooperative binding sites. *Proc. Natl. Acad. Sci.* 96, 2042–2047 (1999).
3. Evans, E. G. B. & Millhauser, G. L. Copper- and Zinc-Promoted Interdomain Structure in the Prion Protein: A Mechanism for Autoinhibition of the Neurotoxic N-Terminus. in *Progress in Molecular Biology and Translational Science* vol. 150 35–56 (Elsevier, 2017).
4. Gielnik, M. et al. PrP (58–93) peptide from unstructured N-terminal domain of human prion protein forms amyloid-like fibrillar structures in the presence of Zn²⁺ ions. *RSC Adv.* 9, 22211–22219 (2019).

X-ray absorption fine structure study on bioactive Cu(II) complex with thiourea derivative in organic solvents

Poster Presentation
Thursday 10.09.2020
15:20-16:30

A. Wolska*, A. Drzewiecka-Antonik, M.T. Klepka, P. Rejmak

Institute of Physics, Polish Academy of Sciences, Al. Lotnikow 32/46, 02-668 Warsaw, Poland

*e-mail: wolska@ifpan.edu.pl

Metal complexes with organic ligands are widely studied due to their potential bioactive properties. Among them there are the copper complexes containing thiourea moiety. They are studied to be used as anticancer chemotherapeutics, antimicrobial drugs and neuroprotective agents for curing Alzheimer disease. In this communication the structural study of the Cu(II) complex with 1,3-disubstituted thiourea derivative is presented. In order to get structural information on the studied compound the X-ray absorption fine structure (XAFS) spectroscopy was used. XAFS is an ideal tool to investigate compounds regardless on their form or state. It can be used to powders, as well as to solutions. The XAFS measurements were performed at Elettra (XAFS beamline). The powder sample was measured in the transmission mode, the solutions in the fluorescence one. Common organic solvents such as dimethyl sulfoxide (DMSO) and dimethylformamide (DMF) were used. The analysis of the XAFS of the powder complex revealed two S and two N atoms in the first coordination sphere¹. Subsequently the solutions were examined. The aim was to investigate whether the presence of the solvent molecules modifies the structure. It was already observed that DMSO as well as DMF molecules can modify the coordination sphere of metal cation and change the structure of a bioactive compound². The investigations revealed that the complex in the DMSO solution didn't undergo major structural changes. However, in case of the DMF solution, changes in the shape of the XANES spectrum indicate that the solvent interacts with part of the complexes and the reduction of Cu(II) to Cu(I) is observed.

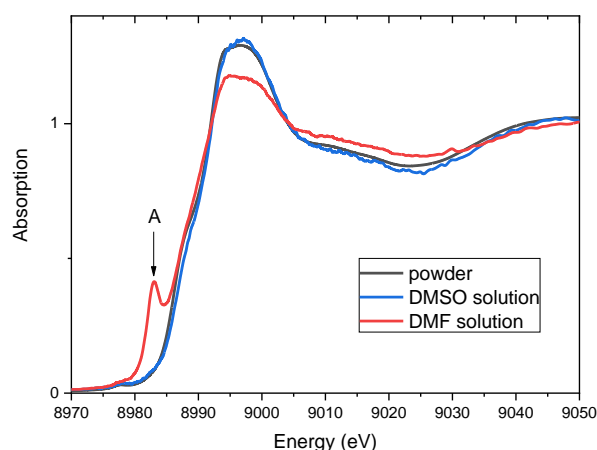


Fig. 1 XANES spectra of the powder complexes and the solutions. Peak A is characteristic for Cu(I) compounds.

References

1. Drzewiecka-Antonik, A., Rejmak, P., Klepka, M.T., Wolska, A., Pietrzyk, P., Stępień, K., Sanna, G. & Struga, M. J. *Inorg. Biochem.* 176, 8 (2017).
2. Klepka, M.T., Wolska, A., Drzewiecka-Antonik, A., Rejmak, P., Hatada, K. & Aquilanti, G., *Chem. Phys. Lett.* 673, 113 (2017).

Insight into precursor effects in selected superconducting stannides

Poster Presentation
Thursday 10.09.2020
15:20-16:30

P. Zajdel^{1*}, M. Fijałkowski¹, A. Ślebarski¹, A. Balerna², M. Cestelli-Guidi²,
M. Romani²

¹Institute of Physics, University of Silesia, ul. 75 Pułku Piechoty 1, PL-41-500, Chorzów, Poland

²INFN-Laboratori Nazionali di Frascati, Via E. Fermi 40, Frascati, I-00044, Italy

*e-mail: pawel.zajdel@us.edu.pl

The competition and coexistence of charge density wave (CDW) and superconductivity (SC) are one of the most important topics in the recent years¹. Multiple CDW forms are predicted to exist well above the T_{SC} although they are typically limited to a static CDW. Dynamic or gliding CDWs are very difficult to observe^{1,2} and their signatures are weak and hard to interpret.

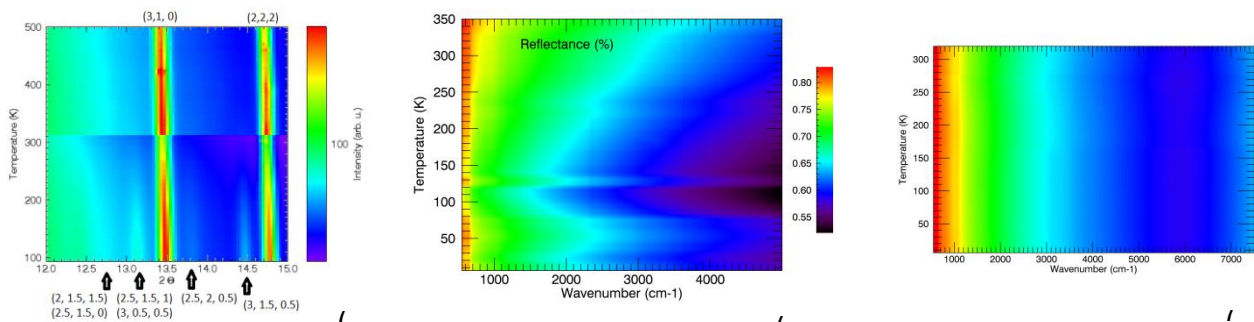


Fig. 1 Precursor effect in $\text{Ca}_{0.2}\text{La}_{2.8}\text{Rh}_4\text{Sn}_{13}$ seen in (a) XRD (SNBL) and (b) reflectivity (DAFNE-Light) compared to (c) no CDW in $\text{Ca}_3\text{Rh}_4\text{Sn}_{13}$

In our recent studies^{2,3}, new precursor effects were observed in several SC stannides as multiple weak perturbations of diffraction patterns (Fig. 1a). In order to obtain corroborating evidence, a Mid-IR measurements were also carried out correlating well with existence (b) or lack (c) of anomalies in other properties. The use of synchrotron sources is here of paramount importance due to limited mass of samples and weak character of the phenomena.

Acknowledgements: The research leading to these results received funding from the European Community Horizon 2020 research and innovation program under the grant agreement N. 730872 project CALIPSOPlus. We thank the Kosciuszko Foundation (New York) for the partial support of the research. We would like to thank the SNBL(ESRF) staff for their help in collecting the data.

References

1. Arpaia, R., Caprara, S., Fumagalli, R., De Vecchi, G., Peng, Y. Y., Andersson, E., Betto, D., De Luca, G. M., Brookes, N. B., Lombardi, F., Salluzzo, M., Braicovich, L., Di Castro, C., Grilli, M. & Ghiringhelli, G. Dynamical charge density fluctuations pervading the phase diagram of a Cu-based high- T_c superconductor, *Science* 365, 906-910 (2019).
2. Ślebarski, A., Zajdel, P., Fijałkowski, M., Maška, M. M., Witas, P., Goraus, J., Fang, Y., Arnold, D. C. & Maple, M. B. The effective increase in atomic scale disorder by doping and superconductivity in $\text{Ca}_3\text{Rh}_4\text{Sn}_{13}$, *New J. Phys.* 20, 103020 (2018).
3. Ślebarski, A., Zajdel, P., Maška, M.M., Deniszczyk, J. & Fijałkowski, M. Superconductivity of $\text{Y}_5\text{Rh}_6\text{Sn}_{18}$ Coexistence of the high temperature thermal lattice relaxation process and superconductivity *Journal of Alloys and Compounds* 819, 152959 (2020).

Interactions between amyloid-beta peptides, human serum albumin and human cystatin C studied by the use of X-ray and light scattering, NMR spectroscopy and bioinformatics

Poster Presentation
Thursday 10.09.2020
15:20-16:30

A. Żyła^{1,2*}, A. Szymańska³, J. Wolak¹, M. Taube¹, D. Grobys¹, E. Banachowicz¹, I. Zhokov⁴, M. Kozak^{1,5}

¹ Department of Macromolecular, Physics. Faculty of Physics, Adam Mickiewicz University, Poznań, Poland

² NanoBioMedical Centre, Adam Mickiewicz University, Poznań Poland

³ Department of Biomedical Chemistry, Faculty of Chemistry, Gdansk University, Gdańsk, Poland

⁴ Institute of Biochemistry and Biophysics Polish Academy of Sciences, Warszawa, Poland

⁵ SOLARIS National Synchrotron Radiation Centre, Jagiellonian University, Kraków, Poland

*e-mail: adrzyl@amu.edu.pl

Neurodegeneration process observed during the development of Alzheimer disease is associated with the formation of amyloid deposits, containing A β peptides, in human brain. However, in last years it was observed that human serum albumin (HSA) and, probably, human cystatin C (HCC) could inhibit or slow down the aggregation process of A β peptides and formation of amyloid¹⁻³.

The goal of our studies was to characterize the the interactions in a binary system involving HCC and HSA and a ternary system HSA/HCC with selected A β peptides. Therefore we used a combination of dynamic light scattering, nuclear magnetic resonance spectroscopy, NMR diffusometry, small angle X-ray scattering and molecular dynamics studies for estimation of the model of interactions between these proteins. Among others the SAXS profiles obtained for HSA/HCC monomer (V58G variant) were used for parametrization of NMR modelling. Moreover, we characterized also long-term dimerization process of HCC in solution.

Based on docking studies, molecular dynamics and experimental structural parameters a theoretical models of interactions between A β peptides and HCC molecule and also between HCC and HSA molecules were proposed.

Acknowledgements: P. Czaplowska is acknowledged for MS experiment carried out under her supervision. The studies were supported by research grant 2017/27/B/ST4/00485 from National Science Centre. Adriana Żyła acknowledge also a financial support of POWR.03.02.00-00- I032/16.

References

1. Castello M. A. & Soriano, S. On the origin of Alzheimer's disease. Trials and tribulations of the amyloid hypothesis. Ageing Res Rev 13, 10-12 (2014).
2. Choi, T. S. et al. Molecular Insights into Human Serum Albumin as a Receptor of Amyloid- β in the Extracellular Region. J. Am. Chem. Soc. 139, 15437-15445 (2017).
3. Spodzieja M. et al. Interaction of serum amyloid A with human cystatin C-identification of binding sites. J Mol Recognit. 25, 513-524 (2012).

Wybrane zagadnienia synchrotronowej absorpcyjnej spektroskopii rentgenowskiej (SXAS)

A. Kisiel^{1*}

¹*Instytut Fizyki im. Mariana Smoluchowskiego, Uniwersytet Jagielloński, 30-348 Kraków*

*e-mail: andrzej.kisiel@uj.edu.pl

Przedstawiono przykłady zastosowania promieniowania synchrotronowego w rentgenowskiej spektroskopii absorpcyjnej (SXAS). Szczególną uwagę poświęcono wynikom badań struktury subtelnej rentgenowskiej krawędzi absorpcji (XANES) niektórych związków półprzewodnikowych grupy II-VI, związków chemicznych pierwiastków na różnym stopniu utlenienia oraz wybranym związkom międzymetalicznym. Zaprezentowano również zastosowanie analizy struktury subtelnej powyżej krawędzi absorpcji rentgenowskiej (analiza EXAFS) do badania struktury lokalnej tetraedrycznie uporządkowanych potrójnych związków półprzewodnikowych.

Selected topics of the Synchrotron X-ray Absorption Spectroscopy (SXAS)

Abstract: The applications of the synchrotron radiation to the X-ray Absorption Spectroscopy (XAS) has been presented. The attention has been devoted to the X-Ray Absorption Near Edge Structure (XANES) analysis of the II-VI semiconductor compounds, chemical compounds with elements at various oxidation states and the selected class of the intermetallic compounds. Moreover, the application of the Extended X-ray Absorption Fine Structure (EXAFS) analysis to study the local structure of the ternary compound has been presented.

DOI:
10.36184/SRNS.2020.20.099
Received: 25.08.2020
Published: 09.11.2020
PACS; SXAS, XANES, EXAFS.
Binary and ternary
semiconductors and intermetallic
compounds

Wstęp

Promieniowanie synchrotronowe użyte do badań naukowych ponad 70 lat temu, znalazło szerokie zastosowanie w badaniach spektroskopowych we wielu dziedzinach nauk przyrodniczych. Udział ten widać w fizyce i chemii ciała stałego, biologii molekularnej i niektórych dziedzinach nauk medycznych. Zostały uzyskane nadzwyczaj wartościowe wyniki badawcze w fizyce i chemii układów uporządkowanych (kryształy, ciekłe kryształy) oraz nieuporządkowanych (materiały amorficzne, polimery) z uwzględnieniem dyfrakcyjnych metod rentgenowskiej analizy struktury krystalicznej i dynamiki przemian fazowych w funkcji temperatury i ciśnienia. Po zastosowaniu promieniowania synchrotronowego do badań nastąpił istotny postęp w fizyce i chemii polimerów, koloidów, membran biologicznych, jak również w analizie powierzchni i międzypowierzchni (ang. interfaces) oraz w układach niskowymiarowych takich jak nanostruktury, studnie i kropki kwantowe. Cenne rezultaty zostały uzyskane w biologii molekularnej (struktura przestrzenna atomów w dużych molekułach) oraz w analitycznych działach medycyny (diagnostyka czynników kancero-

gennych w komórkach organizmu ludzkiego, mammografia itp.). Wśród metod badawczych stosowanych z użyciem promieniowania synchrotronowego ważną rolę odgrywa synchrotronowa absorpcyjna spektroskopia rentgenowska (Synchrotron X-ray Absorption Spectroscopy (SXAS)) dostarczająca ważnych informacji o strukturze elektronowej pasma przewodnictwa w ciele stałym, a także o tzw. strukturze lokalnej struktury krystalicznej mieszanych roztworów stałych. Ten artykuł jest znacznie zmodyfikowaną i rozszerzoną wersją fragmentu publikacji¹, poświęconej zastosowaniu promieniowania synchrotronowego w spektroskopii ciała stałego.

Absorpcja promieniowania rentgenowskiego w ciele stałym

W ciele stałym złożonym z odpowiednio uporządkowanych atomów, elektrony z atomowych powłok elektronowych (stanów rdzeniowych), w wyniku pochłaniania promieniowania synchrotronowego, są wzbudzone rezonansowo do odpowiednich stanów pasma przewodnictwa, tworząc krawędź rentgenowską i nałożoną na nią strukturę przy-krawędziową XANES (X-ray Absorption Near Edge Structure)

oraz ponad krawędzią absorpcji rentgenowskiej zazwyczaj oscylacyjną strukturę nazywaną potocznie strukturą EXAFS (Extended X-ray Absorption Fine Structure).

Elektryczne dipolowe przejścia elektronowe z powłok elektronowych do pasma przewodnictwa, podlegają znanym ze spektroskopii atomowej dipolowym regułom wyboru, $\Delta L = \pm 1$ i $\Delta J = 0, \pm 1$. Zatem elektrony wzbudzone ze stanów rdzeniowych o określonych liczbach kwantowych do zhybrydowanej gęstości stanów pasma przewodnictwa mogą wypełniać tylko te stany kwantowe, które spełniają przytoczone powyżej spektroskopowe reguły wyboru. Przejścia wyższych połowicy np. elektryczne kwadrupolowe i magnetyczne dipolowe, są rządzone innymi regułami wyboru, jednakże jako przejścia dwa lub trzy rzędy wielkości mniej prawdopodobne, nie będą rozpatrywane w dalszym ciągu rozważań. W myśl reguł dipolowych, elektrony rdzeniowe wybierają w paśmie przewodnictwa jedynie stany opisane funkcjami falowymi o określonej parzystości to znaczy, że wybierają tzw. rzutowane gęstości stanów. Krawędzie absorpcyjne K , leżące w obszarze energii rentgenowskich, odpowiadają przejściom z najniższego stanu rdzeniowego $1s^2$ do stanów rzutowanych gęstości stanów w paśmie przewodnictwa, opisanych antysymetrycznymi funkcjami falowymi typu p (reguła Laporte). Krawędzie absorpcji L , dla których konfiguracją podstawową są stany rdzeniowe $2s^2 2p^6$ opisują liczby kwantowe: moment orbitalny $L = 0, \pm 1$, spin elektronu $S = \pm 1/2$ i moment całkowity $J = L + S = 0, \pm 1/2$ i $\pm 3/2$. Krawędź absorpcji L_1 jest wynikiem przejścia, podobnie jak w przypadku krawędzi K , ze stanu rdzeniowego $s_{\pm 1/2}$ do rzutowanych gęstości stanów $p_{1/2}$ i $p_{3/2}$ pasma przewodnictwa. Łatwo zauważyć wynikające z tego podobieństwo struktury przykrawędziowej krawędzi K i L_1 . Krawędzie L_2 i L_3 są odpowiednio rezultatem przejść ze stanu rdzeniowego $p_{1/2}$ do rzutowanych gęstości stanów $s_{1/2}$ i $d_{3/2}$, oraz stanu $p_{3/2}$ do rzutowanych gęstości stanów $s_{1/2}$ i $d_{5/2}$. Elementy macierzowe przejść $s_{-1/2} \rightarrow p_{1/2}$ i $s_{+1/2} \rightarrow p_{3/2}$ są różne wskutek różnych oddziaływań spinów z momentem orbitalnym (pochłanianie światła prowadzi do polaryzacji spinu elektronów i konieczności uwzględnienia tej polaryzacji w opisie krawędzi absorpcji).

W wyniku oddziaływania synchrotronowej fali

elektromagnetycznej z elektronem w powłoce elektronowej atomu, współczynnik absorpcji $\mu(\omega)$ i urojona część stałej dielektrycznej $\varepsilon_2(\omega)$ są opisane wzorami zaczerpniętymi z publikacji^{1,2}.

$$\mu(\omega) = \frac{4\pi^2 e^2}{ncm^2 \omega} |eM_{(c,v)}|^2 J_{(c,v)}(\hbar\omega) \cong A J_{(c,v)}(\hbar\omega) \quad (1)$$

$$\varepsilon^2(\omega) = \frac{4\pi^2 e^2}{ncm^2 \omega^2} |eM_{(c,v)}|^2 J_{(c,v)}(\hbar\omega) \cong \frac{A}{\omega} J_{(c,v)}(\hbar\omega) \quad (2)$$

gdzie

$$J_{(c,v)}(\hbar\omega) = \int_{BZ} \left(\frac{2dk}{(2\pi)^3} \right) \delta(E_c - E_v - \hbar\omega) \quad (3)$$

$J_{cv}(\hbar\omega)$ jest nazywana funkcją łącznej gęstości stanów JDOS (Joint Density of States), która opisuje zmieszane cechy gęstości stanów pasma walencyjnego względnie atomowego stanu rdzeniowego oraz pasma przewodnictwa. Wzory (1), (2) i (3) są stosowane w analizie przejść elektronowych z pasma walencyjnego względnie atomowych stanów rdzeniowych do pasma przewodnictwa a także do analizy dozwolonych przejść elektronowych w niektórych klasach materiałów amorficznych. Rozszerzenie stosowalności tych wzorów można uzyskać zastępując Ψ_v przez funkcję falową dowolnego stanu początkowego Ψ_i (również np. stanu rdzeniowego), Ψ_c przez funkcję falową stanu końcowego Ψ_f a elementy macierzowe przejścia $|M_{v,c}|$ przez elementy macierzowe $|M_{fi}| = \langle \Psi_f | e^{i\mathbf{k}\cdot\mathbf{r}} \mathbf{e} \cdot \mathbf{p} | \Psi_i \rangle$. Analizując wzór (3) na funkcję łącznej gęstości stanów J_{vc} dochodzimy do konkluzji, że w przypadku, gdy energia stanu początkowego jest funkcją słabo zależną od wektora falowego \mathbf{k} , lub jest stała czyli niezależna od \mathbf{k} , wtedy pochodna (gradient) funkcji $E_i(\mathbf{k})$ jest równa 0. W takim przypadku funkcja J_{vc} zależy tylko od gęstości stanów końcowych $E_f(\mathbf{k})$ DOS (Density of States,) to znaczy od DOS pasma przewodnictwa. Z tego wynika, że współczynnik absorpcji promieniowania rentgenowskiego $\mu(E)$ opisuje tzw. złota reguła

$$\mu(E) = |M_{fi}|^2 \rho(E) \quad (4)$$

gdzie $|M_{fi}|^2$ jest powyżej zdefiniowanym elementem macierzowym oddziaływania stanu początkowego i końcowego, a $\rho(E)$ gęstością stanów pasma przewodnictwa. Równanie (4) ma szerokie zastosowanie w absorpcyjnej spektroskopii rentgenowskiej, w której są analizowane przejścia z leżących głębiej atomowych stanów rdzeniowych do położonych wyżej stanów rdzeniowych (przejścia oznaczone

K_{α} , K_{β} , L_{α} , L_{β} , itp.) względnie do odpowiednich stanów pasma przewodnictwa (przejścia oznaczone K , L , M itp.).

Jak wspomniano wcześniej w obszarze XANES współczynnik absorpcji gwałtownie wzrasta, tworząc ostrą krawędź absorpcji rentgenowskiej, będącą wynikiem rezonansowego wzbudzenia elektronów z powłok rdzeniowych K , L , M itp. do stanów powyżej energii poziomu Fermiego tzn. do jego wyższych pasm powyżej dna pasma przewodnictwa. W związku z tym na krawędź absorpcji i obszar przy-krawędziowy nakłada się bogata struktura subtelna. Wzbudzenie elektronów do stanów niezajętych pasma przewodnictwa jest opisane, zgodnie z równaniem (4) przez rozkład gęstości stanów energetycznych pasma przewodnictwa $\rho(E)$. Rozkład ten, obliczany teoretycznie, można potwierdzić doświadczalnie przez pomiar współczynnika absorpcji krawędzi rentgenowskiej i obszaru przy-krawędziowego. Atomowe stany rdzeniowe³ posiadają określoną szerokość energetyczną a rozkład energetyczny stanów opisuje funkcja rozkładu Lorentza. Każdy elektronowy stan rdzeniowy posiada określoną pół-szerokość energetyczną Γ , czyli szerokość w połowie wysokości rozkładu Lorentza. Energetyczna szerokość lorentzowska jest związana z czasem życia wzbudzonego stanu elektronowego Δt zasadą nieoznaczoności Heisenberga $\Delta E \cdot \Delta t < \hbar$. Z tej relacji wynika, że im krótszy jest czas życia stanu elektronowego w stanie wzbudzenia, tym większa jest jego pół-szerokość energetyczna. Powyższe cechy stanów rdzeniowych wpływają na stromość rentgenowskiej krawędzi absorpcji. Jeżeli założyć, że elektron zostaje wzbudzony ze stanu rdzeniowego opisanego rozkładem Lorentza do pasma przewodnictwa o gęstości stanów stałej i niezależnej od energii, oznacza że w takim paśmie przewodnictwa zachowuje się jak elektron swobodny. W takim przypadku całkowita absorpcja $\mu(E)$ będąca sumą współczynników absorpcji lorenzowskich oscylatorów elementarnych opisuje formuła

$$\mu(E) = \int_0^{\infty} \left[\frac{B(E')}{1 + 4 \left[\frac{E-E'}{\Gamma} \right]^2} \right] dE' \quad (5)$$

gdzie $B(E')$ jest słabo zmienną funkcją energii. Wobec tego można przyjąć, że $B(E') = const$. Po scałkowaniu wzór (5) przyjmie postać

$$\mu(E) = \frac{1}{2} + \frac{1}{\pi} \arctan \left(\frac{2E}{\Gamma} \right) \quad (6)$$

Stąd wynika, że teoretycznie przewidywana krawędź rentgenowska dla elektronów swobodnych jest opisana przez gładką funkcję \arctg ⁴. Przytoczone rozważania teoretyczne Richtmyer i współpracownicy⁵ potwierdzili doświadczalnie analizując krawędzie rentgenowskie L_1 , L_2 i L_3 metalicznego złota. W złocie rozkład gęstości stanów elektronowych w paśmie przewodnictwa praktycznie nie zależy od energii i wobec tego elektrony wzbudzone z poziomów rdzeniowych do pasma przewodnictwa odtwarzają z niewielkim błędem zachowanie elektronów swobodnych. Punkt przegięcia na krzywej \arctg jest związany z położeniem energii poziomu Fermiego ośrodka pochłaniającego i wobec tego określa położenie krawędzi absorpcji względem poziomu próżni. Punkt przegięcia łatwo wyznaczyć ponieważ w tym punkcie pierwsza pochodna krzywej absorpcji ma największą wartość (maksimum). Struktura subtelna widma XANES, która pojawia się zwykle wokół rzeczywistej krawędzi absorpcji rentgenowskiej, jest rezultatem nałożenia się rozkładu gęstości stanów charakterystycznych dla pasma przewodnictwa analizowanego materiału na rozkład gęstości stanów elektronów swobodnych w paśmie przewodnictwa. Często w praktyce ze względu na występowanie również struktury przy-krawędziowej na stromości krawędzi absorpcji, jest wygodnie porównywać widma absorpcji odnosząc je, nie do punktu przegięcia zmodyfikowanego nałożoną strukturą subtelną, ale do pierwszego maksimum powyżej stromości krzywej absorpcji. To maksimum jest nazywane z motywów historycznych białą linią. Badanie struktury subtelnej przy krawędzi absorpcji rentgenowskiej (XANES) odsłania bogactwo struktury elektronowej pasma przewodnictwa i zatem służy do cennej charakteryzacji własności elektronowych fazy skondensowanej.

Struktura subtelna nałożona na rentgenowską krawędź absorpcyjną (struktura XANES)

Analiza struktury subtelnej rentgenowskiej krawędzi absorpcyjnej (XANES), różnych rentgenowskich krawędzi absorpcji, dostarcza unikatowych informacji o odpowiednich udziałach rzutowanych gęstości stanów w całkowitej gęstości stanów pasma przewodnictwa badanych materiałów. Zapewnia to pełniejszą weryfikację danych eksperymentalnych z teoretycznie obliczoną strukturą elektro-

nową pasma przewodnictwa. Położenie i kształt krawędzi absorpcji w widmie XANES zależy od kilku istotnych czynników wymagających bardziej szczegółowego omówienia.

Istotnym i nie elementarnym problemem poprawnych teoretycznych obliczeń rozkładu gęstości stanów⁶ jest uwzględnienie w obliczeniach oddziaływania wzbudzanego elektronu z utworzoną dziurą po elektronie. Uwzględnienie tego oddziaływania istotnie modyfikuje funkcje falowe i energie własne opisujące strukturę elektronową ciała stałego. Oprócz modyfikacji rozkładu gęstości stanów w funkcji energii, ten rozkład doznaje znacznych przesunięć na skali energii sięgających kilku a nawet kilkunastu eV. Jednakże ze względu na poważne trudności powstające w trakcie obliczeń z pierwszych zasad z uwzględnieniem oddziaływania elektron – dziura, rezultaty teoretyczne są często porównywane z wynikami doświadczalnymi z zaniechaniem tej ważnej poprawki.

Eksperymentalna krawędź absorpcji rentgenowskiej i przy-krawędziowa struktura subtelna są rozmywane nie tylko przez lorentzowską szerokość rdzeniowego stanu podstawowego Γ_L , ale również przez poszerzenie ΔE_ϵ spowodowane skracaniem czasu życia stanów elektronowych wzbudzonych powyżej energii poziomu Fermiego³. Zwykle przyjmuje się, że to poszerzenie wynosi ok. 0,1 eV na każdy eV powyżej energii poziomu Fermiego. Również istotne jest poszerzenie eksperymentalne Γ_G narzucone przez zdolności rozdzielcze monochromatora oraz układu detekcyjnego. Jak wiadomo, poszerzenie to jest opisane rozkładem Gaussa. Ostatecznie poszerzenie całkowite eksperymentalnej krawędzi absorpcji Γ_{catk} po odpowiednim dopasowaniu szerokości rozkładów lorentzowskiego i gaussowskiego, wyraża się przybliżonym wzorem

$$\Gamma_{catk} = \Gamma_L + \frac{1}{2}\Gamma_G + \Delta E_\epsilon \quad (7)$$

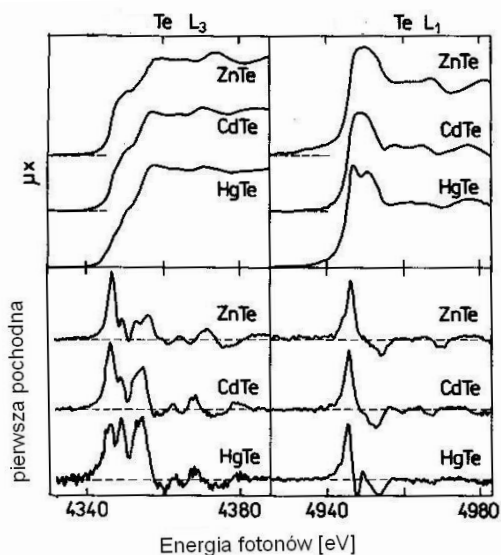
współczynnik $\frac{1}{2}$ wynika z dopasowania szerokości energetycznej rozkładów Lorentza i Gaussa. Otrzymana eksperymentalnie struktura XANES jest zwykle porównywana z pasmowymi obliczeniami teoretycznymi rzutowanych gęstości stanów pasma przewodnictwa. Przy porównywaniu wyników teoretycznie obliczonych krawędzi absorpcji z rezultatami eksperymentalnymi zawierającymi opisane

poszerzenia jest konieczne uwzględnianie w obliczeniach poszerzenia Γ_{catk} . Eksperymentalną strukturę XANES można wyznaczać w szerokim zakresie energii, niestety na obliczenia teoretyczne są nałożone zwykle drastyczne ograniczenia, w wyniku których zakres energetyczny wiarygodnych obliczeń, wynikających z natury przybliżeń teoretycznych stosowanych metod, nie przekracza 25 eV (2 Rydbergów). Wyjątkiem są obliczenia teoretyczne dla niektórych czystych metali, w których rozważa się przejścia z atomowo-podobnych stanów rdzeniowych do orbitali z potencjałem miseczkowym (maffin tin orbitals) gazu elektronowego w paśmie przewodnictwa metalu. Odpowiednią metodą obliczeniową dla tych metali jest zwykle metoda dołączonych fal płaskich APW (Augmented Plane Waves). Bardzo dobrym przykładem możliwości teoretycznych obliczeń dla metali są rezultaty otrzymane dla palladu⁷. Rzutowane gęstości stanów pasma przewodnictwa palladu były obliczane w szerokim zakresie energii przy pomocy zlinearyzowanej wersji metody APW, która umożliwia bardzo wiarygodne obliczenia w szerokim zakresie energii. Zgodność obliczeń teoretycznych z eksperymentem jest bardzo dobra i sięga aż do około 200 eV. Warto podkreślić, że obliczenia teoretyczne, w tym przypadku, odtwarzają powyżej 50 eV oscylacyjną strukturę EXAFS. Niestety, tak dogodne warunki do wiarygodnych obliczeń teoretycznych z pierwszych zasad są raczej rzadkim wyjątkiem.

XANES związków półprzewodnikowych grupy II – VI

Rozkład gęstości stanów pasma przewodnictwa w kryształach różnych związków chemicznych jest określany przez rozmieszczenie i rodzaj atomów w otoczeniu wzbudzanego atomu. Dobrą ilustracją są związki półprzewodnikowe ZnTe, CdTe i HgTe⁸, które krystalizują w strukturze regularnej blendy cynkowej i posiadają takie same tetraedryczne uporządkowanie bliskiego zasięgu. Jednakże ze względu na różne otoczenie atomu Te w tetraedrze (Zn, Cd lub Hg) mają różną strukturę XANES. Jest to szczególnie widoczne na Rys. 1 przy porównywaniu przebiegu pierwszych pochodnych. Za wyjątkiem raczej nielicznych obliczeń teoretycznych dla metali, obliczenia struktury elektronowej kryształów są zwykle obłożone poważny-

mi ograniczeniami. Dotyczy to wspomnianego już wcześniej ograniczenia interwału energetycznego wiarygodnych obliczeń. Właściwe porównanie eksperymentalnych wyników XANES mierzonych w szerokim zakresie energii z obliczeniami teoretycznymi otrzymywanymi w bardzo ograniczonym zakresie energii, wymaga albo (1) uzupełnienia obliczonego rozkładu rzutowanej gęstości stanów powyżej zakresu wiarygodnych obliczeń przez stałą gęstość stanów (niezależną od energii) lub (2) dopasowania eksperymentalnego widma XANES do zakresu obliczeń przez odcięcie (zredukowanie) widma doświadczalnego powyżej poziomu wiarygodności obliczeń.

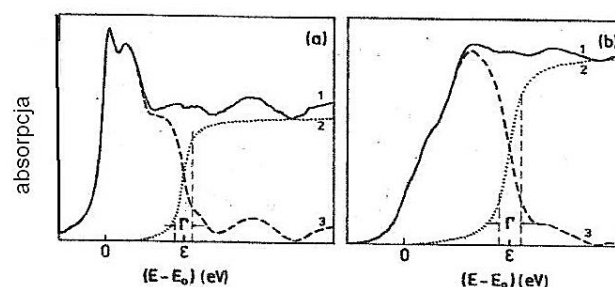


Rys. 1 Struktura subtelna krawędzi rentgenowskiej L_1 i L_3 Te w ZnTe, CdTe i HgTe.

Reprinted Fig. 1 with permission from A Kisiel, A., G. Dalba, P. Fornasini, M. Podgórnny, J. Oleszkiewicz, F. Rocca & E. Burattini, . Phys. Rev. B 39, 7895-7904 (1989-1). Copyright 2020 by the American Physical Society. Licence Number RNP/20/NOV/032730.

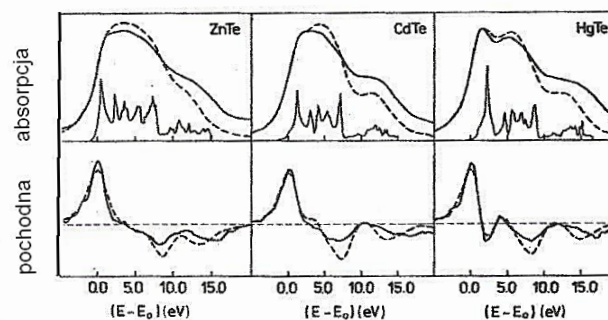
Dogodniejsze i bardziej poprawne wydaje się stosowanie rozwiązania (2). Redukcję widma doświadczalnego⁸ dokonuje się odcinając z tego widma krawędź arctg dla elektronów swobodnych przy szacowanej granicy wiarygodności obliczeń teoretycznych ϵ . Procedurę i rezultat redukcji zaznaczony linią przerywaną ilustruje Rys. 2. Rys. 3 pokazuje zredukowane eksperymentalne widma rentgenowskie dla krawędzi absorpcji L_1 Te dla ZnTe, CdTe i HgTe z Rys. 2. Rezultat redukcji danych eksperymentalnych został porównany z teoretyczną absorpcją przy-

krawędziową wyliczoną na podstawie, pokazanych na Rys. 1, rzutowanych DOS typu p pasma przewodnictwa dla wymienionych związków.



Rys. 2 Procedura redukcji rezultatów doświadczalnych dla dwu (a) i (b) typów krawędzi absorpcji rentgenowskiej. 1 widmo eksperymentalne, 2 udział widma elektronów swobodnych powyżej energii odcięcia. Linia przerywana ilustruje rezultat redukcji.

Reprinted Fig. 5 with permission from A Kisiel, A., G. Dalba, P. Fornasini, M. Podgórnny, J. Oleszkiewicz, F. Rocca & E. Burattini, . Phys. Rev. B 39, 7895-7904, (1989-1). Copyright 2020 by the American Physical Society. Licence Number RNP/20/NOV/032730.

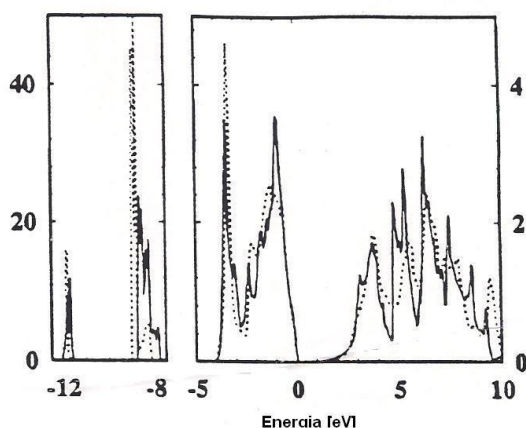


Rys. 3 Porównanie zredukowanego doświadczalnego widma absorpcji (linia ciągła) z wyliczonym teoretycznie (linia przerywana) oraz ich pierwszych pochodnych dla krawędzi rentgenowskiej L_1 Te. Pod krzywymi pokazano teoretycznie wyliczone rzutowane DOS typu p pasma przewodnictwa.

Reprinted Fig. 8 with permission from A Kisiel, A., G. Dalba, P. Fornasini, M. Podgórnny, J. Oleszkiewicz, F. Rocca & E. Burattini, . Phys. Rev. B 39, 7895-7904 (1989-1). Copyright 2020 by the American Physical Society. Licence Number RNP/20/NOV/032730.

W strukturach krystalicznych przy takim samym otoczeniu chemicznym i identycznym uporządkowaniu bliskiego zasięgu wokół wzbudzanego atomu, lecz o różnym uporządkowaniu dalekiego zasięgu, pasmo przewodnictwa takich różnych faz krystalicznych, posiada inny rozkład rzutowanych gęstości stanów. Ilustracją takiego przypadku⁹ jest Rys. 4 prezentujący rozkład gęstości stanów pasma przewodnictwa dla CdSe. CdSe posiada tetraedryczne uporządkowanie bliskiego zasięgu

ale może krystalizować w strukturze regularnej powierzchniowo centro-wanej *fcc*. blendy cynkowej oraz w heksagonalnej strukturze wurcytu. Rozkład DOS dla tych obydwu faz krystalicznych CdSe różni się⁹ i w konsekwencji należy spodziewać się różnic w strukturze XANES dla tych faz. Powyżej wykazano, że przy jednakowym sąsiedztwie atomu wzbudzonego i różnym uporządkowaniu dalekiego zasięgu jest obserwowana odmienna struktura XANES. Warto zaznaczyć, że zazwyczaj w takich przypadkach położenie energetyczne krawędzi absorpcji rentgenowskiej różni się tylko nieznacznie.



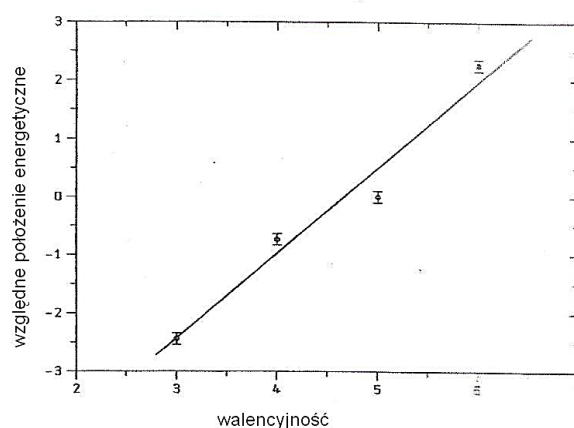
Rys. 4 Rozkład gęstości stanów w strukturze pasmowej CdSe krystalizującej w strukturze krystalicznej, kubicznej blendy cynkowej (linia przerywana) i heksagonalnej wurcytu (linia ciągła).

Reprinted Fig. 1 with permission from J. Konior & S. Kaprzyk Acta Phys Pol A 87, 269 (1995). Copyright 2020 by Acta Physica Polonica A.

XANES związków chemicznych pierwiastków na różnym stopniu utlenienia

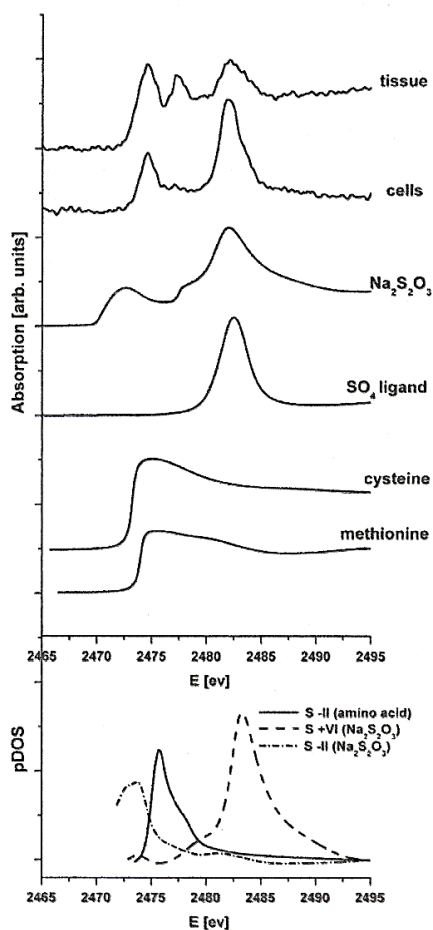
W wielu związkach chemicznych, w których występuje ten sam pierwiastek w otoczeniu złożonym z różnej liczby najbliższych sąsiadów, jego struktura XANES nie tylko różni się strukturą subtelną lecz także położenia energetyczne krawędzi absorpcji rentgenowskiej mogą różnić się między sobą nawet o kilka elektronowoltów w porównaniu z pozycją energetyczną krawędzi dla czystego pierwiastka. Jednym z najbardziej istotnych czynników jest w tym przypadku możliwość występowania w związkach chemicznych analizowanego pierwiastka na różnym stopniu utlenienia, z którym może się wiązać odmienna symetria przestrzenna rozmieszczenia najbliższych sąsiadów. Problem jest złożony bo stopień utlenienia jest definiowany ściśle jedynie dla

wiązań jonowych, które występują jednakże rzadko w czystej postaci. Pełniejszy obraz można uzyskać przez analizę funkcji termodynamicznych opisujących własności tworzenia się związków chemicznych. Warunki równowagi termodynamicznej w związkach chemicznych są określane przez potencjał chemiczny, który z kolei definiuje w ciele stałym położenie energetyczne poziomu Fermiego w temperaturze 0 K. Hormes i współpracownicy¹⁰ pokazali, że w kilku związkach chromu, które mogą występować na 3, 4, 5 i 6 stopniu utlenienia, położenia energetyczne krawędzi absorpcji K Cr z dobrym przybliżeniem zależą liniowo od stopnia utlenienia (Rys. 5). Podobnie jak Cr inne pierwiastki mogą również występować w związkach chemicznych na różnych stopniach utlenienia. W szczególności w analizie materiałów biologicznych ważną rolę odgrywa stopień utlenienia siarki zawartej w tych materiałach. Stopień utlenienia istotnie modyfikuje kształt krawędzi absorpcji rentgenowskiej siarki i przesuwa położenie krawędzi rentgenowskiej na skali energii. Pickering i inni¹¹ pokazali takie zależności dla kilku związków nieorganicznych biologicznie czynnych. Podobnie Kwiatek i inni¹² porównali obliczone pakietem FEF8 teoretyczne krawędzie rentgenowskie K S kilku referencyjnych związków nieorganicznych i organicznych z eksperymentalnymi krawędziami absorpcji rentgenowskiej dla komórek rakowych i wycinków tkanek rakowych prostaty.



Rys. 5 Położenia energetyczne rentgenowskich krawędzi K Cr w zależności od stopnia utlenienia Cr w związkach chemicznych.

Reprinted Fig. 4 with permission from Hormes, J., Chauvistré, R., Schmitt, W. & Pantelouris, M. Acta Phys Pol A 82, 37 (1992). Copyright 2020 by Acta Physica Polonica A.



Rys. 6 Porównanie obliczonych teoretycznie rentgenowskich krawędzi K S dla referencyjnych związków organicznych i nieorganicznych z eksperymentalnymi krawędziami K S wycinków i komórek rakowych prostaty (górne krzywe). W dolnej części rysunku teoretycznie obliczone p-DOS dla siarki na -II (aminokwas metionina) i -II i IV ($\text{Na}_2\text{S}_2\text{O}_3$) stopniu utlenienia.

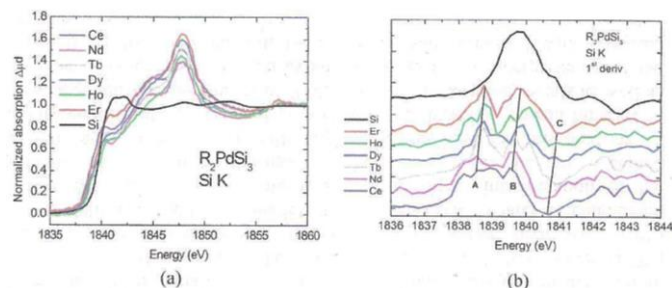
Reprinted from Radiation Physics and Chemistry, vol. 80, W.M. Kwiatek, J. Czapla, M. Podgórczyk, A.Kisiel, J. Konior, A. Balerna, "First approach to studies of sulfur electron DOS in prostate cancer cell lines and tissues studied by XANES", 1104-1108 (2011). Copyright 2020 with permission from Elsevier.

Rozległe możliwości badawcze XANES w zastosowaniu do analizy struktury elektronicznej materii skondensowanej powodują, że ta metoda znajduje zastosowanie i jest doskonała. Nieustannie rozwija się technika pomiarowa i opracowywanie danych doświadczalnych widm XANES a także są doskonałe skomplikowane teoretyczne obliczenia struktury elektronicznej badanych materiałów. Dobrym przykładem dokonującego się postępu mogą być kompleksowe badania XANES dla międzymetalicznych

związków krzemu z metalami ziem rzadkich i metalami przejściowymi.

XANES związków międzymetalicznych¹

Analiza widm XANES związków międzymetalicznych pozwala określić rodzaj tworzonego wiązania pomiędzy atomami, jak pokazano poniżej nie zawsze są to jedynie wiązania metaliczne. Międzymetaliczne związki krzemu z metalami ziem rzadkich i metalami przejściowymi budzą uzasadnione zainteresowanie ze względu na zdiagnozowaną obecność w niektórych z nich ciężkich fermionów, magnetyzmu wynikającego z geometrycznej frustracji kryształów oraz zauważalne współistnienie w strukturze elektronicznej elektronów zlokalizowanych i wędrownych. Obserwowane efekty mogą wskazywać na nieznane do końca interesujące cechy magnetyczne. Osobliwe własności tych materiałów wiąże się przede wszystkim z modyfikacjami struktury elektronicznej, powodowanej zmianami liczby elektronów w obsadzeniu częściowo wypełnionych powłok związków typu R_2PdSi_3 ($\text{R}=\text{Ce}, \text{Nd}, \text{Tb}, \text{Dy}, \text{Ho}$ i Er) oraz $\text{oRh}_{2-x}\text{Pd}_x\text{Si}_2$ ($x=0,0, 0,5, 0,75, 1, 1,5, 1,8, 2$)¹³.



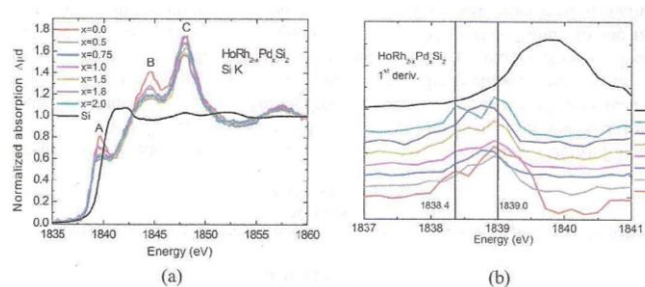
Rys. 7 Krawędzie K Si dla rodziny związków R_2PdSi_3 ($\text{R} = \text{Ce}, \text{Nd}, \text{Tb}, \text{Dy}, \text{Ho}, \text{Er}$) (a) i ich pierwsze pochodne dla obszaru przy-krawędziowego (b).

Reprinted from Nuclear Instruments and Methods in Physics Research B, vol. 364, P. Zajdel, A. Kisiel, A. Szytuła J. Goraus, A. Balerna A. Banaś. P. Starowicz, J. Konior, G. Cinque, A. Grilli, "Studies of valence of selected rare earth silicides determined using Si K and Pd/Rh $L_{2,3}$ XANES and LAPW numerical studies" 76-84 (2015). Copyright 2020 with permission from Elsevier.

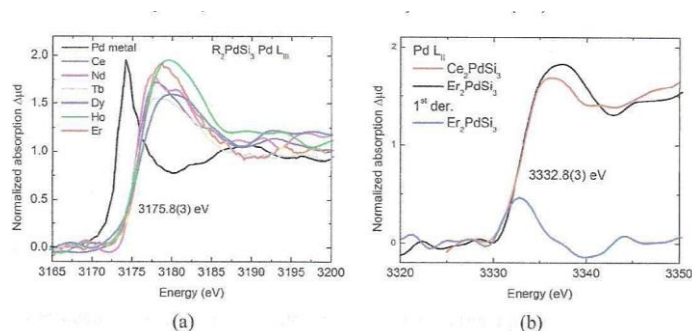
Dane doświadczalne XANES zostały uzyskane przy użyciu promieniowania synchrotronowego z 510 MeV colidera DAΦNE w Frascati², a następnie opracowane z użyciem programu ATHENA¹⁴. Normalizacje przeprowadzono w oparciu o model CL_{norm} bazujący na atomowych przekrojach czynnych (C-L) Cromera-Libermana¹⁵. Szczegółowa analiza widm

¹ Ten rozdział został zredagowany wspólnie z dr hab. Pawłem Zajdlem

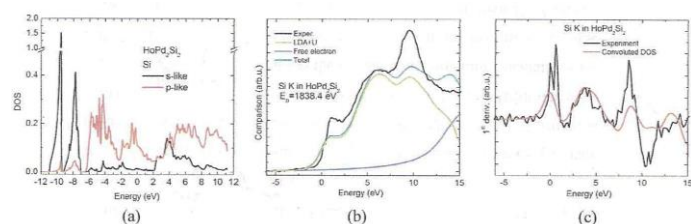
² Colider DAΦNE Light w Laboratori Nazionali di Frascati, Istituto Nazionale di Fisica Nucleare, Frascati



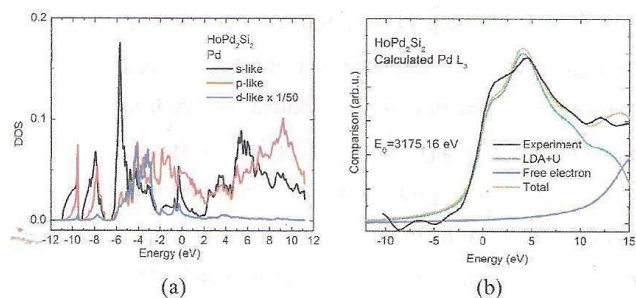
Rys. 8 Krawędzie K Si dla rodziny związków $\text{HoRh}_{2-x}\text{Pd}_x\text{Si}_2$ ($x = 0, 0, 5, 0, 75, 1, 1, 5, 1, 8, 2$) (a) i ich pierwsze pochodne wokół maksimum A (b). Reprinted from Nuclear Instruments and Methods in Physics Research B, vol. **364**, P. Zajdel, A. Kisiel, A. Szytuła J. Goraus, A. Balerna A. Banaś. P. Starowicz, J. Konior, G. Cinque, A. Grilli, "Studies of valence of selected rare earth silicides determined using Si K and Pd/Rh $L_{2,3}$ XANES and LAPW numerical studies" 76–84 (2015). Copyright 2020 with permission from Elsevier.



Rys. 9 Krawędzie L_3 Pd dla rodziny związków R_2PdSi_3 ($\text{R} = \text{Ce}, \text{Nd}, \text{Tb}, \text{Dy}, \text{Ho}, \text{Er},$) (a) i krawędzie L_2 Pd dla Ce_2PdSi_3 i Er_2PdSi_3 (b). Reprinted from Nuclear Instruments and Methods in Physics Research B, vol. **364**, P. Zajdel, A. Kisiel, A. Szytuła J. Goraus, A. Balerna A. Banaś. P. Starowicz, J. Konior, G. Cinque, A. Grilli, "Studies of valence of selected rare earth silicides determined using Si K and Pd/Rh $L_{2,3}$ XANES and LAPW numerical studies" 76–84 (2015). Copyright 2020 with permission from Elsevier.



Rys. 10 Udział Si w DOS Ho_2PdSi_3 (a), porównanie eksperymentalnej zredukowanej krawędzi K Si z krawędzią obliczoną teoretycznie (b) i porównanie ich pierwszych pochodnych (c). Reprinted from Nuclear Instruments and Methods in Physics Research B, vol. **364**, P. Zajdel, A. Kisiel, A. Szytuła J. Goraus, A. Balerna A. Banaś. P. Starowicz, J. Konior G. Cinque, A. Grilli, "Studies of valence of selected rare earth silicides determined using Si K and Pd/Rh $L_{2,3}$ XANES and LAPW numerical studies" 76–84 (2015). Copyright 2020 with permission from Elsevier.



Rys. 11 Udział Pd w DOS Ho_2PdSi_3 (a), porównanie eksperymentalnej zredukowanej krawędzi L_3 Pd z teoretycznie obliczoną krawędzią absorpcji (b). Reprinted from Nuclear Instruments and Methods in Physics Research B, vol. **364**, P. Zajdel, A. Kisiel, A. Szytuła J. Goraus, A. Balerna A. Banaś. P. Starowicz, J. Konior, G. Cinque, A. Grilli, "Studies of valence of selected rare earth silicides determined using Si K and Pd/Rh $L_{2,3}$ XANES and LAPW numerical studies" 76–84 (2015). Copyright 2020 with permission from Elsevier.

zakwestionowała występowanie jedynie wiązań międzymetalicznych w obydwu analizowanych rodzinach związków. Wiązania krzem – ziemie rzadkie mają charakter polarny na co wskazują, przesunięcia energii krawędzi K Si wraz ze zmianą ziemi rzadkiej (Rys. 7). Natomiast brak przesunięć krawędzi K Si przy stopniowej zamianie Rh przez Pd potwierdza metaliczny charakter wiązania ich pasma $4d5s$ (Rys. 8).

Podobnie metale ziem rzadkich i Pd (Rys. 10) oraz Rh mają metaliczny charakter wiązania. Obliczenia teoretyczne gęstości stanów pasma przewodnictwa zostały przeprowadzone dla Ho_2PdSi_3 i HoPd_2Si_2 . Do obliczeń użyto pakietu obliczeniowego Wien2K'09¹⁶ z formalizmem LDA + U (tzn. z uwzględnieniem oddziaływania Hubbarda dla Ho)¹⁷. Porównania skomplikowanych obliczeń teoretycznych gęstości stanów pasma przewodnictwa ze zredukowanymi wynikami doświadczalnymi dla krawędzi K Si i L_3 Pd wykazują zadawalającą zgodność, która świadczy o rozległych możliwościach badawczych analizy XANES (Rys. 10 i Rys. 11).

Struktura subtelna powyżej rentgenowskiej krawędzi absorpcyjnej (struktura EXAFS)

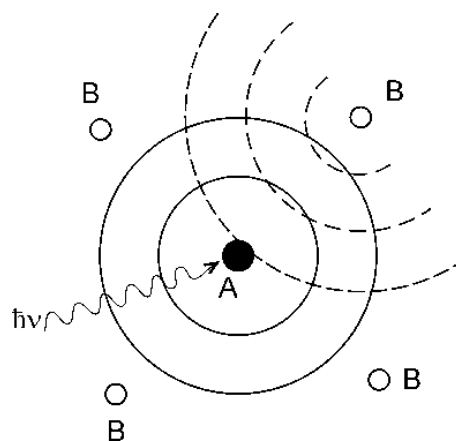
Powyżej rentgenowskiej krawędzi absorpcji, współczynnik absorpcji promieniowania rentgenowskiego posiada słabą, subtelną, strukturę zwykle o charakterze oscylacyjnym. Takiej struktury nie obserwuje się dla wzbudzanych atomów swobodnych np. dla gazów szlachetnych, natomiast taką strukturę oscylacyjną obserwuje się już w drobinach dwu atomowych. Subtelna struktura ponad

rentgenowską krawędzią absorpcji, nazwana strukturą EXAFS (Extended X-ray Absorption Fine Structure), dostarcza przede wszystkim cennych informacji o odległościach i liczbie najbliższych sąsiadów wokół centrum wybranego przez eksperymentatora. Te informacje, określające tzw. strukturę lokalną materiału, są nadzwyczaj cenne przy bardziej szczegółowym opisie struktury kryształów i materiałów amorficznych.

W celu opisanego mechanizmu powstawania oscylacji współczynnika absorpcji promieniowania rentgenowskiego powyżej krawędzi absorpcji rentgenowskiej, należy prześledzić proces propagacji elektronów, wzbudzonych z głębokich stanów rdzeniowych, do wysoko wzbudzonych stanów pasma przewodnictwa¹⁸⁻²⁰. Jak wiadomo, elektron poruszający się w paśmie może być opisany również przez rozchodzącą się w ośrodku kulistą falę materii elektronu o energii kinetycznej $E_{kin} = (\hbar\omega - E_0)$ i o wektorze falowym \mathbf{k} równym

$$k = \sqrt{\frac{2m}{\hbar^2} (\hbar\omega - E_0)} \quad (8)$$

Rozchodzenie się tej fali może być rozpatrywane w oparciu o teorię uwzględniającą porządek dalekiego zasięgu z wykorzystaniem własności funkcji Blocha lub o teorię porządku bliskiego zasięgu uwzględniającą rozproszenia pochodzące tylko od sąsiednich atomów. Jak zostało udowodnione obydwie podejścia okazały się równoważne i komplementarne. W rozważaniach uwzględniających uporządkowanie dalekiego zasięgu należy mieć na uwadze, że przy wzbudzeniu elektronu do pasma przewodnictwa pojawia się dodatkowe oddziaływanie elektron-dziura, a ponadto elektron w stanie wzbudzonym posiada skończony czas życia, odpowiedzialny za tłumienie amplitudy elektronowej fali materii. Z tych powodów elektrony atomów wzbudzonych są opisywane przez inne funkcje Blocha niż elektrony rdzeniowe i walencyjne atomów nie wzbudzonych. W końcu należy również pamiętać o drganiach sieci krystalicznej będących źródłem rozproszeń fali elektronowej. Nie wchodząc zatem w kolizję z bezrozproszeniowym opisem propagacji elektronów Blocha w idealnej sieci krystalicznej, jest w pełni umotywowane rozważanie rozpraszania fali materii elektronów ze wzbudzonego atomu centralnego na powłokach elektronowych



Rys. 12 Ilustracja rozproszenia elektronowej fali materii elektronu wzbudzonego w atomie centralnym A (krążek zaczerniony) na sąsiednich atomach B. Pierścienie oznaczone linią przerywaną ilustrują czoła fal rozproszonych wstecznie.

atomów sąsiadujących (Rys. 12). Elektronowe fale materii rozproszone wstecz, przez atom rozpraszający, interferują z elektronową falą rozpraszaną, dając w wyniku oscylacje współczynnika absorpcji. Można wykazać, że oscylacyjny charakter współczynnika absorpcji tkwi w elementach macierzy oddziaływania M_{if} z wzoru (4), a nie w modyfikacji gęstości stanów pasma przewodnictwa ρ wokół atomu wzbudzonego. W strukturach uporządkowanych (w kryształach) oscylacje współczynnika absorpcji mogą być wzmacniane, gdy kilka jednakowych atomów znajduje się w takich samych odległościach wokół analizowanego centrum. Taki zespół atomów tworzy tzw. strefę koordynacyjną. Proces interferencji fal materii, opisany teoretycznie w przybliżeniu jednoelektronowym, można wyrazić w przestrzeni wektorów falowych \mathbf{k} funkcją EXAFS-u

$$\chi(k) = \frac{1}{k} \sum_j A_j(k) \sin \phi_j(k) \quad (9)$$

gdzie $\Phi(k)$ jest fazą rozproszonej fali elektronowej, wskaźnik j wyraża sumowanie po kolejnych strefach koordynacyjnych, a $A_j(k)$ — amplitudą funkcji $\chi(k)$, daną wzorem

$$A_j(k) = \frac{N_j}{R_j^2} f_j(\pi, k) e^{\left(\frac{-2R_j}{\lambda}\right)} e^{(-2\sigma_j^2 k^2)} \quad (10)$$

w tym wzorze $f_j(\pi, k)$ jest amplitudą rozproszenia wstecznego od sąsiednich atomów leżących w tej samej strefie koordynacyjnej, o liczbie koordynacyjnej N_j , oddalonej od wzbudzonego centrum o odległość R_j , $\exp(-2\sigma_j^2 k^2)$ jest czynnikiem Debye'a-Wallera opisującym termiczne drgania wibracyjne sieci o kwadra-

towym średnim przesunięciu σ_j ; czynnik $\exp(-2R_j/\lambda)$ jest odpowiedzialny za straty energii spowodowane niesprężystym rozpraszaniem elektronów z czynnikiem tłumienia λ . Łatwo zauważyć, że amplituda funkcji $\chi(k)$ jest proporcjonalna do liczby sąsiadów (liczby koordynacyjnej) w kolejnych strefach i odwrotnie proporcjonalna do kwadratu odległości od wzbudzanego centrum. Wskutek silnego tłumienia amplitudy (wywołanego tłumieniem fali elektronowej w ciele stałym), istotną rolę w tej analizie odgrywają głównie pierwsi (NN) i drudzy sąsiedzi (NNN), tzn. atomy z pierwszej i drugiej strefy koordynacyjnej. Tylko w wyjątkowo dogodnych warunkach eksperymentalnych mogą być analizowane trzecia i dalsze strefy koordynacyjne. Fourierowska analiza oscylacji ponad krawędziowego współczynnika absorpcji promieniowania rentgenowskiego, przy znajomości amplitudy i fazy funkcji $\chi(k)$, prowadzi do określenia odległości R_j oraz liczby atomów N_j leżących w tych samych odległościach od atomu centralnego. W rezultacie otrzymuje się średnie odległości atomów od wybranego centrum, dla którego jest mierzona krawędź absorpcji rentgenowskiej i ciąg oscylacji pojawiający się powyżej krawędzi absorpcji. Rozpatrywanie tych oscylacji jako superpozycji rozprożeń wielokrotnych od wszystkich sąsiadów z kolejnych stref koordynacyjnych tworzy złożony układ, który jest opisywany przez sieć rozprożeń wielokrotnych. Obecnie w praktyce do symulacji sieci rozprożeń wielokrotnych w zadanej sieci krystalicznej oraz porównania tej analizy z danymi eksperymentalnymi absorpcji rentgenowskiej stosuje się pakiet IFEFFIT¹⁴.

Analizowanie metodą EXAFS położeń atomów z najbliższych stref koordynacyjnych względem wybranego atomu centralnego otwiera tej metodzie rozległe obszary zastosowania w badaniach struktur uporządkowanych (krystalicznych) a także nieuporządkowanych (amorficznych). Opis struktury lokalnej materiału, znalazł zastosowanie w badaniach procesów katalitycznych, w których określanie otoczenia atomowego stosowanych katalizatorów ma istotne znaczenie techniczne. EXAFS jest stosowany w biologii i medycynie przy określaniu bardzo złożonych sekwencji procesów zachodzących w organizmach żywych, np. w analizie procesów przyswajania wapnia i strontu przez organizm oraz odkładania ich w kościach względnie w układzie krążenia. Analiza

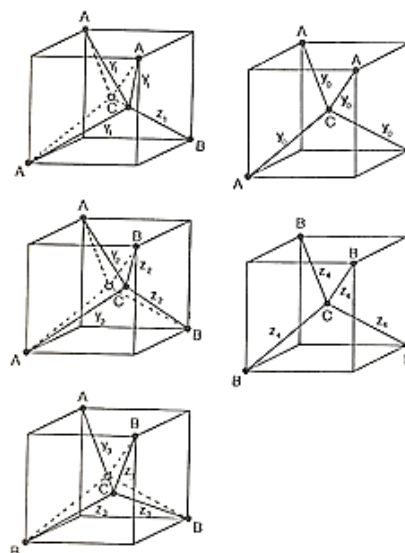
EXAFS stała się również źródłem ważnych informacji o strukturze lokalnej potrójnych i poczwórnych roztworów stałych (stopów) związków półprzewodnikowych. Badania te łączą wraz z ważnymi celami poznawczymi nadzieje na cenne zastosowania w elektronice roztworów stałych, przede wszystkim związków półprzewodnikowych, należących do związków grup III-V i II-VI.

EXAFS w analizie struktury lokalnej potrójnych związków półprzewodnikowych

Stopy (roztwory stałe) półprzewodników powstają ze stopienia i krystalizacji dwu lub więcej mieszających się ze sobą półprzewodników np. C, Si i Ge lub związków półprzewodnikowych takich jak np. GaAs i InAs lub ZnTe i CdTe, itp. Z dowolnych dwu związków binarnych AC i BC lub AC i BD otrzymujemy odpowiednio potrójny stop (roztwór stały) ABC, lub poczwórny roztwór stały ABCD. Binarne związki półprzewodnikowe typu AC lub BC, gdzie A i B są atomami (kationami) z kolumn II lub III, a C i D odpowiednio atomami (anionami) z kolumn VI lub V tablicy Mendelejewa, krystalizują w strukturze regularnej blendy cynkowej (struktura sfalerytu) lub rzadziej w heksagonalnej strukturze wurcytu. Obydwie te struktury charakteryzują się przestrzennym uporządkowaniem tetraedrycznym, tzn., że atom (kation) A lub B leżący w centrum tetraedru jest otoczony czterema atomami (anionami) C lub D położonymi w narożach tetraedru i na odwrót każdy atom C lub D jest otoczony przez 4 atomy A lub B. Każdy atom w takiej sieci krystalicznej ma w pierwszej strefie koordynacyjnej czterech najbliższych sąsiadów, a w drugiej i następnych strefach koordynacyjnych po 12 atomów. Wzajemne odległości atomowe w pierwszej (NN) i drugiej (NNN) strefie koordynacyjnej oraz liczby koordynacyjne N_j dla tych związków można wyznaczyć posługując się analizą EXAFS. Jeżeli binarne składniki AC i BC lub AC i AD stopu potrójnego względnie poczwórne, rozpuszczają się w sobie w dowolnych proporcjach, można otrzymać wówczas nieograniczoną liczbę różnych stopów (roztworów stałych), różniących się między sobą kontrolowanymi zmianami własności fizycznych. Związki potrójne i poczwórne powstałe ze związków binarnych o strukturze blendy cynkowej zachowują strukturę krystaliczną składników binarnych i tetraedryczne uporządkowanie atomów. W przypadku, gdy jeden ze składników

binarnych krystalizuje w strukturze blendy cynkowej lub wurcytu, a drugi w innej strukturze krystalicznej, wówczas tworzony stop potrójny zachowuje strukturę pierwszego składnika binarnego do określonego składu, przy którym zachodzi strukturalne przejście fazowe. Powyżej tego składu stop potrójny krystalizuje w strukturze drugiego składnika lub tworzy mieszaninę kilku różnych faz. Typowym przykładem takiego zachowania są stopy związków grupy II-VI z metalami przejściowymi (np. Mn, Fe itp.). Związki binarne metali przejściowych z S, Se i Te nie krystalizują w strukturze regularnej i w związku z tym powyżej strukturalnego przejścia fazowego układy takie mogą się stać mieszaniną kilku faz. Przy tworzeniu się kryształu potrójnego typu $A_xB_{1-x}C$ o strukturze blendy cynkowej lub wurcytu, można wyróżnić w kryształce pięć różnych rodzajów tetraedrów elementarnych: $T_0(4AC)$, $T_1(3A1BC)$, $T_2(2A2BC)$, $T_3(1A3BC)$ i $T_4(4BC)$, pokazanych na Rys. 13. Ich obecność powinna być uwzględniana w opisie teoretycznym własności stopów potrójnych (roztworów stałych). Dla stopów poczwórnych liczba możliwych różnych tetraedrów elementarnych wynosi 15 lub 18 w zależności czy składają się odpowiednio z dwu kationów i dwu anionów czy z trzech kationów (anionów) i jednego anionu (kationu).

W celu określenia wzajemnych położenia atomów w stopach potrójnych z użyciem analizy EXAFS, opisanej formułami (9) i (10), na początku lat osiemdziesiątych ubiegłego wieku zostały przeprowadzone badania przez Mikkelsona i Boyce^{21,22} ³. Badania te dotyczyły, krystalizujących w strukturze blendy cynkowej, półprzewodnikowych potrójnych roztworów stałych $In_{1-x}Ga_xAs$. Roztwory stałe $In_{1-x}Ga_xAs$ otrzymuje się z $InAs$, gdy sukcesywnie atomy In podstawiane są atomami Ga. Stała sieci wyznaczona dla tego roztworu metodami dyfrakcji rentgenowskiej zależy liniowo od zawartości Ga w kryształce. Pomiary EXAFS wykazały, że atomy Ga nie podstawiają atomów In w odległościach charakterystycznych dla związku $InAs$, lecz w przybliżeniu lokują się w odległościach charakterystycznych dla $GaAs$. (Rys. 14a). Takie zachowanie par atomów In-As i Ga-As nie było wtedy w pełni zrozumiałe.



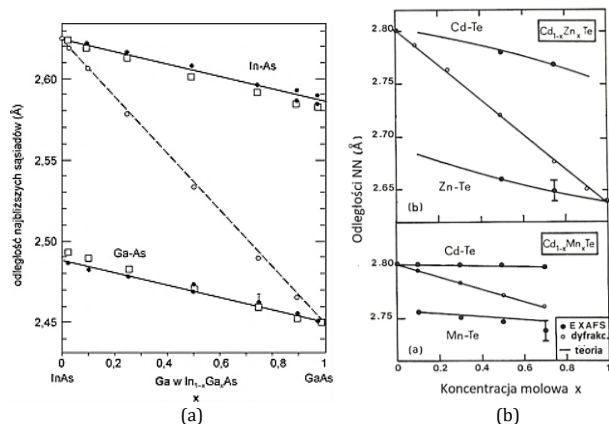
Rys. 13 Pięć możliwych położenia anionu C w tetraedrach elementarnych modelu sztywnej sieci kationów. W tetraedrach otwarte punkty i linie przerywane pokazują położenie anionu C oraz wiązania w przypadkach bez dystorsji. Zaczernione punkty i linie ciągłe wyznaczają tetraedry z dystorsją.

Wy tłumaczeniem tworzenia się takiej struktury dwumodułowej, były różne promienie jonowe Ga i In a więc różne oddziaływania pomiędzy In-As i Ga-As. Zaskakujące wyniki badań EXAFS dla $In_{1-x}Ga_xAs$ wyjaśnił, teoretyczny model sztywnej sieci kationów zastosowany do interpretacji wyników EXAFS dla potrójnych związków $Cd_{1-x}Mn_xTe$ ^{23,24} ⁴. Model ten również wyjaśnił zadawalająco podobne zachowanie związków $Cd_{1-x}Zn_xTe$ ^{23,24} i $HgSe_{1-x}Te_x$ ²⁵. Rys. 14 ilustruje wyniki badań dla struktury lokalnej $In_{1-x}Ga_xAs$ ²¹ (a) oraz $Cd_{1-x}Zn_xTe$ i $Cd_{1-x}Mn_xTe$ ²⁶ (b). Model sztywnej sieci kationów przyjmował arbitralnie, że, pokazane na Rys. 13 tetraedry elementarne z kationami A i B w narożach nie są zdeformowane, natomiast anion C znajdujący się wewnątrz tetraedru lokuje się w położeniu określonym przez oddziaływania atomów AC i BC, opisane przez przybliżenie pola sił walencyjnych Keatinga²⁷ i Martina²⁸. Według tego modelu wszystkie 5 rodzajów tetraedrów elementarnych rozmieszczone są chaotycznie w objętości kryształu zgodnie z dwumianowym rozkładem statystycznym Bernoulli'ego, który przewiduje, pokazany na Rys. 15 rozkład statystyczny dla tetraedrów elementarnych $T_0(4AC)$, $T_1(3A1BC)$, $T_2(2A2BC)$, $T_3(1A3BC)$

³ Przy użyciu the wiggler site station at the Stanford Synchrotron Radiation Laboratory (SSRL)

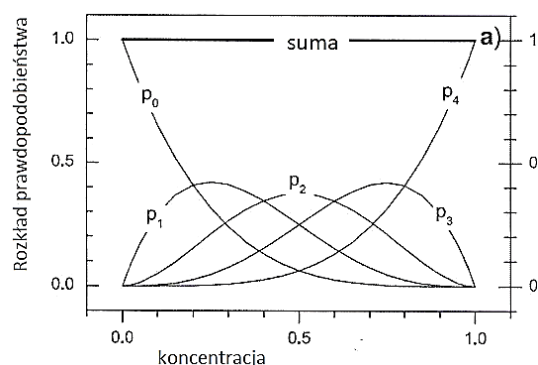
⁴ Rentgenowska linia pomiarowa DX1+PWA (Programma della Luce ADONE), Programa Utilizazione di Luce Sinchrotrone (PULS) ADONE, Frascati.

i $T_4(4BC)$. Suma jednakowych udziałów wszystkich wymienionych tetraedrów elementarnych opisywała z dobrym przybliżeniem rezultaty uzyskane z analizy EXAFS. Model sztywnej sieci kationów był pierwszym, ale jeszcze niedoskonałym opisem wyników



Rys. 14 Analiza EXAFS struktury lokalnej $In_{1-x}Ga_xAs$ ²¹ (a) oraz $Cd_{1-x}Zn_xTe$ i $Cd_{1-x}Mn_xTe$ ²⁴ (b). Na rysunku (a) punkty pełne oznaczają doświadczalnie wyznaczone odległości par jonów In-As i Ga-As, kwadraty niewypełnione – przewidywania teoretyczne modelu sztywnej sieci kationów. Średnią odległość jonów w funkcji składu wyznaczoną metodą dyfrakcji rentgenowskiej ilustrują punkty doświadczalne (małe otwarte kółka) oraz krzywa przerywana (krzywa Vegarda). Na rysunku (b) pełne punkty oznaczają wyniki doświadczalne. Linie ciągłe są przewidywaniami teoretycznymi modelu sztywnej sieci kationów.

Reprinted from Opto-Electronic Review, vol. 25, A. Kisiel, B.V. Robouch & A. Marcelli, „Local crystalline structure of multinary semiconducting alloys: Random vs. ordered distribution”, 242-250 (2017). Copyright 2020 with permission from Elsevier.

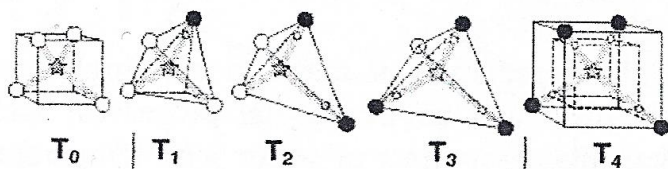


Rys. 15 Dwumianowy rozkład Bernoulliego chaotycznego rozmieszczenia tetraedrów elementarnych w kryształach potrójnym $A_{1-x}B_xC$. Rozkłady prawdopodobieństwa p_i w funkcji składu dla tetraedrów elementarnych T_0 4AC (p_0), T_1 3A1BC (p_1), T_2 2A2BC (p_2), T_3 1A3BC (p_3), T_4 4BC (p_4).

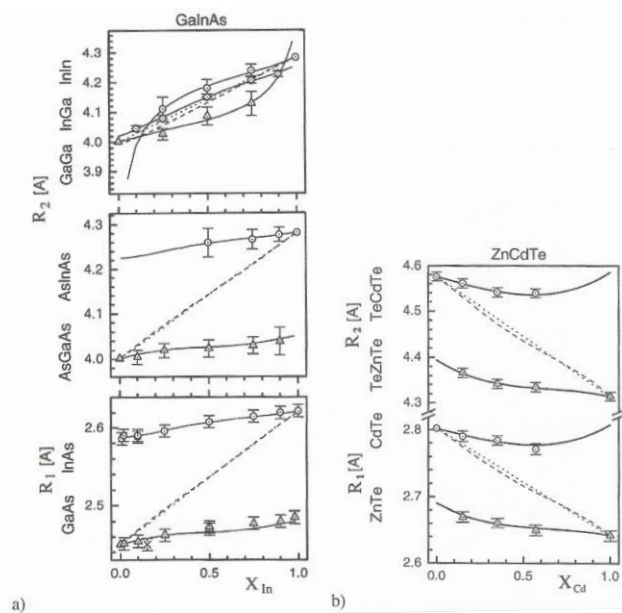
doświadczalnych uzyskiwanych z analizy EXAFS dla związków potrójnych. Niedostatkami tego modelu było nieuwzględnianie możliwości występowania deformacji elementarnych tetraedrów. Ten niedostatek usuwały częściowo prace wykorzystujące symulacje Monte Carlo i zmodyfikowane przybliżenia quasi-chemiczne^{26,29}. Startując z modelu sztywnej sieci kationów Wiedmann i inni³⁰ rozwinęli elementy teorii relaksacji naprężeń elastycznych dla związków potrójnych $A_{1-x}B_xC$ i włączyli relaksowanie tetraedrów elementarnych przez wprowadzenie klasterów w schemacie iteracyjnym (random iterative cluster model). Znacznie pełniejszy opis struktury lokalnej związków potrójnych przyniósł jednak dopiero statystyczny model zdeformowanych tetraedrów (Strained tetrahedra model)^{31,32}, który uwzględnił możliwość wprowadzania w rozważaniach udziału, pokazanych na Rys. 16, zdeformowanych tetraedrów T_1 , T_2 i T_3 z różnymi wagami statystycznymi. Wprowadzone w tym modelu aksjomaty umożliwiły jednoczesne rozszerzenie modelu sztywnej sieci kationów i modelu klasterów w schemacie iteracyjnym. Model zdeformowanych tetraedrów uwzględnił deformacje elementarnych tetraedrów i relaksacyjny wpływ drugiej strefy koordynacyjnej. Model wykorzystywał wyznaczone z analizy EXAFS odległości atomów w pierwszej (NN) i drugiej strefie koordynacyjnej (NNN), kąty pomiędzy parami wiązań oraz liczby koordynacyjne jonów N_j . Umożliwiło to analizę statystyczną odległości atomów w zdeformowanych tetraedrach w pierwszej i drugiej strefie koordynacyjnej dla badanych związków potrójnych. Na Rys. 17 pokazano dopasowanie krzywych teoretycznych modelu zdeformowanych tetraedrów z uwzględnieniem odstępstw od stochastycznego obsadzania tetraedrami elementarnymi do doświadczalnych odległości między atomami dla pierwszej i drugiej strefy koordynacyjnej w $Ga_{1-x}In_xAs$ i $Cd_{1-x}Zn_xTe$ ³¹. Porównując te wyniki z pokazanymi na Rys. 13 wynikami dopasowania modelem sztywnej sieci kationów widać, że model zdeformowanych tetraedrów jest lepszy. Model ten umożliwił wyznaczenie odstępstw od stochastycznego obsadzania realnej sieci krystalicznej tetraedrami elementarnymi dla $Ga_{1-x}In_xAs$ oraz dla wielu innych stopów potrójnych^{31,32}.

Pierwsze doniesienia o preferencyjnym (niestochastycznym) obsadzaniu miejsc atomów (Site Occupation Preferences (SOP)) w strukturze

krystalicznej związków potrójnych znalazły się w pracach Verleura i Barkera^{33,34}. Proponowany przez nich model teoretyczny opisujący dane doświadczalne przejść fononowych w $\text{GaAs}_y\text{P}_{1-y}$ i $\text{CdSe}_y\text{S}_{1-y}$ uwzględniał w skali mikroskopowej efekt klasterowania par jonów, czyli przyjmował niestochastyczny rozkład atomów w kryształach, wyrażony przez parametr klasterowania β .



Rys. 16 Tetraedry elementarne w modelu zdeformowanych tetraedrów. T_0 i T_4 to binarne tetraedry regularne, T_1 , T_2 i T_3 to tetraedry zdeformowane. Reprinted from J. Alloys Compounds, vol. 339, B.V. Robouch, A. Kisiel, & J. Konior, "Statistical model for the occupation preferences and shapes of elemental tetrahedral in the zinc-blende type semiconductors GaInAs , GaAsP , ZnCdTe ", 1-17 (2002). Copyright 2020 with permission from Elsevier.

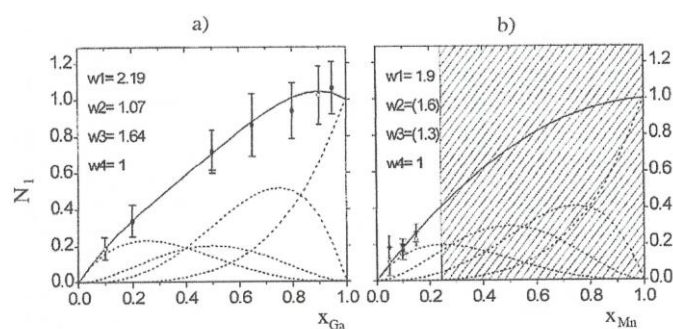


Rys. 17 Dopasowanie średnich odległości atomów w pierwszej i drugiej strefie koordynacyjnej dla $\text{Ga}_{1-x}\text{In}_x\text{As}$ i $\text{Cd}_{1-x}\text{Zn}_x\text{Te}$ modelem zdeformowanych tetraedrów³¹.

Reprinted from Opto-Electronics Review, vol. 25, A. Kisiel, B.V. Robouch & A. Marcelli, „Local crystalline structure of multinary semiconducting alloys: Random vs. ordered distribution”, 242-250 (2017). Copyright 2020 with permission from Elsevier.

Preferencyjne obsadzenia atomów Ga wokół As zaobserwowano w badaniach EXAFS związków poczwórnych $\text{Ga}_x\text{In}_{1-x}\text{As}_y\text{Sb}_{1-y}$ ³⁵ (Rys. 18a). Onabe³⁶, analizując termodynamiczne własności związków poczwórnych grupy III-V, wykazał, że

preferencje zaburzające chaotyczne rozmieszczenie par atomów mogą być wynikiem klasterowania bliskiego zasięgu najbliższych par odznaczających się silnym wiązaniem. Wiązanie par może być opisywane przez potencjał chemiczny μ . W przypadku $\text{Ga}_x\text{In}_{1-x}\text{As}_y\text{Sb}_{1-y}$ zachodzi relacja $\mu_{\text{GaAs}} + \mu_{\text{InSb}} > \mu_{\text{InAs}} + \mu_{\text{GaSb}}$. Preferencje obsadzania miejsc atomów zostały zaobserwowane również w badaniach EXAFS dla krawędzi rentgenowskich K Mn i K Se w poczwórnych związkach $\text{Cd}_x\text{Mn}_{1-x}\text{Te}_y\text{Se}_{1-y}$ ^{37,38}. Badania zostały przeprowadzone dla składów $x < 0,2$ i $y < 0,2$ gdyż związek ten tylko w tym zakresie składów krystalizuje w strukturze blendy cynkowej, a poza tymi granicami jest układem wielofazowym. Stwierdzono preferencje par atomów Mn-Se (Rys. 18b) w porównaniu z parami Cd-Se, co wskazuje na odstępstwo od rozkładu statystycznego dla Mn wokół Se. Do opisanego zachowania została zastosowana analiza probabilistyczna uwzględniająca najlepsze dopasowanie do punktów doświadczalnych. Podane na Rys. 18 współczynniki w_1 , w_2 , w_3 i w_4 w wielomianach czwartego stopnia, najlepiej dopasowanych do danych doświadczalnych, wyrażają odpowiednie prawdopodobieństwa obsadzania tetraedrami elementarnymi^{39,40}. Bunker⁴¹ oraz Pong i inni⁴² analizując dystorsje w kryształach roztworu stałego $\text{Zn}_{1-x}\text{Mn}_x\text{Se}$, przeprowadzili w temperaturze pokojowej i ciekłego azotu, szczegółowe badania odległości pierwszych (NN) i drugich (NNN) sąsiadów oraz kątów w zdeformowanych tetraedrach elementarnych.



Rys. 18 (a) Średnia liczba atomów Ga otaczająca każdy atom As. $N(\text{Ga})$ w poczwórnym roztworze stałym $\text{Ga}_x\text{In}_{1-x}\text{As}_y\text{Sb}_{1-y}$ dla różnych składów x ³⁵ (b) Średnia liczba atomów Mn wokół Se w $\text{Cd}_{1-x}\text{Mn}_x\text{Te}_{1-y}\text{Se}_y$ ³⁸. Linia przerywana opisuje stochastyczne rozmieszczenie atomów.

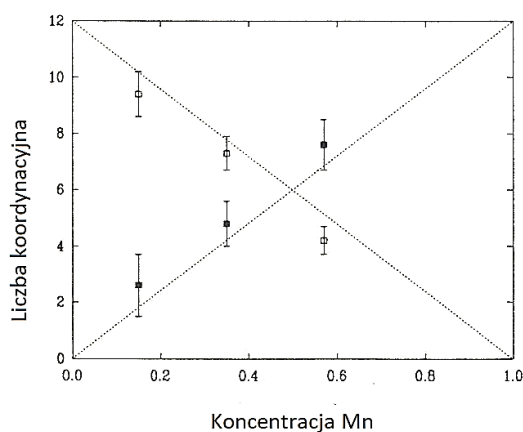
Reprinted from Opto-Electronics Review, vol. 25, A. Kisiel, B.V. Robouch & A. Marcelli, „Local crystalline structure of multinary semiconducting alloys: Random vs. ordered distribution”, 242-250 (2017). Copyright 2020 with permission from Elsevier.

Przeprowadzili również szczegółową analizę liczb koordynacyjnych N_j (definiowanych w formule (10)) dla rentgenowskich krawędzi K Zn, Mn i Se. Stwierdzili oni, że pokazane na Rys. 19, wartości liczb koordynacyjnych dla par Zn-Zn są nieco niższe od wartości przewidywanych rozkładem stochastycznym (linie przerywane na Rys. 19) a wartości dla par Zn-Mn są nieco wyższe. Różnice te zostały związane przez nich z niepełną relaksacją naprężeń w drugiej strefie koordynacyjnej. Aby rozpatrzyć ewentualną możliwość preferencyjnego obsadzenia parami jonów, dane doświadczalne Ponga i innych⁴² zostały przeanalizowane przy użyciu modelu zdeformowanych tetraedrów^{31,32}. Przeprowadzona analiza wykazała, że obserwowane w $Zn_{1-x}Mn_xSe$ odchylenia od rozkładu statystycznego rzeczywiście można wytłumaczyć preferencyjnym obsadzeniem struktury krystalicznej zdeformowanymi tetraedrami elementarnymi. W modelu zdeformowanych tetraedrów^{31,32} obsadzenie struktury krystalicznej tetraedrami elementarnymi określa prawdopodobieństwo W_k , które definiuje się jako

$$\{W_k\} = \{p_k w_k\} \text{ dla } k = 1, 2, 3 \quad (11)$$

gdzie p_k jest statystycznym rozkładem prawdopodobieństwa Bernoulli'ego.

Dla przypadku tetraedrów zdeformowanych T_1 , T_2 i T_3 prawdopodobieństwa obsadzenia W_1 , W_2 i W_3 mogą być $\neq 1$. Na podstawie tej analizy



Rys. 19 Średnie wartości liczb koordynacyjnych drugiej strefy koordynacyjnej dla Zn (kółka otwarte) i Mn (kółka wypełnione) w $ZnMnSe$ ⁴². Linie przerywane ilustrują liczby koordynacyjne w przypadku stochastycznego rozmieszczenia Zn i Mn.

Reprinted Fig. 12 with permission from W.-F. Pong, R. A. Mayanovic, B. A. Bunker, J. K. Furdyna, & U. Debska, Phys. Rev. B **41**, 8440–8448 (1990). Copyright 2020 by the American Physical Society. Licence Number RNP/20/NOV/032732.

można określić zatem preferencyjne obsadzenia parami atomów (SOP). W tym modelu przyjmuje się arbitralnie, że prawdopodobieństwa obsadzania W_0 i W_4 niezdeformowanymi tetraedrami elementarnymi T_0 i T_4 są równe 1. Wartości prawdopodobieństwa obsadzenia $\{W_k\}$ mają sens fizyczny, gdy posiadają wartość dodatnią, tzn. gdy współczynnik w_k mieści się w granicach $0 \leq w_k \leq N/k$. Oznacza to, że przy uporządkowaniu tetraedrycznym dla najbliższych sąsiadów (NN)

$$0 \leq W_1 \leq 4, 0 \leq W_2 \leq 2, 0 \leq W_3 \leq \frac{4}{3} \quad (12)$$

W związku z tymi ograniczeniami jest wygodne zdefiniowanie dla najbliższych sąsiadów współczynnik populacji konfiguracji C_k jako

$$C_k = \min \left[W_k, 1, \frac{(4-k)W_k}{4-k} \right] \leq 1 \quad (13)$$

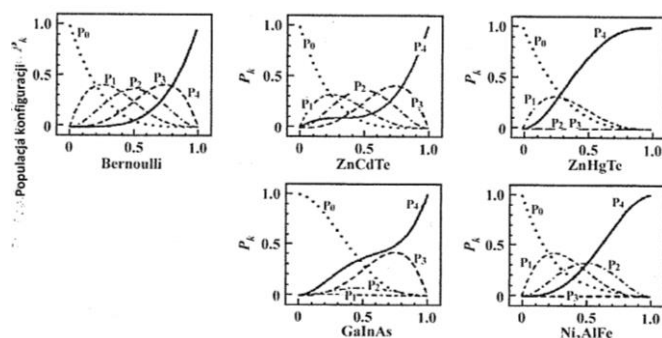
Z formuły (13) wynika, że rozkład prawdopodobieństwa dla zdeformowanych tetraedrów T_k jest obniżony w porównaniu do statystycznego rozkładu Bernoulli'ego p_k . Wielkość tego obniżenia jest wyrażana za pomocą współczynnika populacji konfiguracji C_k , który jest zawsze mniejszy lub co najwyżej równy jedności. Tak więc dla zdeformowanych tetraedrów T_1 , T_2 i T_3 rozkłady prawdopodobieństwa można wyrazić w prostszej formie

$$\{P_k\} = \{C_k p_k\} \text{ dla } k = 1, 2 \text{ i } 3 \quad (14)$$

Z warunku (14) wynika, że skoro współczynnik populacji konfiguracji C_k jest mniejszy a co najwyżej równy jedności, to rozkłady prawdopodobieństwa P_k dla tetraedrów zdeformowanych T_k są niższe lub co najwyżej równe chaotycznemu rozkładowi prawdopodobieństwa Bernoulli'ego p_k . Dla omawianego powyżej związku potrójnego $Zn_{1-x}Mn_xSe$ ^{41,42} wyznaczone preferencje obsadzania zdeformowanymi tetraedrami elementarnymi wynoszą odpowiednio $\{W_1, W_2, W_3\} = \{0,67, 1,67, 0\}$ a związane z nimi współczynniki $\{C_1, C_2, C_3\}$, opisujące populacje konfiguracji tetraedrów zdeformowanych, są równe odpowiednio $\{0,67, 0,33, 0,0\}$ ²⁶. Przytoczone wartości C_k informują, że w $Zn_{1-x}Mn_xSe$ najbardziej preferowanymi są tetraedry elementarne T_1 natomiast brak jest tetraedrów elementarnych T_3 . Podobny brak tetraedrów T_3 zaobserwowano również w kilku innych związkach potrójnych grupy II-VI z manganem (patrz Tabela II).

Rys. 20⁴³ pokazuje obliczone na podstawie danych doświadczalnych rozkłady prawdopodobieństwa P_k dla tetraedrów zdeformowanych

(T_1 , T_2 i T_3) oraz niezdeformowanych (T_0 i T_4) dla roztworów stałych ZnCdTe, ZnHgTe, GaInAs i $Ni_3(Al,Fe)$. Dla porównania zostały pokazane dodatkowo na Rys. 20 odpowiednie rozkłady prawdopodobieństwa dla statystycznego rozkładu Bernoulli'ego. Łatwo zauważyć różnice pomiędzy populacjami konfiguracji statystycznego rozkładu Bernoulli'ego i populacjami konfiguracji tetraedrów zdeformowanych P_1 , P_2 i P_3 oraz populacjami konfiguracji niezdeformowanych tetraedrów, opisanymi w realnych kryształach przez krzywe P_0 i P_4 .



Rys. 20 Populacja konfiguracji p_k stochastycznego rozkładu Bernoulliego i wyznaczone z eksperymentu populacje konfiguracji tetraedrów elementarnych P_k dla ZnCdTe, ZnHgTe, GaInAs i Ni_3AlFe ⁴³.

Reprinted from Opto-Electronics Review, 25, A. Kisiel, B.V. Robouch & A. Marcelli, „Local crystalline structure of multinary semiconducting alloys: Random vs. ordered distribution”, 242-250 (2017). Copyright 2020 with permission from Elsevier.

Model zdeformowanych tetraedrów^{31,32} został użyty do analizy wyników EXAFS szeregu tetraedrycznie uporządkowanych potrójnych stopów półprzewodnikowych, jak również do analizy tetraedrycznie uporządkowanego kubicznego (*fcc*) międzymetalicznego związku $Ni_3(Al,Fe)$ ⁴⁴. Model ten po odpowiednim uogólnieniu mógł być zastosowany również do analizy nadprzewodnika $Ce_{1-x}La_xRu_2$ o strukturze krystalicznej C15⁴⁵. Niektóre wyniki analizy zaczerpnięte z publikacji⁴⁶ zestawia Tabeli I. Ocenę wewnętrznych preferencji dla tetraedrów zdeformowanych również umożliwiły prowadzone w dalekiej podczerwieni (FIR) badania doświadczalne częstości drgań i natężeń poprzecznych fononów optycznych (TO) dla potrójnych roztworów stałych ZnCdTe^{47,48} oraz CdHgTe i ZnHgTe⁴⁹ analizowane przy użyciu modelu statystycznego⁵⁰. Zastosowanie tego modelu umożliwiło bezpośrednie porównanie preferencji wewnętrznych uzyskanych z badań częstości i natężeń drgań fononowych z

odpowiednimi preferencjami uzyskanymi z analizy wyników doświadczalnych EXAFS przy użyciu modelu zdeformowanych tetraedrów. Takie porównanie wyników jest uprawnione gdyż częstości i natężenia w widmie drgań fononowych, podobnie jak położenie rentgenowskiej krawędzi absorpcji i struktura EXAFS, są funkcjami mas atomowych drgających par atomów, ich wzajemnych odległości i stałych siłowych oddziaływujących par. Model zdeformowanych tetraedrów stosowany do analizy EXAFS i model statystyczny użyty do analizy struktury widma fononowego umożliwiają liczbowe określenie i porównanie preferencyjnego obsadzenia elementarnymi tetraedrami w realnych kryształach. Tabeli II zestawia wartości preferencyjnego obsadzenia tetraedrami elementarnymi W_k , wartości populacji konfiguracji C_k oraz sumę wartości C_k (ΣC_k) dla kilkunastu stopów półprzewodnikowych grupy III-V, II-VI oraz II-VI z Mn i związku międzymetalicznego $Ni_3Al_{1-x}Fe_x$. Preferencje wewnętrzne uzyskane z analizy EXAFS oraz z analizy drgań fononowych wykazują dla obydwu podejść podobne tendencje zachowania współczynników C_k . Stopy zebrane w Tabeli I zostały uporządkowane w zależności od zestawionej w przedostatniej kolumnie wielkości ΣC_k . ΣC_k jest miarą odchodzenia rozkładów prawdopodobieństwa struktury lokalnej określonego roztworu stałego od chaotycznego rozkładu Bernoulli'ego. Dla maksymalnej wartości $\Sigma C_k = 3$ struktura lokalna roztworu stałego jest opisywana przez statystyczny rozkład Bernoulli'ego. Wyniki zestawione w Tabeli II reprezentują związki potrójne, dla których wartość ΣC_k jest, jak w przypadku ZnCdTe, dla różnych eksperymentów równa lub bliska 3. Oznacza to, że struktura lokalna tego związku może być opisana z dobrym przybliżeniem przez statystyczny rozkład Bernoulli'ego. Na końcu Tabeli II są zestawione stopy takie jak ZnSeS i ZnSeTe posiadające bardzo małe lecz niezerowe wartości ΣC_k . Na gruncie modelu zdeformowanych tetraedrów wartość $\Sigma C_k = 0$ oznacza brak tetraedrów mieszanych (zdeformowanych) w badanym układzie potrójnym ABC. W konsekwencji tego brakuje drogi oddziaływania wzajemnego pomiędzy składnikami binarnymi AC i BC. W takim przypadku składniki te powinny się zachowywać się nie jak jednorodny stop lub roztwór stały ABC a jedynie jako mieszanina składników binarnych AC i BC. Tak postawiona hipoteza wymaga jednakże potwierdzenia doświadczalnego.

Tab. I Współczynniki preferencji dla zdeformowanych tetraedrów elementarnych w niektórych związkach potrójnych o uporządkowaniu tetraedrycznym.

Reprinted from Opto-Electronics Review, vol.25, A. Kisiel, B.V. Robouch & A. Marcelli, „Local crystalline structure of multinary semiconducting alloys: Random vs. ordered distribution”, 242-250 (2017). Copyright 2020 with permission from Elsevier.

Alloy	Experiment	W ₁	W ₂	W ₃	C ₁	C ₂	C ₃	ΣC _k	Ref.
ZnCdTe	Exafs ^{23,24}	1.0	1.0	1.0	1.0	1.0	1.0	3.00	31
ZnCdTe	FIR ^{48,50}	1.66	1	1	0.780	1	1	2.78	48,51
CdHgTe	FIR ^{48,50}	1.01	1.20	1.01	1.0	0.80	1.0	2.80	48,51
ZnCdTe	Exafs ⁵²	0.93	1.15	1.07	0.930	0.85	0.79	2.57	46
AlFeNi ₃	Exafs ⁵³	1.01	0.86	1.33	0.997	0.86	0.0	1.86	44
GaInAs	Exafs ^{21,22}	0.58	0.25	1.05	0.58	0.25	0.85	1.68	31
CdMnTe	Exafs ^{54,55}	0.68	1.33	0.003	0.68	0.67	0	1.35	32
ZnMnSe	Exafs R ₁ ^{41,42}	0.67	1.67	0.04	0.67	0.33	0.04	1.04	32
ZnMnSe	Exafs N ₁ ^{41,42}	0.62	1.7	0	0.62	0.3	0	0.92	32
HgSeTe	Exafs ⁴⁵	0.217	1.944	0.517	0.217	0.056	0.517	0.79	
ZnHgTe	FIR ⁴⁸	0.76	2.0	1.33	0.76	0.0	0.0	0.76	51,56
ZnMnS	Exafs ⁵⁷⁻⁵⁹	1.78	0	0.01	0.74	0	0.01	0.75	32
HgMnTe	Exafs ⁶⁰	0.33	1.75	0	0.33	0.25	0	0.58	32
ZnHgTe	Exafs ⁶¹	0.37	2.0	1.33	0.37	0.0	0.0	0.37	48,51
ZnMnTe	Exafs ⁶²	0.37	2.0	0	0.37	0.0	0	0.37	32
ZnSeS	Exafs ⁶³	0.12	0	0.03	0.12	0	0.03	0.15	52
ZnSeTe	Exafs ⁶⁴ & N-Scater ⁶⁵	0.037	0	1.299	0.037	0	0.103	0.14	51

Tab. II Wartości liczbowe całek Δp₀ i Δp₄ dla niektórych stopów potrójnych.

Związki grupy II - VI	Stopy	Metody	Δp ₀	Δp ₄	Preferencje
	ZnCdTe	EXAFS	0.00	0.00	ZnTe = CdTe
	ZnCdTe	FIR	0.01	0.07	ZnTe < CdTe
	ZnCdTe	EXAFS	0.01	0.12	ZnTe < CdTe
	ZnHgTe	EXAFS	0.13	0.66	ZnTe < HgTe
	ZnHgTe	FIR	0.05	0.67	ZnTe < HgTe
	CdHgTe	FIR	0.0	0.23	HgTe > CdTe
	ZnSeS	EXAFS	0.38	0.32	ZnSe > ZnS
	ZnSeTe	EXAFS	0.35	0.33	ZnSe > ZnTe
	HgSeTe	EXAFS	0.25	0.31	HgTe > HgSe
Związki grupy III - V	GaInAs	EXAFS	0.11	0.10	GaAs > InAs
Związki grupy II-VI z Mn	ZnMnS	EXAFS	0.40	0.09	ZnS > MnS
	ZnMnSe	EXAFS (N ₁)	0.26	0.22	ZnSe > MnSe
	ZnMnSe	EXAFS (R ₁)	0.26	0.13	ZnSe > MnSe
	ZnMnTe	EXAFS	0.35	0.33	ZnTe > MnTe
	CdMnTe	EXAFS	0.26	0.11	CdTe > MnTe
	HgMnTe	EXAFS	0.33	0.25	HgTe > MnTe
Związek międzymetaliczny	AlFeNi ₃	EXAFS	0.11	0.10	AlNi ₃ > FeNi ₃

Dla tetraedrów niezdeformowanych T₀ i T₄ rozkłady prawdopodobieństwa⁴⁶ można wyrazić jako

$$P_0 = p_0 + \Delta p_0, P_4 = p_4 + \Delta p_4 \quad (15)$$

gdzie p₀ i p₄ są odpowiednimi rozkładami prawdopodobieństwa Bernoulli'ego dla niezdeformowanych tetraedrów, a Δp₀ i Δp₄ są tymi częściami rozkładów prawdopodobieństwa niezdeformowanych tetraedrów AC i BC związku potrójnego ABC, które w wyniku minimalizowania energii układu w procesie naturalnego

wzrostu kryształu, nie mogły uczestniczyć w tworzeniu zdeformowanych tetraedrów T₁, T₂ lub T₃. Na Rys. 20 krzywe P₀ i P₄ przedstawiają udziały niezdeformowanych tetraedrów T₀ i T₄ związków potrójnych. Są one funkcjami koncentracji składnika BC w roztworze stałym ABC. Zgodnie z formułami funkcje Δp₀ i Δp₄ mogą wносить, widoczny na Rys. 20, istotny wkład w kształt krzywych P₀ i P₄. Porównanie rozkładów prawdopodobieństwa P₀ i P₄ w całym zakresie składników związku potrójnego niesie zatem ważne

informacje o wewnętrznych preferencjach w związkach potrójnych. Łatwo widać, że za wielkość preferencji wewnętrznych pomiędzy P_0 i P_4 będą odpowiadały funkcje Δp_0 i Δp_4 całkowane w całym zakresie koncentracji związków potrójnych. Tak więc wartości tych całek opisują preferencje wewnętrzne związane z niezdeformowanymi tetraedrami T_0 i T_4 w strukturze krystalicznej realnych kryształów. Tabela II zestawia wartości liczbowe całek Δp_0 i Δp_4 dla związków potrójnych zestawionych w Tabeli II. Warto zauważyć, że dla niektórych związków potrójnych wartości liczbowe całek Δp_0 i Δp_4 znacznie różnią się między sobą a zatem preferencje wewnętrzne pomiędzy populacjami tetraedrów typu T_0 i T_4 mogą być znaczne. Trzeba podkreślić, że preferencje wewnętrzne obserwowane dla tetraedrów zdeformowanych i niezdeformowanych wzajemnie się kompensują zgodnie z prawem zachowania masy i nie naruszają stechiometrii roztworów stałych.

Model zdeformowanych tetraedrów^{31,32} po odpowiednich modyfikacjach^{47,66} był również zastosowany do analizy danych doświadczalnych EXAFS poczwórnych związków półprzewodnikowych GaInAsSb³⁵, CdMnTeSe^{37,38}, ZnCdHgTe⁴⁷ i InAsPSb^{67,68}. Analiza wyników dla GaInAsSb i CdMnSeTe przy użyciu zmodyfikowanego modelu zdeformowanych tetraedrów potwierdziła i uzupełniła rezultaty wcześniejszych badań^{39,40}. Podobnie jak dla związków potrójnych, użycie modelu statystycznego do badań częstości drgań i natężeń poprzecznych fononów optycznych (TO) do poczwórnych związków $Cd_xMn_{1-x}Te_ySe_{1-y}$ ⁶⁶ i $Zn_xCd_yHg_{1-x-y}Te$ ^{47,69} istotnie wzbogaciło wiedzę o istniejących preferencjach wewnętrznych w strukturze lokalnej związków poczwórnych.

Literatura

1. Kisiel A. *Spektroskopia fazy skondensowanej w skrypcie Promieniowanie synchrotronowe w spektroskopii i badaniach strukturalnych: wybrane zagadnienia*. pod redakcją Kowalski, B. J., Paszkowicz, W. & Görlicha, E. A. (Polskie Towarzystwo Promieniowania Synchrotronowego, 2011).
2. Bassani, G. F. & Pastori Parravicini, G. *Electronic states and optical transitions in solids*. (Pergamon Press, 1975).
3. Parratt, L. G. Electronic Band Structure of Solids by X-Ray Spectroscopy. *Rev. Mod. Phys.* **31**, 616–645 (1959).
4. Agarwal, B. K. *X-ray spectroscopy: an introduction*. (Springer-Verlag, 1991).
5. Richtmyer, F. K., Barnes, S. W. & Ramberg, E. The Widths of the L-Series Lines and of the Energy Levels of Au(79). *Phys. Rev.* **46**, 843–860 (1934).
6. *Unoccupied Electronic States*. vol. 69 (Springer Berlin Heidelberg, 1992).
7. Müller, J. E. & Wilkins, J. W. Band-structure approach to the x-ray spectra of metals. *Phys. Rev. B* **29**, 4331–4348 (1984).
8. Kisiel, A. *et al.* X-ray-absorption spectroscopy of ZnTe, CdTe, and HgTe: Experimental and theoretical study of near-edge structures. *Phys. Rev. B* **39**, 7895–7904 (1989).
9. Konior, J. & Kaprzyk, S. Electronic Structure of Zinc-Blende and Hexagonal Semiconductors: Comparative Theoretical Study. *Acta Phys. Pol. A* **87**, 269–274 (1995).
10. Hormes, J., Chauvistré, R., Schmitt, W. & Pantelouris, M. Examples for the Industrial Use of Synchrotron Radiation. *Acta Phys. Pol. A* **82**, 37–50 (1992).
11. Pickering, I. J., Prince, R. C., Divers, T. & George, G. N. Sulfur K-edge X-ray absorption spectroscopy for determining the chemical speciation of sulfur in biological systems. *FEBS Lett.* **441**, 11–14 (1998).
12. Kwiatek, W. M. *et al.* First approach to studies of sulphur electron DOS in prostate cancer cell lines and tissues studied by XANES. *Radiat. Phys. Chem.* **80**, 1104–1108 (2011).
13. Zajdel, P. *et al.* Studies of valence of selected rare earth silicides determined using Si K and Pd/Rh L_{2,3} XANES and LAPW numerical studies. *Nucl. Instrum. Methods Phys. Res. Sect. B Beam Interact. Mater. At.* **364**, 76–84 (2015).
14. Ravel, B. & Newville, M. ATHENA, ARTEMIS, HEPHAESTUS: data analysis for X-ray absorption spectroscopy using IFEFFIT. *J. Synchrotron Radiat.* **12**, 537–541 (2005).
15. Cromer, D. T. & Liberman, D. Relativistic Calculation of Anomalous Scattering Factors for X Rays. *J. Chem. Phys.* **53**, 1891–1898 (1970).
16. Blaha, P., Schwarz, K., Sorantin, P. & Trickey, S. B. Full-potential, linearized augmented plane wave programs for crystalline systems. *Comput. Phys. Commun.* **59**, 399–415 (1990).
17. Miletić, G. I. & Blažina, Ž. Magnetic properties of and from the electronic structure calculations. *J. Magn. Magn. Mater.* **321**, 3888–3892 (2009).
18. *EXAFS Spectroscopy*. (Springer US, 1981). doi:10.1007/978-1-4757-1238-4.
19. Stern, E. A., Bunker, B. A. & Heald, S. M. Many-body effects on extended x-ray absorption fine structure amplitudes. *Phys. Rev. B* **21**, 5521–5539 (1980).

20. Lee, P. A., Citrin, P. H., Eisenberger, P. & Kincaid, B. M. Extended x-ray absorption fine structure—its strengths and limitations as a structural tool. *Rev. Mod. Phys.* **53**, 769–806 (1981).
21. Mikkelsen, J. C. & Boyce, J. B. Atomic-Scale Structure of Random Solid Solutions: Extended X-Ray-Absorption Fine-Structure Study of Ga_{1-x}In_xAs. *Phys. Rev. Lett.* **49**, 1412–1415 (1982).
22. Mikkelsen, J. C. & Boyce, J. B. Extended x-ray-absorption fine-structure study of Ga_{1-x}In_xAs random solid solutions. *Phys. Rev. B* **28**, 7130–7140 (1983).
23. Motta, N. *et al.* EXAFS of Cd_{1-x}Zn_xTe: A test of the random distribution in zincblende ternary alloys. *Solid State Commun.* **53**, 509–512 (1985).
24. Motta, N. *et al.* Random distribution and miscibility of Cd_{1-x}Zn_xTe alloy from exafs. *J. Cryst. Growth* **72**, 205–209 (1985).
25. Balzarotti, A *et al.* 'EXAFS of Cd_{1-x}Zn_xTe: A Test of the Random Distribution in Zinc-blende Ternary Alloys' *Festkorperprobleme XXV, Advances in Solid State Physics 25 (1985) 689.* (Vieweg, 1985).
26. Balzarotti, A *et al.* "The Local Structure of Random Ternary Alloys by EXAFS" *Internat. Conf. on Ternary and Multinary Compounds, Caracas 1984, Progress in Crystalline Growth and Characterization 10 (1985) 55.*
27. Keating, P. N. Effect of Invariance Requirements on the Elastic Strain Energy of Crystals with Application to the Diamond Structure. *Phys. Rev.* **145**, 637–645 (1966).
28. Martin, R. M. Elastic Properties of ZnS Structure Semiconductors. *Phys. Rev. B* **1**, 4005–4011 (1970).
29. Czyżyk, M. T. *et al.* Thermodynamic properties of ternary semiconducting alloys. *Z. Für Phys. B Condens. Matter* **62**, 153–161 (1986).
30. Weidmann, M. R., Gregg, J. R. & Newman, K. E. Local structure in Zn_{1-x}Mn_xSe alloys. *J. Phys. Condens. Matter* **4**, 1895–1904 (1992).
31. Robouch, B. V., Kisiel, A. & Konior, J. Statistical model for site occupation preferences and shapes of elemental tetrahedra in the zinc-blende type semiconductors GaInAs, GaAsP, ZnCdTe. *J. Alloys Compd.* **339**, 1–17 (2002).
32. Robouch, B. V., Kisiel, A. & Konior, J. Statistical model for atomic distances and site occupation in zinc-blende diluted magnetic semiconductors (DMSs). *J. Alloys Compd.* **340**, 13–26 (2002).
33. Verleur, H. W. & Barker, A. S. Infrared Lattice Vibrations in GaAs_yP_{1-y} Alloys. *Phys. Rev.* **149**, 715–729 (1966).
34. Verleur, H. W. & Barker, A. S. Optical Phonons in Mixed Crystals of CdSe_yS_{1-y}. *Phys. Rev.* **155**, 750–763 (1967).
35. Islam, S. M. & Bunker, B. A. Studies of atomic correlations in quaternary semiconductor alloys using the extended X-ray absorption fine structure technique. *Phys. Lett. A* **156**, 247–252 (1991).
36. Onabe, K. Thermodynamics of type A_{1-x}B_xC_{1-y}D_y III–V quaternary solid solutions. *J. Phys. Chem. Solids* **43**, 1071–1086 (1982).
37. Kisiel, A., Łazewski, J., Zimnal-Starnawska, M., Burattini, E. & Mycielski, A. Manganese Distribution in CdMnTeSe Crystals. EXAFS Data Analysis. *Acta Phys. Pol. A* **90**, 1032–1034 (1996).
38. Kisiel, A., Lazewski, J., Zimnal-Starnawska, M., Burattini, E. & Mycielski, A. Site Occupation Preferences in CdMnTeSe Quaternary Alloys. EXAFS Data Analysis. *J. Phys. IV* **7**, C2-1197–C2-1198 (1997).
39. Robouch, B. V. & Kisiel, A. Probabilistic Analysis of Site-Occupation Preferences in Ga_xIn_{1-x}As_ySb_{1-y} and Cd_{1-x}Mn_xSe_yTe_{1-y} Quaternary Compounds. *Acta Phys. Pol. A* **94**, 497–502 (1998).
40. Robouch, B. V. & Kisiel, A. EXAFS data resolved into individual site occupation preferences in quaternary compounds with tetrahedral coordinated structure. *J. Alloys Compd.* **286**, 80–88 (1999).
41. Bunker, B. A. Extended x-ray absorption fine-structure studies of semiconductor structure. *J. Vac. Sci. Technol. Vac. Surf. Films* **5**, 3003–3008 (1987).
42. Pong, W.-F., Mayanovic, R. A., Bunker, B. A., Furdyna, J. K. & Debska, U. Extended x-ray-absorption fine-structure studies of Zn_{1-x}Mn_xSe alloy structure. *Phys. Rev. B* **41**, 8440–8448 (1990).
43. Robouch, B. V., Marcelli, A., Robouch, P. & Kisiel, A. Occupation preferences in doped CmIm' multinary by correlated analysis of EXAFS and FTIR data. *Low Temp. Phys.* **37**, 241–244 (2011).
44. Robouch, B. V., Burattini, E., Kisiel, A., Suvorov, A. L. & Zaluzhnyi, A. G. Strained-tetrahedra statistical model for atomic distances and site occupations in ternary intermetallic M₃(XX') structures Ni₃(AlFe) case. *J. Alloys Compd.* **359**, 73–78 (2003).
45. Robouch, B. V., Marcelli, A., Saini, N. L. & Kisiel, A. Statistical model structure of A_{1-x}Z_xB₂ Laves phase C₁₅ system—the superconducting alloy Ce_{1-x}La_xRu₂. *Low Temp. Phys.* **35**, 89–93 (2009).
46. Kisiel, A., Robouch, B. V. & Marcelli, A. Local crystalline structure of multinary semiconducting alloys: Random vs. ordered distributions. *Opto-Electron. Rev.* **25**, 242–250 (2017).
47. Robouch, B. V. *et al.* Statistical model analysis of local structure of quaternary sphalerite crystals. *Low Temp. Phys.* **33**, 214–225 (2007).

48. Robouch, B. V. *et al.* Ion distribution preferences in ternary crystals $Zn_xCd_{1-x}Te$, $Zn_{1-x}Hg_xTe$ and $Cd_{1-x}Hg_xTe$. *Eur. Phys. J. B* **84**, 183–195 (2011).
49. Robouch, B. V., Sheregii, E. M. & Kisiel, A. Statistical analysis of inter-ionic distances and occupation preferences in ternary zincblende and wurtzite structured crystals. *Phys. Status Solidi C* **1**, 3015–3018 (2004).
50. Polit, J. J. *et al.* Analysis of phonon spectra of the $Zn_{1-x}Cd_xTe$ solid-solution. *J. Alloys Compd.* **371**, 172–176 (2004).
51. Robouch, B. V. *et al.* The complex stoichiometry of ternary alloys: What lies beyond the canonical Bernoulli distribution? *Solid State Commun.* **192**, 75–78 (2014).
52. Letardi, P., Motta, N. & Balzarotti, A. Atomic bonding and thermodynamic properties of pseudo-binary semiconducting alloys. *J. Phys. C Solid State Phys.* **20**, 2853–2884 (1987).
53. Pascarelli, S., Boscherini, F., Mobilio, S., Lawniczak-Jablonska, K. & Kozubski, R. Local structure of $L_{1-x}A_{2-x}B_{2x}$ -ordered $Ni_{75}(Al_{1-x}Fe_x)_{25}$ alloys. *Phys. Rev. B* **49**, 14984–14990 (1994).
54. Balzarotti, A. *et al.* Local structure of ternary semiconducting random solid solutions: Extended x-ray-absorption fine structure of $Cd_{1-x}Mn_xTe$. *Phys. Rev. B* **30**, 2295–2298 (1984).
55. Balzarotti, A. *et al.* Model of the local structure of random ternary alloys: Experiment versus theory. *Phys. Rev. B* **31**, 7526–7539 (1985).
56. Vodopyanov, L. *et al.* Effect of band inversion on the phonon spectra of $Hg_{1-x}Zn_xTe$ and $Hg_{1-x}Cd_xTe$ semiconductor alloys. *Phys. Status Solidi C* **1**, 2836–2839 (2004).
57. Zimnal-Starnawska, M. *et al.* EXAFS Studies of $Zn_{1-x}Mn_xS$ Ternary Compounds. *Acta Phys. Pol. A* **86**, 763–766 (1994).
58. Łażewski, J. *et al.* Local structure in $Zn_{1-x}Mn_xS$: EXAFS study. *Phys. Status Solidi B* **197**, 7–12 (1996).
59. Iwanowski, R. J., Ławniczak-Jabłońska, K., Winter, I. & Hormes, J. EXAFS studies of local atomic structure in $Zn_{1-x}Mn_xS$. *Solid State Commun.* **97**, 879–885 (1996).
60. Mayanovic, R. A., Pong, W.-F. & Bunker, B. A. X-ray-absorption fine-structure studies of $Hg_{1-x}Cd_xTe$ and $Hg_{1-x}Mn_xTe$ bond lengths: Bond relaxation and structural stability of ternary alloys. *Phys. Rev. B* **42**, 11174–11182 (1990).
61. Marbeuf, A. *et al.* EXAFS and XPS studies of $Hg_{1-x}Zn_xTe$: Determination of local atomic structure and valence band maximum. *J. Phys. Chem. Solids* **50**, 975–979 (1989).
62. Happo, N. *et al.* Zn, Mn and Te K-edge EXAFS studies of the diluted magnetic semiconductor. *J. Phys. Condens. Matter* **8**, 4315–4323 (1996).
63. Valeev, R. G. *et al.* Structure and properties of ZnS_xSe_{1-x} thin films deposited by thermal evaporation of ZnS and $ZnSe$ powder mixtures. *Mater. Res. Express* **2**, 025006 (2015).
64. Pellicer-Porres, J. *et al.* X-ray-absorption fine-structure study of $ZnSe_xTe_{1-x}$ alloys. *J. Appl. Phys.* **96**, 1491–1498 (2004).
65. Peterson, P. F. *et al.* Local atomic strain in $ZnSe_{1-x}Te_x$ from high real-space resolution neutron pair distribution function measurements. *Phys. Rev. B* **63**, 165211 (2001).
66. Robouch, B. V. *et al.* Statistical model of sphalerite structured quaternary $A_{1-x}B_xY_zZ_{1-y}$ systems. *J. Alloys Compd.* **426**, 31–42 (2006).
67. Wu, C.-J. *et al.* In Extended X-ray absorption fine structure of $InAsPSb$, Compound Semiconductor Week (CSW/IPRM), 2011 and 23rd Internat. Conf. on Indium Phosphide and Related Materials, 2011; pp 1-2.
68. Robouch, B. V. *et al.* First attempt to identify site occupation preference coefficients of a quaternary alloy: The $InAs_xPySb_{1-x-y}$ system. *J. Alloys Compd.* **738**, 218–223 (2018).
69. Sheregii, E. *et al.* First interpretation of phonon spectra of quaternary solid solutions using fine structure far-IR reflectivity by synchrotron radiation. *Infrared Phys. Technol.* **49**, 13–18 (2006).

Polish Synchrotron Radiation Society Board
The term of office: 2020 – 2023

Chairman:

Wojciech Kwiatek
Institute of Nuclear Physics PAS
Radzikowskiego 152
31-142 Krakow
wojciech.kwiatek@ifj.edu.pl

Vice Chairman:

Jakub Szlachetko
Institute of Nuclear Physics PAS
Radzikowskiego 152
31-142 Krakow
jakub.szlachetko@ifj.edu.pl

Vice Chairman:

Agnieszka Witkowska
Faculty of Applied Physics and
Mathematics
Narutowicza 11/12
80-233 Gdansk
agnieszka@mif.pg.gda.pl

Treasurer:

Joanna Czapla-Masztafiak
Institute of Nuclear Physics PAS
ul. Radzikowskiego 152
31-142 Krakow
joanna.czapla@ifj.edu.pl

Secretary of the Board:

Edyta Piskorska-Hommel
Institute of Low Temperature
and Structure Research PAS
Okólna 2, 50-422 Wrocław
e.piskorska@intibs.pl

Board Member:

Marcin Klepka
Institute of Physics PAS
al. Lotników 32/46
02-668 Warsaw
mklepka@ifpan.edu.pl

Board Member:

Maciej Kozak
Faculty of Physics
Adam Mickiewicz University
Uniwersytetu Poznańskiego 2
61-614 Poznan
mkozak@amu.edu.pl

Board Member:

Zuzanna Pietralik-Molińska
Faculty of Physics
Adam Mickiewicz University
Uniwersytetu Poznańskiego 2
61-614 Poznan
zuzannap@amu.edu.pl

Board Member:

Marcin Sikora
Academic Centre for Materials and
Nanotechnology AGH
al. Mickiewicza 30
30-059 Krakow
marcin.sikora@agh.edu.pl

Board Member:

Ryszard Sobierajski
Institute of Physics PAS
al. Lotników 32/46
02-668 Warsaw
ryszard.sobierajski@ifpan.edu.pl

Board Member:

Marek Stankiewicz
National Synchrotron
Radiation Centre SOLARIS
Jagiellonian University
Czerwone Maki 98
30-392 Krakow
m.j.stankiewicz@uj.edu.pl



polskie towarzystwo
promieniowania
synchrotronowego



polish synchrotron
radiation society

Bulletin of the Polish Synchrotron Radiation Society

SYNCHROTRON RADIATION IN NATURAL SCIENCE



polish synchrotron
radiation society

Bulletin of the Polish Synchrotron Radiation Society

SYNCHROTRON RADIATION IN NATURAL SCIENCE